Journal of Sound and Vibration (1998) **211**(1), 39–93

ON THE ELASTODYNAMIC RESPONSE OF THICK MULTILAYERED PLATES SUBJECTED TO IMPACT LOADS

K. A. LANGE† AND W. J. BOTTEGA

Department of Mechanical and Aerospace Engineering, Rutgers University, Piscataway, NJ 08854-8058, *U.S.A.*

(*Received* 22 *January* 1997, *and in final form* 8 *October* 1997)

The transient axisymmetric response of thick multilayered plates is considered from a dynamic elasticity point of view. The analysis is based on an exact elasticity formulation and analytical solution, via eigenfunction expansion, for a plate comprised of an arbitrary number of perfectly bonded isotropic layers of arbitrarily differing thicknesses and material properties. Results of numerical simulations based on the exact solution are presented for a single layer plate, for sandwich plates and for bilaminates with a central "adhesive" layer. In each case, frequency spectra and physical through the thickness depictions of selected individual elastodynamic modes representative of the various branches of the spectrum are computed and compared. A forcing function is formulated to simulate transverse impact and results corresponding to both "long" and "short" duration normal impact of each structure are presented in the form of physical depictions of the entire deformed cross-section of the structure as a function of time. In addition, the degree of participation of the various modes for the transient response is monitored by a scaled shade intensity of the frequency spectrum plot. The dimensions of the impactor considered are on the order of the overall thickness of the plate, and the responses are seen to capture the critical wave behavior in the vicinity of the impactor.

© 1998 Academic Press Limited

1. INTRODUCTION

The dynamics of layered media is of interest in a variety of settings, from geophysical applications and semiconductor devices to composite engineering structures. The subject of impact response is particularly germain to layered structures in that large local interfacial stresses may cause delamination at these locations, compromising the effectiveness and integrity of the overall structure. The study of the response of laminates to transverse impact loading has thus been, and continues to be, of much interest. Typically, the structure or medium is considered as either an infinite or semi-infinite domain, or as a thin layered structure with implicit assumptions concerning the variation of the response through the thickness. Both approaches have their place and may be considered appropriate within certain ranges of length scales and load types peculiar to the particular problem under consideration. In the present study, however, the problem of impact of a finite dimensional multilayered plate is examined in the context of an exact, albeit axisymmetric, elasticity solution which captures and demonstrates the contribution of the through the thickness wave effects.

† Present address: General Dynamics/Electric Boat Division, Groton, CT 06340, U.S.A.

0022–460X/98/100039 + 55 $25.00/0/sv971351 © 1998 Academic Press Limited

The impact problem may generally be considered to consist of two parts, the first being the modelling of the impact process and the second being the modelling of the laminate response. Both are, of course, interdependent and must formally be considered simultaneously. Generally, the impact process is simulated by relating the motion of the plate to the motion of the impactor via a contact law. Commonly, the contact law is based on the Hertzian assumption that the stresses and deformations close to the contact region can be calculated at any instant as if the contact were static. With regard to the response of layered plates, approximate thin plate models have commonly been employed such as that due to Whitney and Pagano [1], which was originated by Yang *et al*. [2] who extended the isotropic plate theory of Mindlin [3] to the case of heterogeneous plates. The literature pertaining to elasticity solutions of such problems is less extensive. A comprehensive review of the literature concerning impact of composites may be found in the papers by Abrate [4–6]. A number of such works, grouped according to topic, are discussed below in chronological order.

We begin with the work of Sun and Lai [7] who, in 1974, compared the plate theory of Whitney and Pagano [1] with the exact elasticity solution for transient wave propagation in an anisotropic plate. They found that the plate solution agreed very well with the exact solution except in the vicinity of load. In 1975, Sun and Chattopadhyay [8] examined the response of anisotropic laminated plates under initial stress to impact of a mass. They used the plate theory of Whitney and Pagano [1] to model the laminated plates and the Hertzian contact law to model the impact forces. An approximate numerical scheme was employed to solve the resulting non-linear integral equation of motion. In 1986, Koller [9] investigated the elastic impact of spheres on sandwich plates. In that study, a special sandwich plate theory was used which included bending of the facing sheets and transverse shear of the core. Hertzian contact was assumed. A Laplace transform was carried out on the equations of motion which were then solved in the transform space. As the resulting solution was too cumbersome for an analytical inverse transformation, a power series approximation was taken and a finite number of terms were then inversely transformed. Although the results agreed qualitatively with experiment, the author concluded that

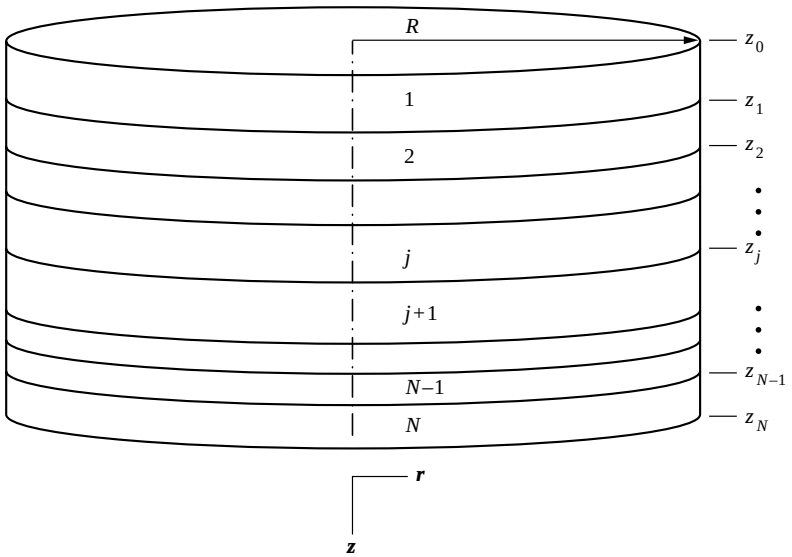

Figure 1. Multilayered elastic solid with co-ordinates and labels.

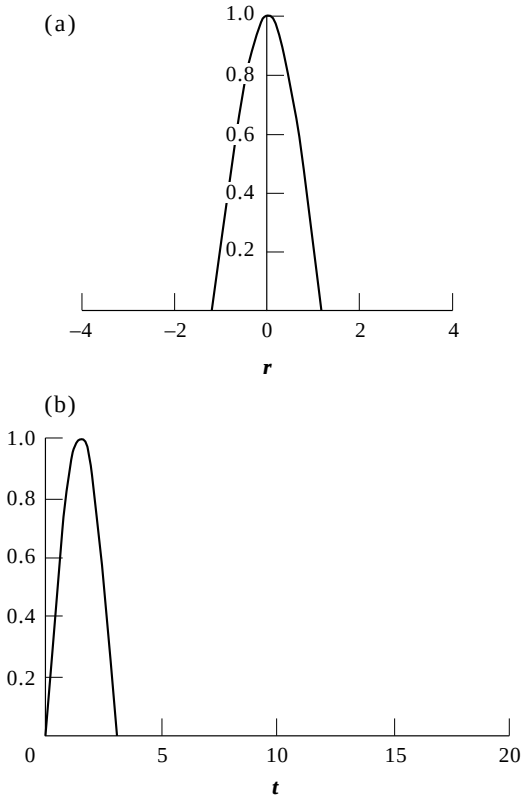

Figure 2. Graphical depiction of the "impact force": (a) radial variation: shown for the case $r_0 = 1{\cdot}2$ ($k_0 = 2$); (b) temporal variation: shown for the case $t_0 = 3{\cdot}14$ ($\omega_0 = 1$).

transverse waves, which were not modelled by the sandwich plate theory, were important and should be included. In 1991, Christoforou and Swanson [10] used the approximate equations of motion developed by Whitney and Pagano [1] to obtain an analytical solution for impact response in composite plates. A closed form solution was obtained by linearizing the equilibrium equation between the impactor and the plate and by assuming a constant contact area. In 1993, Lee *et al*. [11] studied the response of a sandwich plate impacted by a rigid ball using a sandwich theory which modelled the face sheets as separate Mindlin plates with a core that transmits transverse shear as well as transverse normal deformations. They used the finite element method to numerically solve the equations of motion for the plate and impactor with a contact power law determined from static indentation tests. In 1994, Prasad *et al*. [12] conducted experiments of low speed impact on composite plates and compared their results with analysis using the plate theory by Whitney and Pagano [1]. For impact, a constant contact zone was used with the Hertzian contact law. The results of that study showed that the inclusion of transverse shear in the plate theory was very important for correlating the analysis with experiment in the local region of impact. We also note several other studies that have employed higher-order plate theories for the study of laminated plates [13–15].

Studies of one-dimensional elastic wave propagation in periodically layered structures have been conducted by Sun *et al*. [16], Li and Benaroya [17], and by Weaver and Pao [18]. Norris and Wang [19] examined flexural waves in periodic plates using an asymptotic approximation for the dispersion relation of flexural waves in an infinite periodic plate.

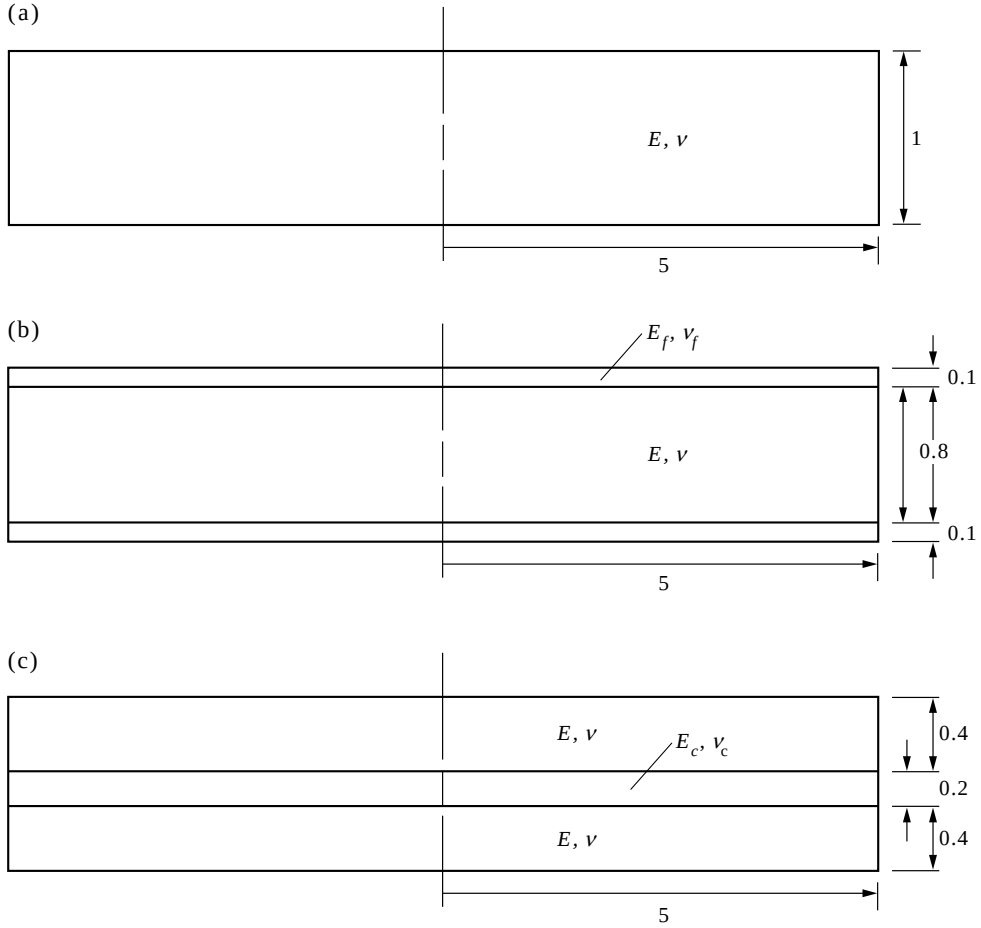

Figure 3. Laminate configurations: (a) single layer (isotropic) plate; (b) sandwich plate; (c) bilaminate with central "adhesive" layer.

In 1988, Bottega [20] extended the exact elasticity solution for the transient axisymmetric response of an isotropic plate, via eigenfunction expansion, by Weaver and Pao [21], to the case of multilayered plates. This solution gives the response to transient loading as an expansion of the axisymmetric elastodynamic modes† for an elastic solid comprised of an arbitrary number of isotropic layers as well as a procedure for evaluating the natural frequencies of the structure. It was noted by the author [20] that the solution to specific problems can be obtained numerically using the presented solution as an algorithm and that the major computational effort would be in the evaluation of the natural frequencies. In 1995, Lih and Mal [23] calculated the field response of laminated plates subjected to a full cycle sine pulse with Gaussian spatial variation over the entire surface of the plate using both an elasticity solution via Fourier transform, and using shear plate and classical plate solutions. Surface motion at various multiples of the plate thickness away from the center of the load, for various durations of the sine pulse, were computed and compared and conclusions were drawn as to the adequacy of the shear plate model within ranges of these parameters. In 1996, El-Raheb and Wagner [24] used an exact elasticity solution

† A condition for the orthogonality of the modes of a general class of multilayered solids was given by Bottega [22]. The multilayered plates considered herein fall into that class.

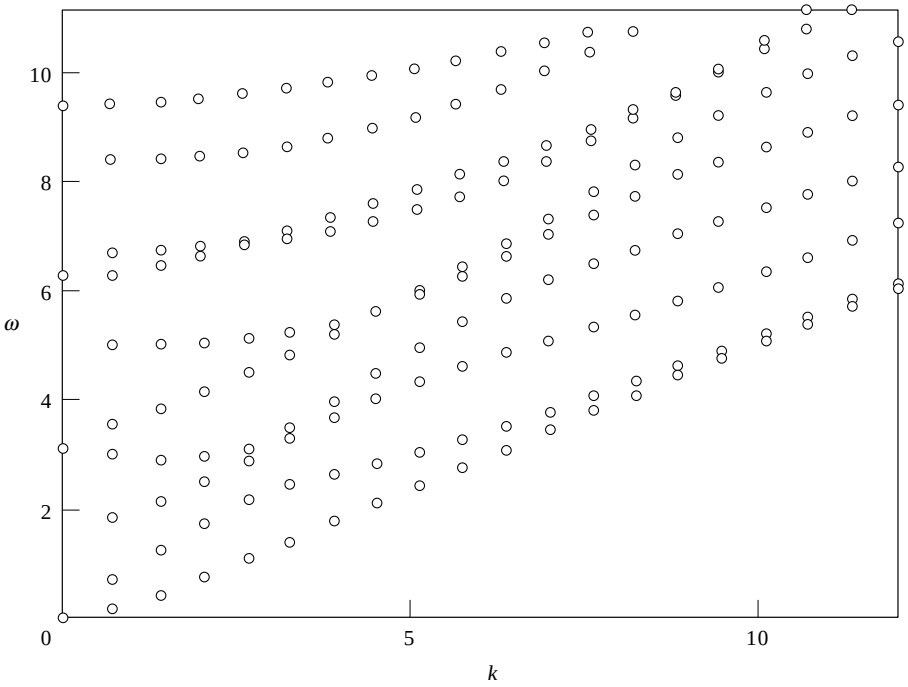

Figure 4. Frequency spectrum for isotropic plate.

similar to Bottega's [20] to examine transient axisymmetric elastic waves in periodic layered media.

In the present work, the exact solution by Bottega [20] is employed to investigate the dynamic response of layered plates to impact loading. A mathematical representation of an impact load is incorporated, which implicitly assumes a form of contact [25]. The frequency spectrum and representative elastodynamic mode shapes are presented for selected structures. In addition, the corresponding response to impact loading is presented in the form of time histories of the deforming structure and reveals the local wave-like behavior in the vicinity of the impactor for a specific contact area and a pair of impact durations. This is first done for a single layer plate, as a benchmark. Corresponding results for the case of sandwich structures and for the case of bilaminates with a central adhesive layer are then presented, and are interpreted through and compared with the results for the single layer plate as well as with each other. In each case, impact areas are considered such that the impact diameter is of the order of the overall thickness of the layered plate. In all cases, critical wave behavior is captured and is seen to occur locally in the vicinity of the impactor. Such behavior has ramifications with regard to interfacial failure of the structure (see, for example, references [26–28]).

2. ANALYTICAL SOLUTION

For this study, the eigenfunction based solution by Bottega [20] for the transient axisymmetric response of a multilayered elastic solid of finite extent is employed. This solution begins by solving the elasticity equations in a single layer. A multilayered structure is considered by incorporating the general form of the solution for each individual layer. Matching conditions imposed at the layer interfaces provide a general response of the

multilayered solid, and boundary conditions imposed on the edges and exterior faces provide a dispersion relation for the entire structure. Finally, the response to time dependent loading is assumed as an expansion of the normal modes with time dependent amplitudes and is expressed in the form of a Duhamel Integral. That solution is briefly summarizd in this section. The reader is referred to reference [20] for a detailed development of the solution.

Consider the N-layer circular plate of radius R depicted in Figure 1, where the displacement field corresponding to each linearly elastic isotropic layer, $\mathbf{u}^{(j)}(\mathbf{r}, t)$ ($j = 1, 2, \ldots, N$), must satisfy Navier's equation which for the jth layer is of the form

$$(\lambda^{(j)} + \mu^{(j)})\nabla(\nabla \cdot \mathbf{u}^{(j)}(\mathbf{r}, t)) + \mu^{(j)}\nabla^2\mathbf{u}^{(j)}(\mathbf{r}, t) = \rho^{(j)}\frac{\partial^2\mathbf{u}^{(j)}(\mathbf{r}, t)}{\partial t^2} - \mathbf{F}(\mathbf{r}, t), \qquad \text{on } z_{j-1} \leqslant z \leqslant z_j. \tag{1}$$

In equation (1), $\lambda^{(j)}$, $\mu^{(j)}$, and $\rho^{(j)}$ correspond to the two Lamé constants and the mass density for the jth layer, respectively, $\mathbf{F}(\mathbf{r}, t)$ is the applied body force field, and t is the time. In addition, $\mathbf{r} = (r, z)$ is the spatial co-ordinate vector where r is the radial co-ordinate and z is the transverse co-ordinate, and ∇ represents the gradient operator.

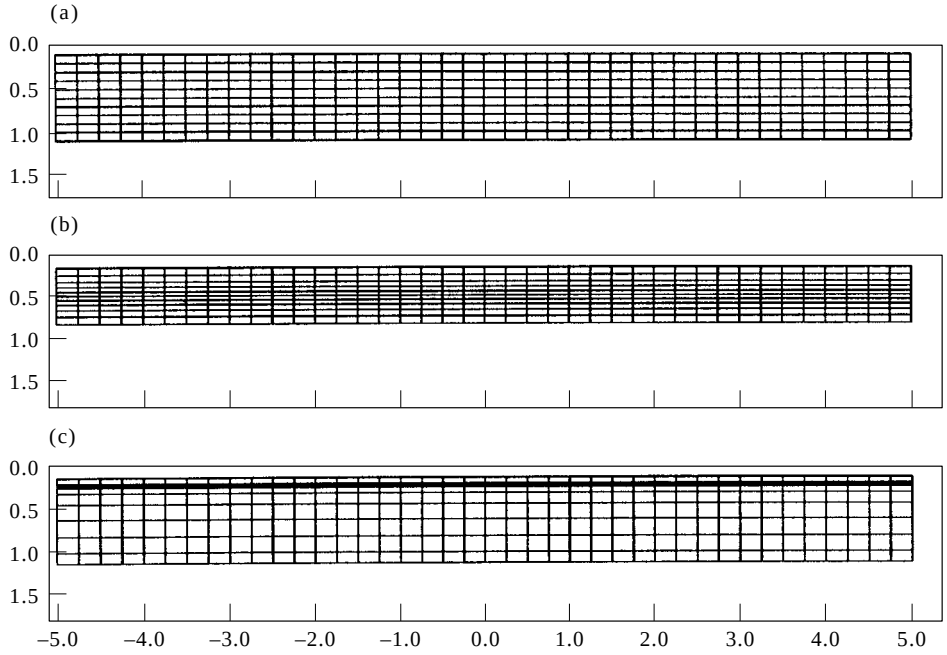

Figure 5. The first three "transverse–longitudinal" ("rod-like") modes of the isotropic plate: (a) $\omega = 0$, $k = 0$; (b) $\omega = 3{\cdot}14$, $k = 0$; (c) $\omega = 6{\cdot}28$, $k = 0$.

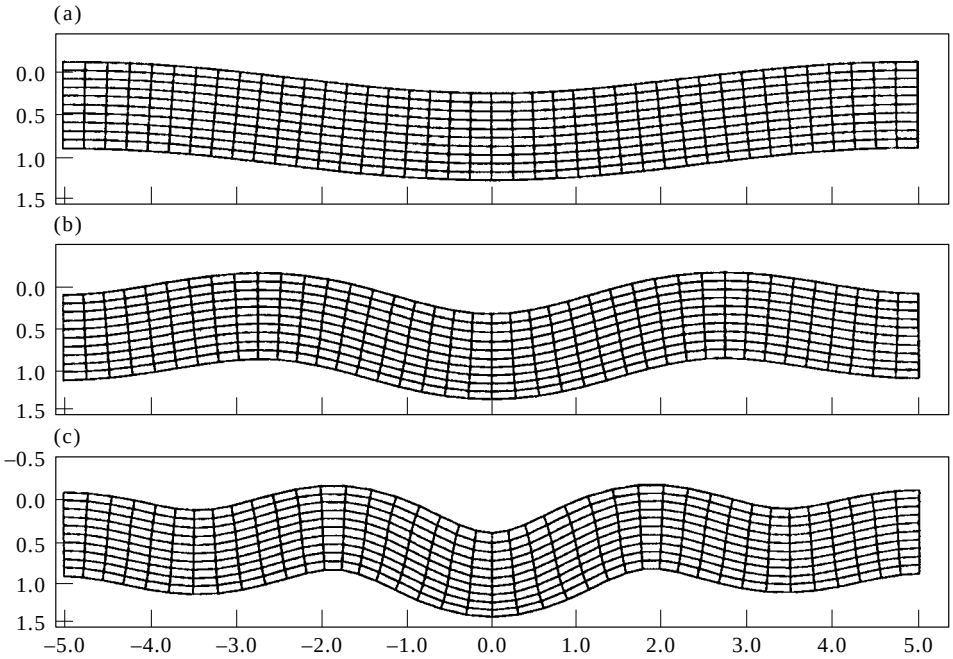

Figure 6. The first three "flexural" modes of the isotropic plate: (a) $\omega = 0{\cdot}14$, $k = 0{\cdot}766$; (b) $\omega = 0{\cdot}401$, $k = 1{\cdot}4$; (c) $\omega = 0{\cdot}713$, $k = 2{\cdot}03$.

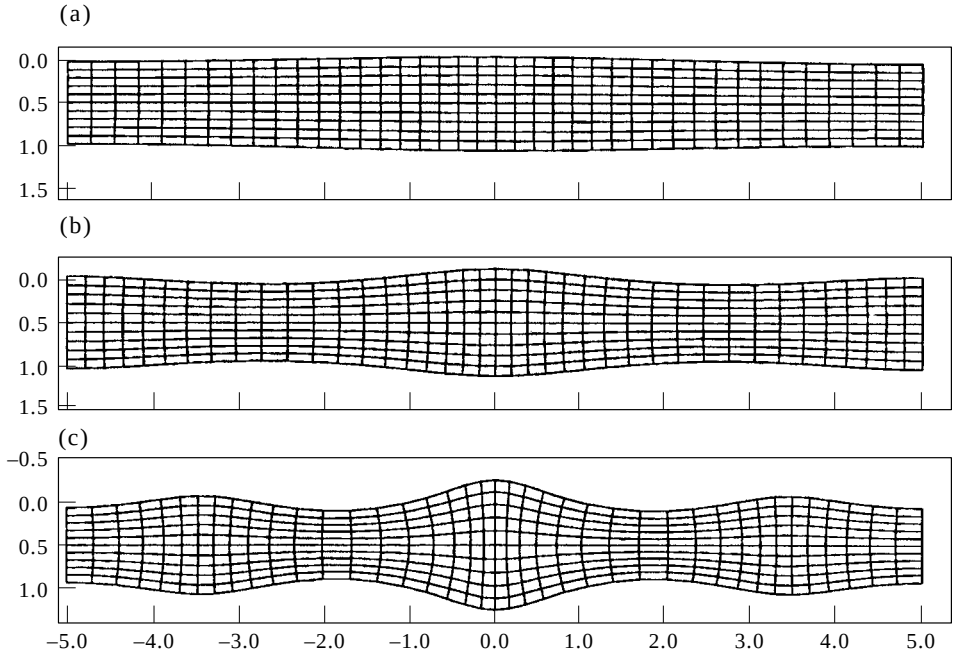

Figure 7. The first three "radial–longitudinal" modes of the isotropic plate: (a) $\omega = 0{\cdot}689$, $k = 0{\cdot}766$; (b) $\omega = 1{\cdot}24$, $k = 1{\cdot}4$; (c) $\omega = 1{\cdot}75$, $k = 2{\cdot}03$.

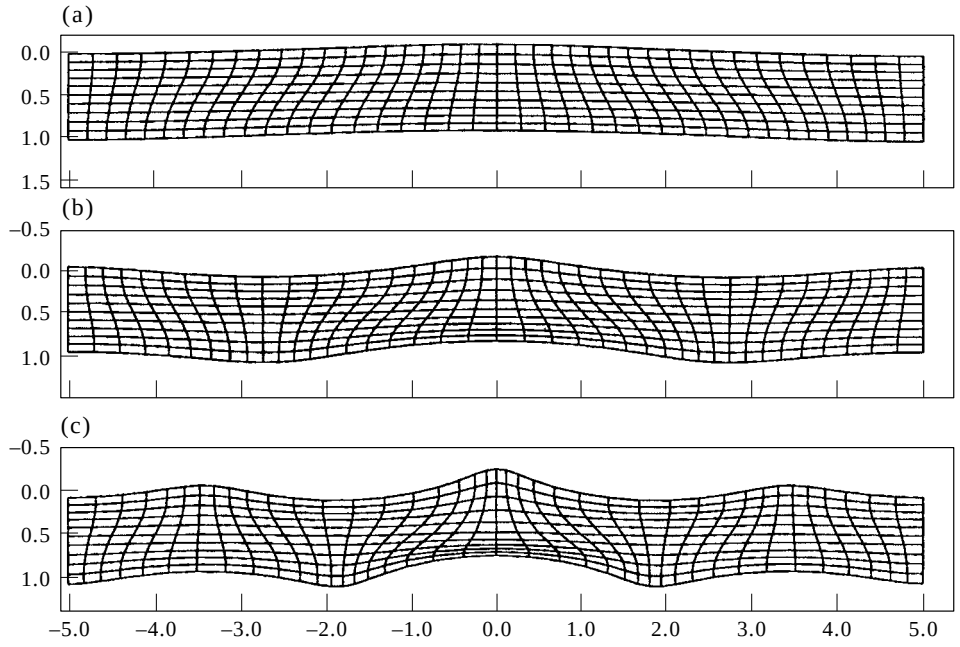

Figure 8. The first three anstisymmetric "thickness–shear" modes of the isotropic plate: (a) $\omega = 1{\cdot}84$, $k = 0{\cdot}766$; (b) $\omega = 2{\cdot}14$, $k = 1{\cdot}4$; (c) $\omega = 2{\cdot}51$, $k = 2{\cdot}03$.

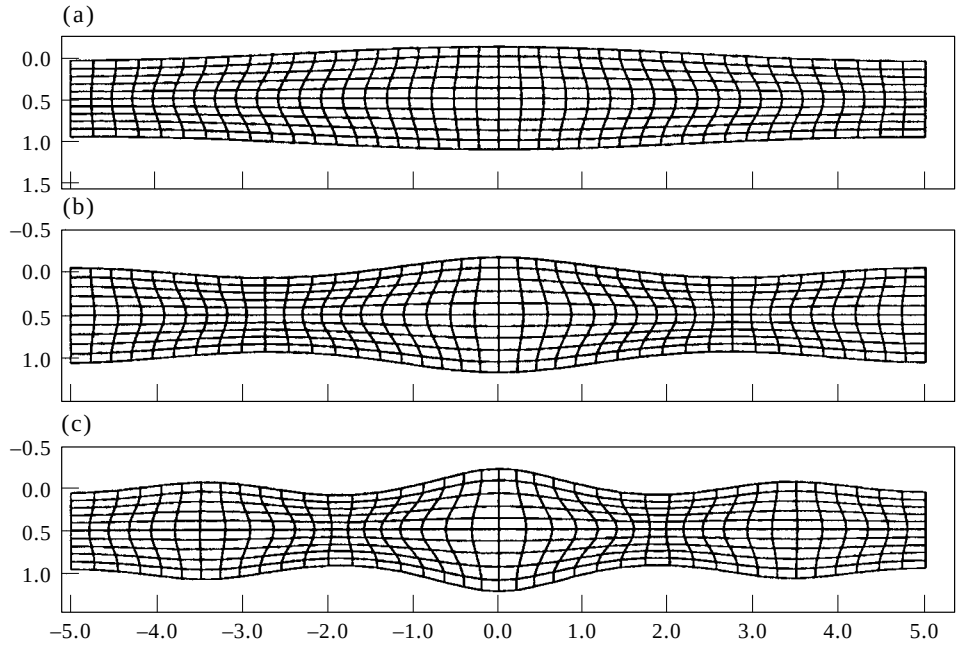

Figure 9. The first three symmetric "thickness–shear" modes of the isotropic plate: (a) $\omega = 3{\cdot}56$, $k = 0{\cdot}766$; (b) $\omega = 3{\cdot}84$, $k = 1{\cdot}4$; (c) $\omega = 4{\cdot}15$, $k = 2{\cdot}03$.

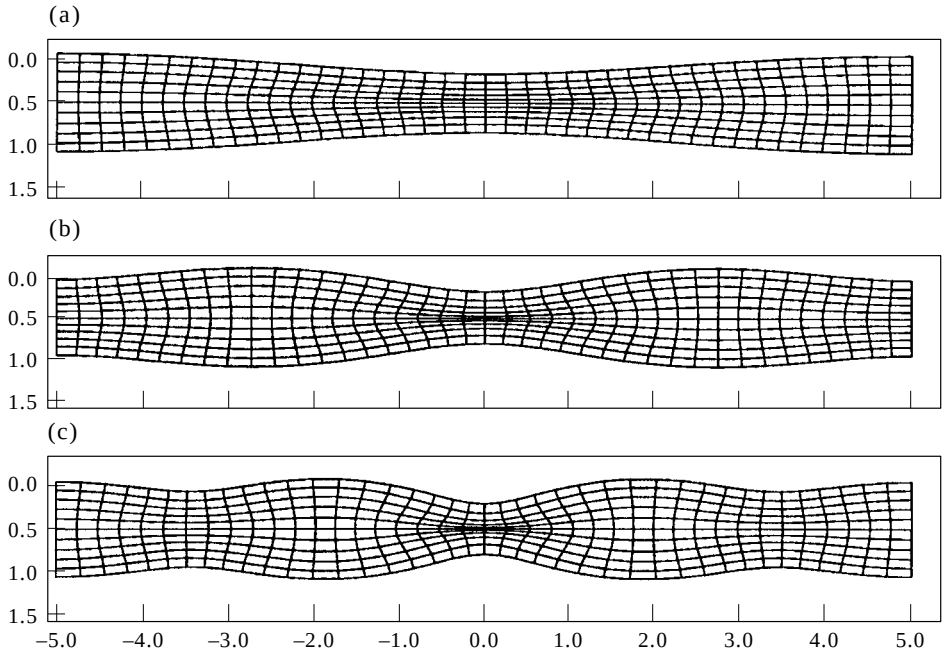

Figure 10. The first three (radially varying) symmetric "thickness–stretch" modes of the isotropic plate: (a) $\omega = 3{\cdot}02$, $k = 0{\cdot}766$; (b) $\omega = 2{\cdot}93$, $k = 1{\cdot}4$; (c) $\omega = 2{\cdot}94$, $k = 2{\cdot}03$.

2.1. MODAL RESPONSE

Consideration of the unforced ($\mathbf{F} = \mathbf{0}$) case yields the modal response in the jth layer given by

$$\hat{\mathbf{d}}^{(j)}(r, z) = \mathbf{J}(kr)\mathbf{S}^{(j)}(z)\mathbf{a}^{(j)}, \tag{2}$$

where

$$\hat{\mathbf{d}}^{(j)}(r, z) \equiv \begin{Bmatrix} \hat{u}^{(j)}(r, z) \\ \hat{w}^{(j)}(r, z) \\ \hat{\sigma}_{zr}^{(j)}(r, z) \\ \\ \hat{\sigma}_{zz}^{(j)}(r, z) \end{Bmatrix} \tag{3}$$

is the "modal array" for the jth layer, with

$$\mathbf{J}(kr) \equiv \begin{bmatrix} kJ_1(kr) & 0 & 0 & 0 \\ 0 & J_0(kr) & 0 & 0 \\ 0 & 0 & kJ_1(kr) & 0 \\ 0 & 0 & 0 & J_0(kr) \end{bmatrix}, \tag{4}$$

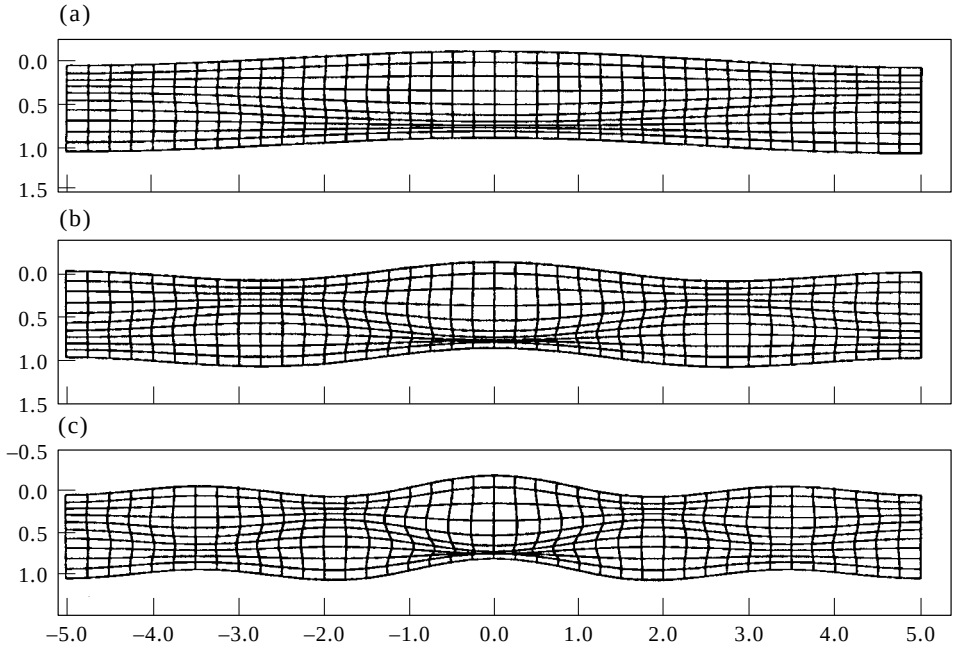

Figure 11. The first three antisymmetric "thickness–stretch" modes of the isotropic plate: (a) $\omega = 6{\cdot}34$, $k = 0{\cdot}766$; (b) $\omega = 6{\cdot}45$, $k = 1{\cdot}4$; (c) $\omega = 6{\cdot}62$, $k = 2{\cdot}03$.

$$\mathbf{S}^{(j)}(z) \equiv \begin{bmatrix} -\cos(\alpha^{(j)}z) & -\sin(\alpha^{(j)}z) & \beta^{(j)}\sin(\beta^{(j)}z) & \beta^{(j)}\cos(\beta^{(j)}z) \\ -\alpha^{(j)}\sin(\alpha^{(j)}z) & \alpha^{(j)}\cos(\alpha^{(j)}z) & k^2\cos(\beta^{(j)}z) & k^2\sin(\beta^{(j)}z) \\ \xi^{(j)}\sin(\alpha^{(j)}z) & -\xi^{(j)}\cos(\alpha^{(j)}z) & \gamma^{(j)}\mu^{(j)}\cos(\beta^{(j)}z) & \gamma^{(j)}\mu^{(j)}\sin(\beta^{(j)}z) \\ -\Gamma^{(j)}\cos(\alpha^{(j)}z) & -\Gamma^{(j)}\sin(\alpha^{(j)}z) & -\eta^{(j)}\sin(\beta^{(j)}z) & \eta^{(j)}\cos(\beta^{(j)}z) \end{bmatrix} \tag{5}$$

and

$$\mathbf{a}^{(j)} \equiv \begin{Bmatrix} A_1^{(j)} \\ A_2^{(j)} \\ A_3^{(j)} \\ A_4^{(j)} \end{Bmatrix}. \tag{6}$$

Further,

$$(\alpha^{(j)})^2 = \left(\frac{\omega}{c_p^{(j)}}\right)^2 - k^2, \qquad (\beta^{(j)})^2 = \left(\frac{\omega}{c_s^{(j)}}\right)^2 - k^2, \tag{7a, b}$$

$$c_p^{(j)} \equiv \sqrt{\frac{\lambda^{(j)} + 2\mu^{(j)}}{\rho^{(j)}}}, \qquad c_s^{(j)} \equiv \sqrt{\frac{\mu^{(j)}}{\rho^{(j)}}}, \tag{8a, b}$$

$$\xi^{(j)} \equiv 2\mu^{(j)}\alpha^{(j)}, \qquad \Gamma^{(j)} \equiv \alpha^{(j)2}[\lambda^{(j)} + 2\mu^{(j)}] + k^2\lambda^{(j)}, \tag{9a, b}$$

$$\gamma^{(j)} \equiv \beta^{(j)2} - k^2, \qquad \eta^{(j)} \equiv 2\mu^{(j)}k^2\beta^{(j)}. \tag{10a, b}$$

In equation (3), $\hat{u}^{(j)}(r, z)$ and $\hat{w}^{(j)}(r, z)$ respectively correspond to the radial and transverse components of the modal displacement vector $\hat{\mathbf{u}}^{(j)}(r, z)$, while $\hat{\sigma}_{zr}^{(j)}(r, z)$ and $\hat{\sigma}_{zz}^{(j)}(r, z)$ respectively correspond to the radial and normal components of the modal traction vector for surfaces with normals parallel to the z-axis, $\hat{\boldsymbol{\tau}}_z^{(j)}(r, z)$ (i.e., the corresponding modal shear stress, and modal normal stress), for the jth layer. In equation (4), the functions J_0 and J_1 correspond to the zeroth order and first order Bessel functions of the first kind, respectively, while in equation (6) the modal amplitude array for the jth layer, $\mathbf{a}^{(j)}$, contains four (as yet arbitrary) constants $A_i^{(j)}$ ($i = 1$–4) for that layer. Finally, the parameter k represents a radial wavenumber and the parameter ω is a circular frequency, both to be determined. When multiplied by a harmonic time signature with circular frequency ω, the components of the modal array satisfy the unforced equations of motion.

The corresponding modal dilatation $\hat{\varepsilon}^{(j)}(r, z)$ and local modal rotation $\hat{\Omega}_\theta^{(j)}(r, z)$ in the jth layer are found as

$$\hat{\varepsilon}^{(j)}(r, z) = -(\omega/c_p^{(j)})^2[A_1^{(j)} \cos(\alpha^{(j)}z) + A_2^{(j)} \sin(\alpha^{(j)}z)]J_0(kr), \qquad (z_{j-1} \leqslant z \leqslant z_j), \quad (11a)$$

$$\hat{\Omega}_\theta^{(j)}(r, z) = (\omega/c_s^{(j)})^2[A_3^{(j)} \cos(\beta^{(j)}z) + A_4^{(j)} \sin(\beta^{(j)}z)]kJ_1(kr), \qquad (z_{j-1} \leqslant z \leqslant z_j), \quad (11b)$$

from which it is seen that $\alpha^{(j)}$ is the transverse wavenumber associated with dilatation and $\beta^{(j)}$ is the transverse wavenumber associated with shear, in the jth layer, and hence that the corresponding terms in the modal response (the first two columns and last two columns, respectively, of the matrix $\mathbf{S}^{(j)}$) are associated accordingly.

For perfect bonding of the layers, it is required that the displacements and tractions associated with each interface, and hence that the modal arrays of adjacent layers, be

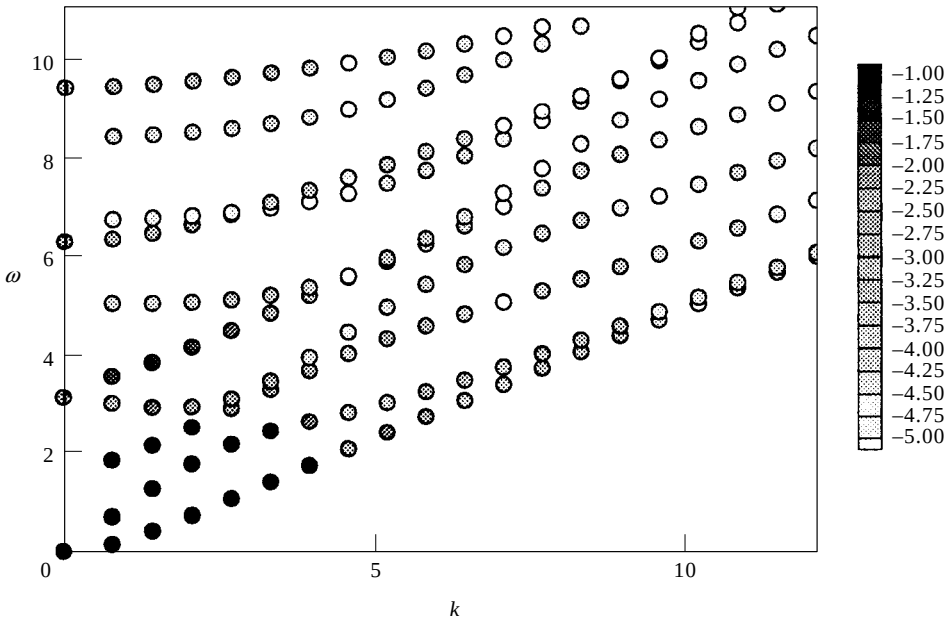

Figure 12. Modal participation spectrum of the impacted isotropic plate (long duration load). Degree of shading indicates relative contribution of mode according to $\log_{10}$ scale of amplitude shown at right.

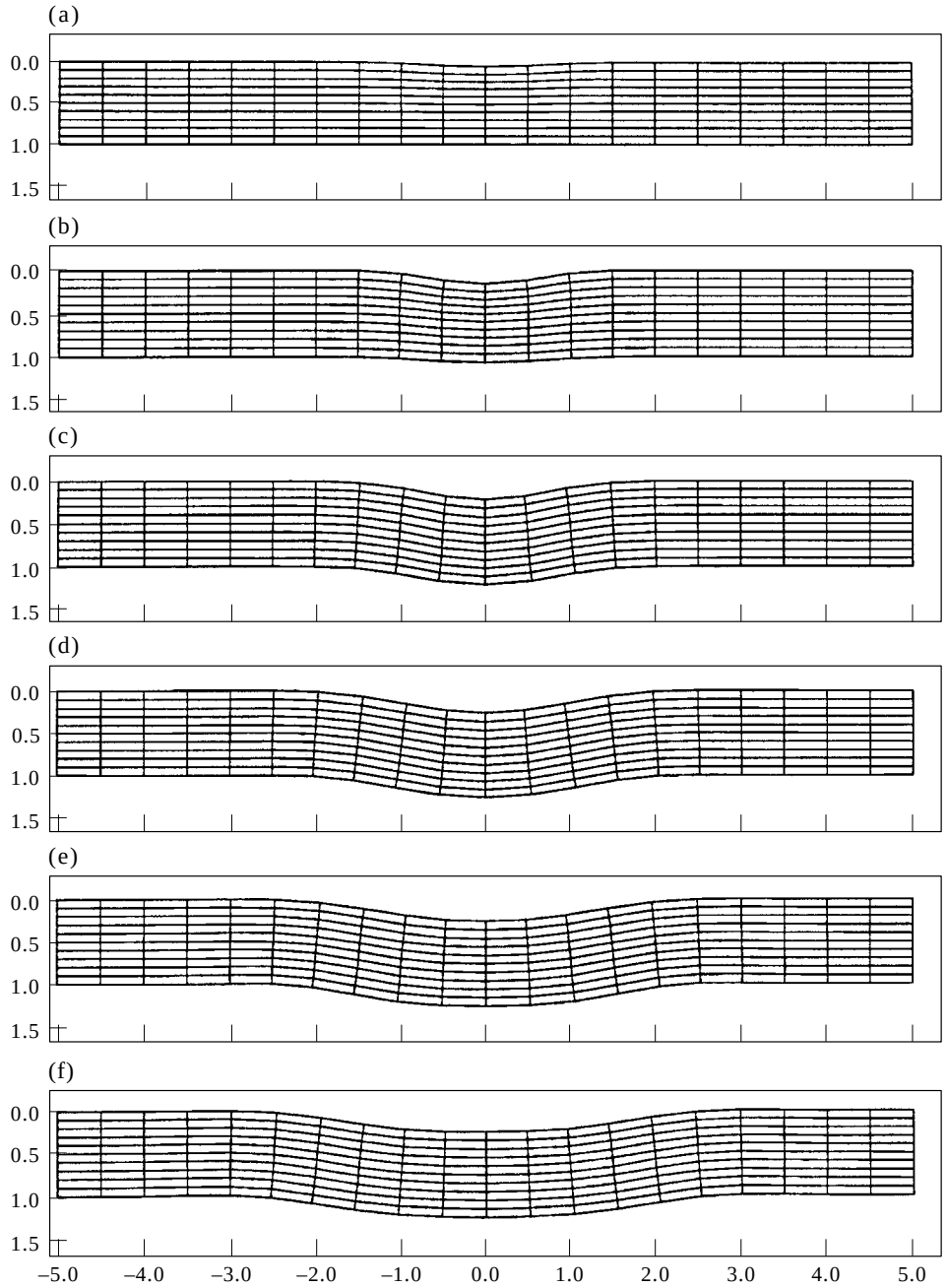

Figure 13. Transient response of the isotropic plate (long duration load). "Freeze frames" of deforming plate at sequential instants in (normalized) time: (a) $t = 1$, (b) 2, (c) 3, (d) 4, (e) 5, (f) 6.

continuous across each interface. This results in distinct relations between the modal amplitude constants of the different layers given by

$$\mathbf{a}^{(j+k)} = \mathbf{T}(z_j, z_{j+k-1})\mathbf{a}^{(j)}, \tag{12}$$

where

$$\mathbf{T}(z_j, z_{j+k-1}) = \mathbf{T}^{(j+k-1)}\mathbf{T}^{(j+k-2)} \ldots \mathbf{T}^{(j)} \tag{13}$$

and

$$\mathbf{T}^{(j)} \equiv [\mathbf{S}^{(j+1)}(z_j)]^{-1}\mathbf{S}^{(j)}(z_j). \tag{14}$$

We refer to $\mathbf{T}$ as the "influence matrix" and to $\mathbf{T}^{(j)}$ as the "transmission matrix". The modal vector and hence the response of any layer is related to the modal vector and therefore the response of any other layer, say the first, by these matrices. There are thus only four independent integration constants associated with each mode, regardless of the number of layers.

2.2. THE DISPERSION RELATION

We will consider support conditions around the perifery of the structure to be rigid-smooth. That is, conditions are such that the radial displacement and the transverse shear stress both vanish on the surface $r = R$. (It will be seen in the results sections of this study that the local impact response of the multilayered structures under consideration is not affected by the periferal support conditions.) Upon examination of equations (2)–(6), it is seen that these particular support conditions are satisfied for all radial wavenumbers $k = k_1, k_2, \ldots$, which are zeroes of the equation

$$J_1(kr) = 0. \tag{15}$$

In addition to the conditions imposed at $r = R$, the bounding surfaces $z = z_0$ and $z = z_N$ are considered to be traction free. That is, it is required that the corresponding normal and shear stresses vanish on these surfaces. (The complete set of boundary conditions considered herein satisfy the conditions for mutual orthogonality of the normal modes for the general class of layered solids established by Bottega [22]. The modes considered herein

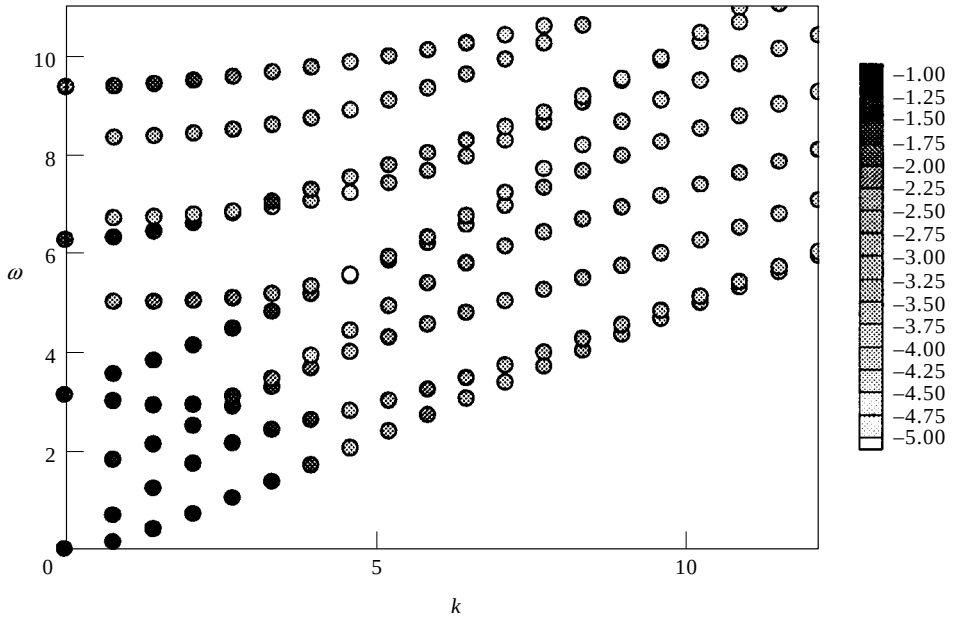

Figure 14. Modal participation spectrum of the impacted isotropic plate (short duration load). Degree of shading indicates relative contribution of mode according to $\log_{10}$ scale of amplitude shown at right.

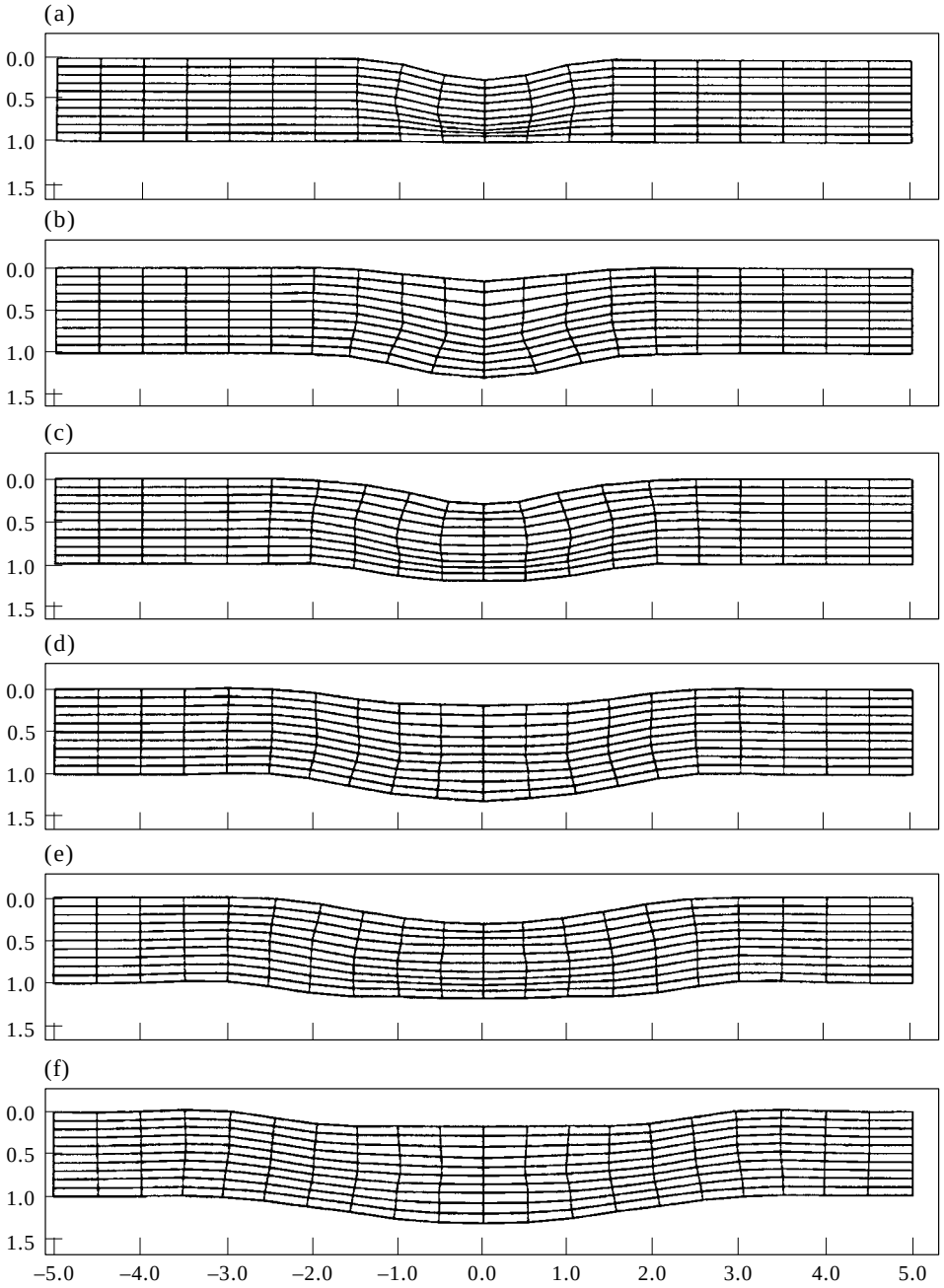

Figure 15. Transient response of the isotropic plate (short duration load). ''Freeze frames'' of deforming plate at sequential instants in (normalized) time: (a) $t = 1$, (b) 2, (c) 3, (d) 4, (e) 5, (f) 6.

are therefore mutually orthogonal.) Expressing the traction-free boundary conditions in terms of the corresponding modal arrays one has

$$\mathbf{S}^*\mathbf{a}^{(1)} = 0, \tag{16}$$

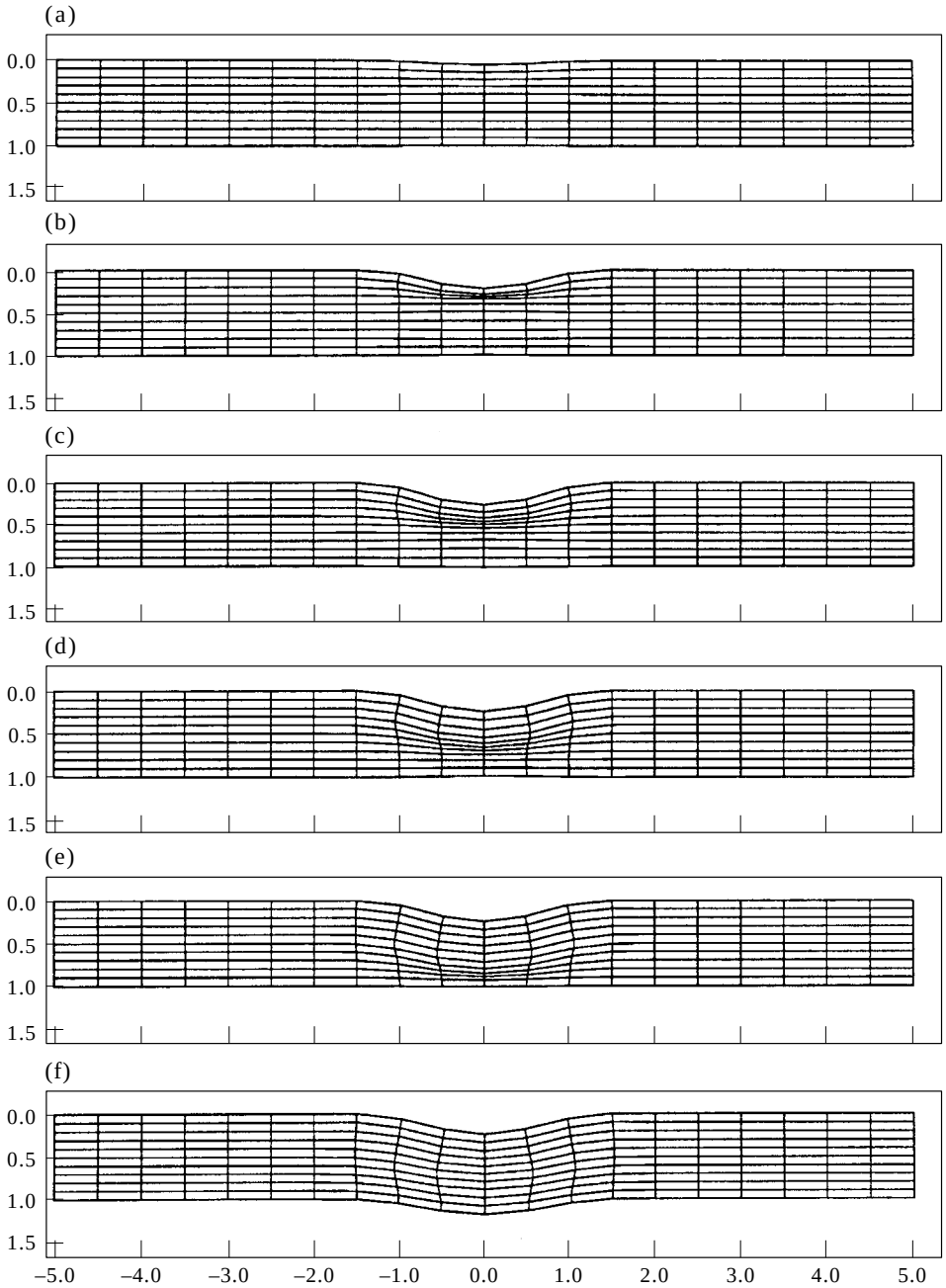

Figure 16. Transient response of the isotropic plate (short duration load—finer time increments). "Freeze frames" of deforming plate at sequential instants in (normalized) time: (a) $t = 0{\cdot}2$, (b) 0·4, (c) 0·6, (d) 0·8, (e) 1·0, (f) 1·2.

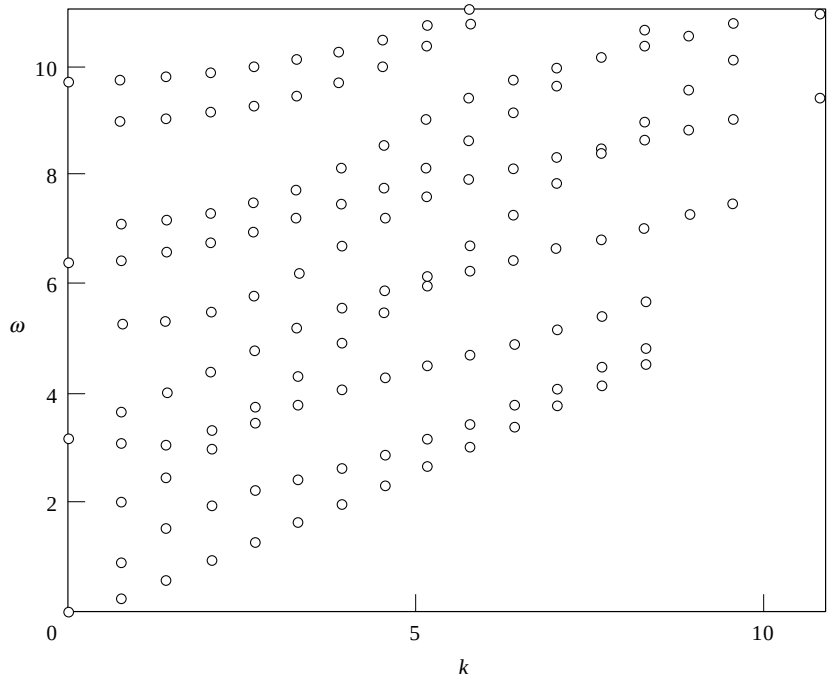

Figure 17. Frequency spectrum for sandwich plate: case 1 (stiff face sheets).

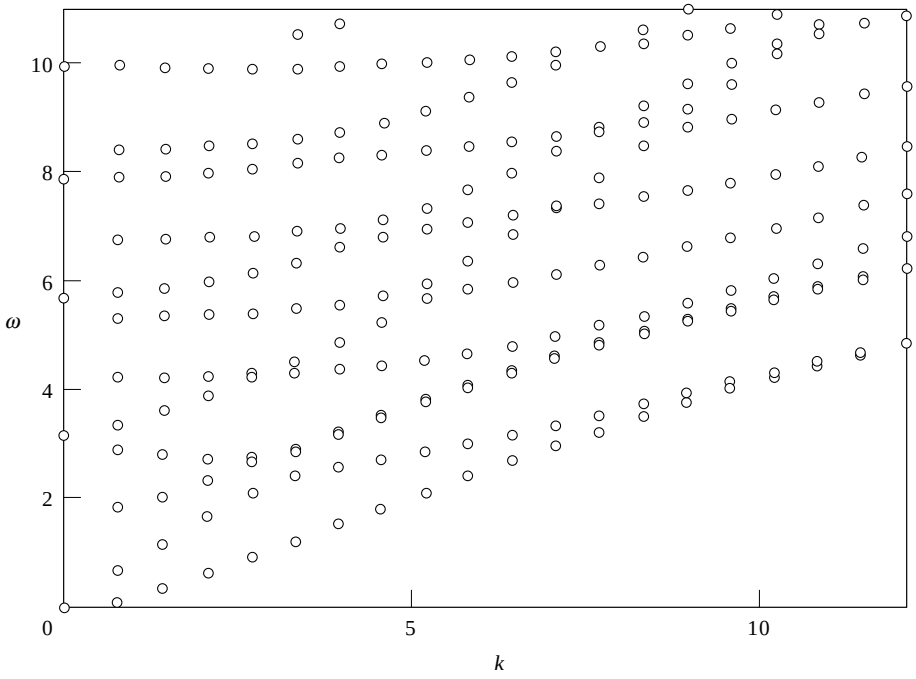

Figure 18. Frequency spectrum for sandwich plate: case 2 (compliant face sheets).

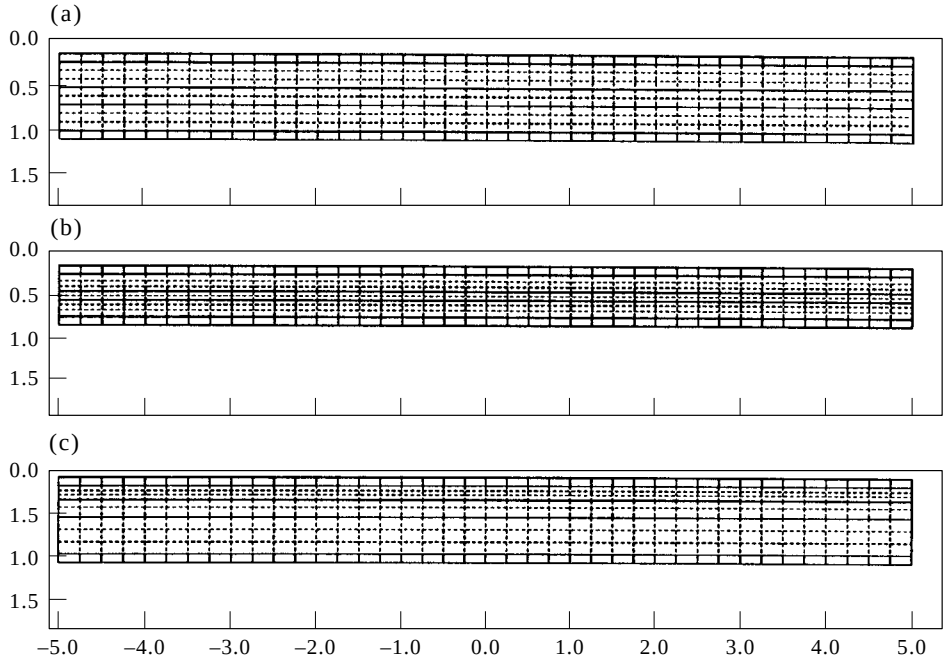

Figure 19. The first three "transverse–longitudinal" ("rod-like") modes for case 1: (a) $\omega = 0$, $k = 0$; (b) $\omega = 3{\cdot}16$, $k = 0$; (c) $\omega = 6{\cdot}39$, $k = 0$.

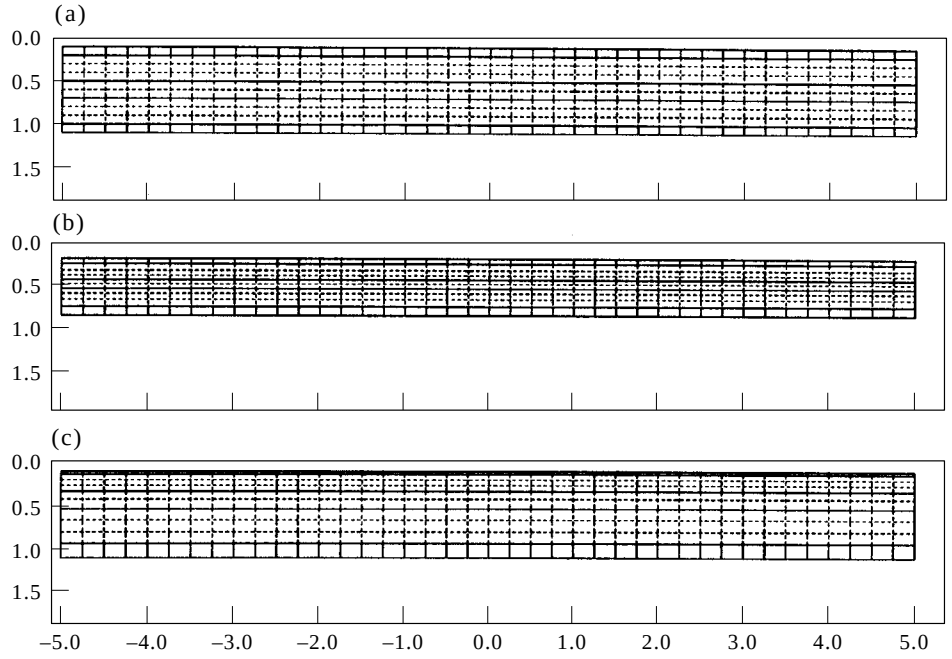

Figure 20. The first three "transverse–longitudinal" ("rod-like") modes for case 2: (a) $\omega = 0$, $k = 0$; (b) $\omega = 3{\cdot}28$, $k = 0$; (c) $\omega = 5{\cdot}75$, $k = 0$.

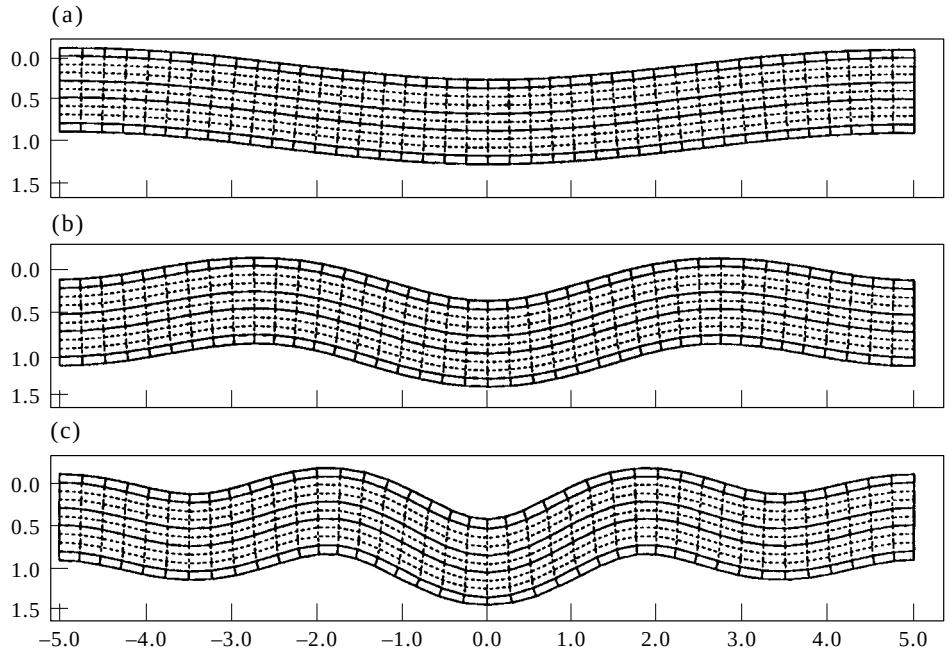

Figure 21. The first three "flexural" modes for case 1: (a) $\omega = 0{\cdot}204$, $k = 0{\cdot}766$; (b) $\omega = 0{\cdot}535$, $k = 1{\cdot}4$; (c) $\omega = 0{\cdot}894$, $k = 2{\cdot}03$.

where

$$\mathbf{S}^* \equiv \mathbf{V}^{(0)}\mathbf{S}^{(1)}(z_0) + \mathbf{V}^{(N)}\mathbf{S}^{(N)}(z_N)\mathbf{T}(z_1, z_{N-1}) \tag{17}$$

and

$$\mathbf{V}^{(0)} \equiv \begin{bmatrix} 0 & 0 & 1 & 0 \\ 0 & 0 & 0 & 1 \\ 0 & 0 & 0 & 0 \\ 0 & 0 & 0 & 0 \end{bmatrix}, \qquad \mathbf{V}^{(N)} \equiv \begin{bmatrix} 0 & 0 & 0 & 0 \\ 0 & 0 & 0 & 0 \\ 0 & 0 & 1 & 0 \\ 0 & 0 & 0 & 1 \end{bmatrix}. \tag{18}$$

For equation (16) to admit non-trivial solutions, the determinant of the matrix $\mathbf{S}^*$ must vanish, resulting in the dispersion relation

$$|\mathbf{S}^*| = f(\omega, k) = 0. \tag{19}$$

Thus, for every value of the radial wavenumber $k = k_n$ $(n = 1, \ldots, \infty)$ that satisfies equation (15), there exists an associated set of frequencies $\omega = \omega_{mn}$ $(m = 1, \ldots, \infty)$ that satisfies the dispersion relation (19). These frequency–wavenumber pairs may be found numerically for any given structure, using numerical root solving techniques. Each resulting frequency–wavenumber pair may then be substituted into equation (16) to determine the associated modal amplitude array $\mathbf{a}^{(1)} = \mathbf{a}^{(1)}_{mn}$. The remaining modal amplitude arrays associated with the particular frequency–wavenumber pair may then be found using equations (12)–(14). Thus, each of the mutually orthogonal modes $\hat{\mathbf{d}}^{(j)}_{mn}(r, z)$ $(m, n = 1, 2, \ldots, \infty)$ is completely determined by a frequency–wavenumber pair that satisfies equation (19).

2.3. TIME DEPENDENT RESPONSE

The time dependent response is expressed in array form as

$$\mathbf{d}^{(j)}(r, z, t) \equiv \begin{Bmatrix} u^{(j)}(r, z, t) \\ w^{(j)}(r, z, t) \\ \sigma_{zr}^{(j)}(r, z, t) \\ \sigma_{zz}^{(j)}(r, z, t) \end{Bmatrix}, \qquad (z_{j-1} \leqslant z \leqslant z_j ; j = 1, 2, \ldots, N), \tag{20}$$

where $\mathbf{d}^{(j)}(r, z, t)$ is the "response array", and $u^{(j)}(r, z, t)$, $w^{(j)}(r, z, t)$, $\sigma_{zr}^{(j)}(r, z, t)$, and $\sigma_{zz}^{(j)}(r, z, t)$ are the actual (time dependent) displacement and stress components whose physical interpretations are in direct correspondence with the analogous modal components defined earlier.

2.3.1. *Free vibration response*

The time-dependent response for the unforced case is obtained by multiplying each of the modes by its corresponding harmonic time signature and summing. Hence, the free vibration response is given by

$$\mathbf{d}^{(j)}(r, z, t) = \sum_{n=1}^{\infty} \sum_{m=1}^{\infty} A_{mn}\, \hat{\mathbf{d}}_{mn}^{(j)}(r, z)\, \mathrm{e}^{-i\omega_{mn} t}, \qquad (z_{j-1} \leqslant z \leqslant z_j ; j = 1, 2, \ldots, N), \tag{21}$$

where A_{mn} is the modal amplitude and $i \equiv \sqrt{-1}$.

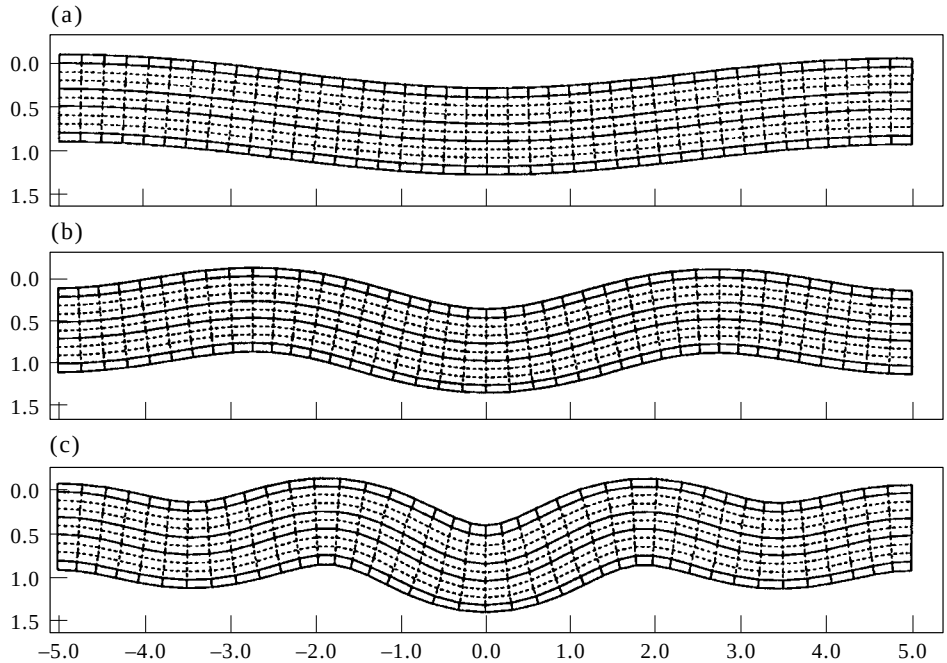

Figure 22. The first three "flexural" modes for case 2: (a) $\omega = 0{\cdot}113$, $k = 0{\cdot}766$; (b) $\omega = 0{\cdot}334$, $k = 1{\cdot}4$; (c) $\omega = 0{\cdot}608$, $k = 2{\cdot}08$.

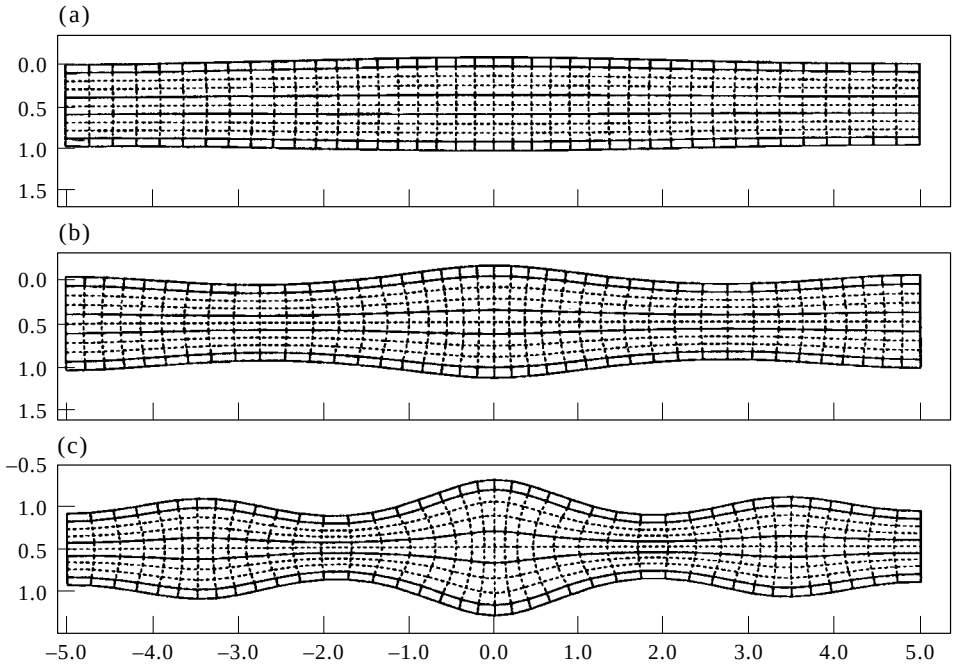

Figure 23. The first three radial–longitudinal modes for case 1: (a) $\omega = 0{\cdot}859$, $k = 0{\cdot}766$; (b) $\omega = 1{\cdot}49$, $k = 1{\cdot}4$; (c) $\omega = 1{\cdot}95$, $k = 2{\cdot}03$.

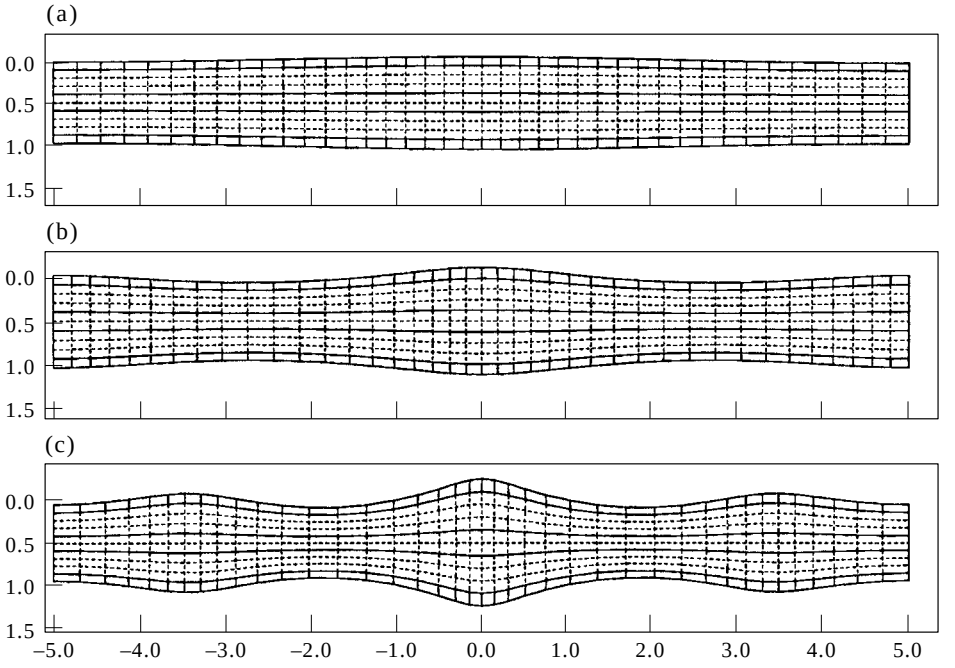

Figure 24. The first three radial–longitudinal modes for case 2: (a) $\omega = 0{\cdot}636$, $k = 0{\cdot}766$; (b) $\omega = 1{\cdot}15$, $k = 1{\cdot}4$; (c) $\omega = 1{\cdot}64$, $k = 2{\cdot}03$.

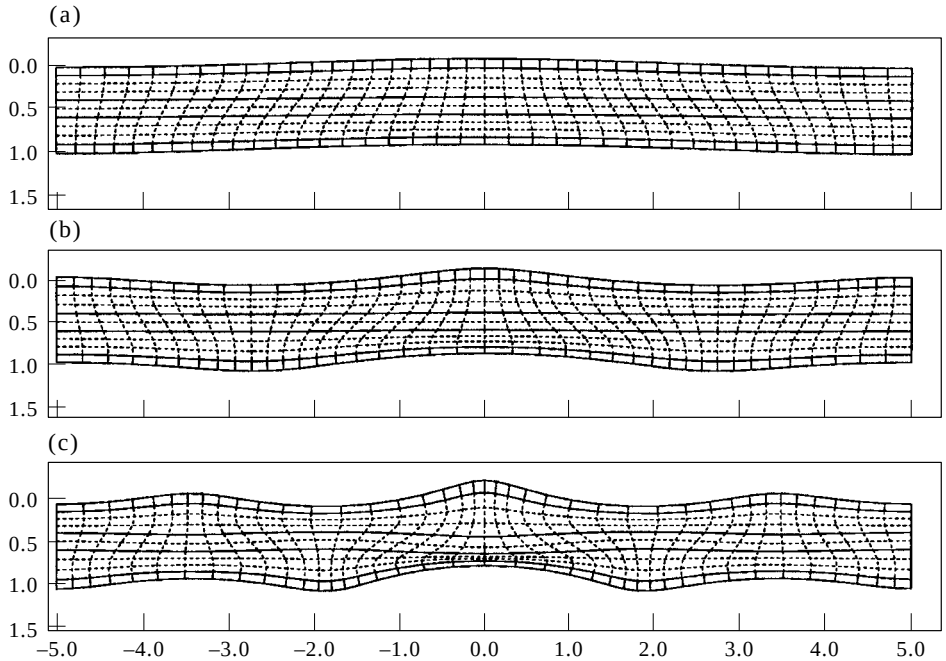

Figure 25. The first three antisymmetric thickness–shear modes for case 1: (a) $\omega = 1{\cdot}98$, $k = 0{\cdot}766$; (b) $\omega = 2{\cdot}47$, $k = 1{\cdot}4$; (c) $\omega = 3{\cdot}0$, $k = 2{\cdot}03$.

2.3.2. *Transient response*

The response to transient loading is found by expressing the displacement field $\mathbf{u}^{(j)}(r, z, t)$ as an expansion in terms of the mutually orthogonal modal displacement vector, $\hat{\mathbf{u}}_{mn}^{(j)}(r, z)$, with time dependent amplitudes $q_{mn}(t)$. The corresponding transient response $\mathbf{d}^{(j)}(r, z, t)$ to the time dependent body force field $\mathbf{F}(r, z, t)$ is then found as an expansion in terms of the modal arrays $\hat{\mathbf{d}}_{mn}^{(j)}(r, z)$ with the time dependent amplitudes $q_{mn}(t)$ as

$$\mathbf{d}^{(j)}(r, z, t) = \sum_{n=1}^{\infty} \sum_{m=1}^{\infty} \hat{\mathbf{d}}_{mn}^{(j)}(r, z) q_{mn}(t), \qquad (z_{j-1} \leqslant z \leqslant z_j \,; j = 1, 2, \ldots, N), \tag{22}$$

where

$$q_{mn}(t) = \frac{1}{\omega_{mn}} \int_0^t F_{mn}(\tau) \sin(\omega_{mn}(t - \tau)) \, \mathrm{d}\tau, \tag{23}$$

$$F_{mn}(t) = 2\pi \sum_{j=1}^{N} \int_{z_{j-1}}^{z_j} \int_0^R \hat{\mathbf{u}}_{mn}^{(j)}(r, z) \cdot \mathbf{F}(r, t) r \, \mathrm{d}r \, \mathrm{d}z. \tag{24}$$

The solution outlined in this section, for the axisymmetric response of a finite multilayered elastic solid, provides the basis for our analysis. The particular loading to be considered is described next.

3. REPRESENTATION OF IMPACT LOADING

The body force vector in equation (1) is used to simulate contact forces due to impact loading of the multilayered plates considered. It has been shown, by Prasad *et al*. [12], that the spatial variation of contact forces on the surface of a plate due to impact of a spherical impactor may be approximated using a cosine distribution which has a maximum at the point of impact and then tapers to zero at a distance equal to the contact radius of the impactor. The time variation of contact forces due to impact on a plate was investigated by Sun and Chattopadhyay [8]. Inspection of their results shows that a typical contact force due to impact will grow from zero at the instant of impact to reach a maximum at about half of the "impact duration" and then taper to zero at the end of the "impact duration".

For the present study, a body force is constructed to approximate contact forces due to impact of spherical objects on a plate. The form of the body force $\mathbf{F}(r, z, t) = (F_r, F_z)$ for this case is taken as

$$F_r(r, z, t) = 0, \tag{25a}$$

$$F_z(r, z, t) = \begin{cases} DJ_0(k_0 r)\delta(z - z_0)\sin(\omega_0 t), & \text{if} \quad 0 \leqslant r \leqslant 2{\cdot}405/k_0 \text{ and } 0 \leqslant t \leqslant \pi/\omega_0, \\ 0, & \text{if} \quad r > 2{\cdot}405/k_0 \quad \text{or} \quad t > \pi/\omega_0, \end{cases} \tag{25b}$$

where D is the intensity of the force and $\delta(z)$ is the Dirac delta function. The "impact duration", t_0, and "impact radius", r_0, are characterized by the relations

$$t_0 \equiv \pi/\omega_0 \quad \text{and} \quad r_0 \equiv 2{\cdot}405/k_0, \tag{26a, b}$$

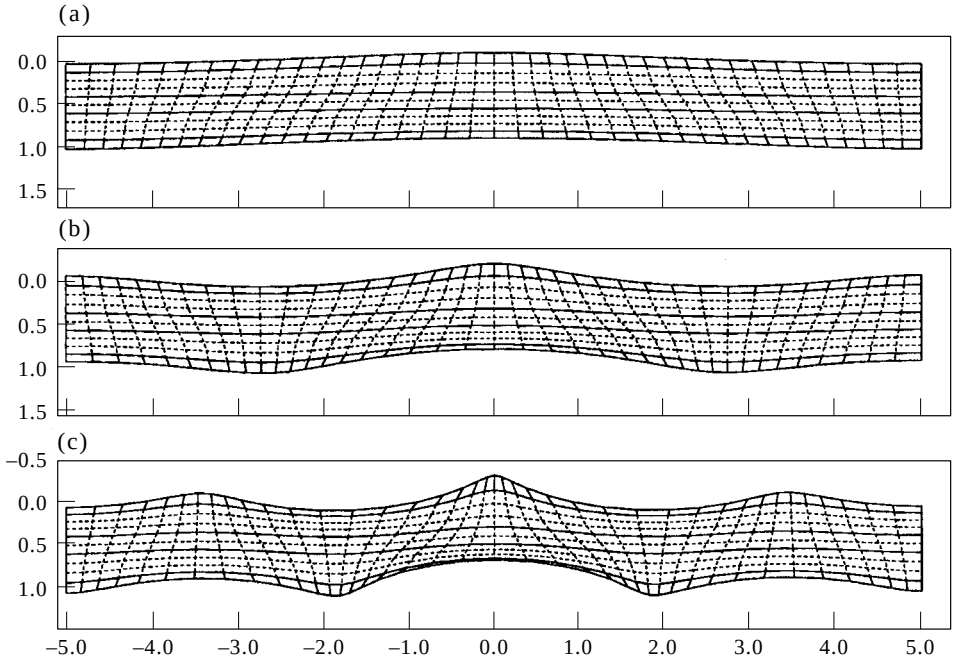

Figure 26. The first three antisymmetric thickness–shear modes for case 2: (a) $\omega = 1{\cdot}76$, $k = 0{\cdot}766$; (b) $\omega = 1{\cdot}99$, $k = 1{\cdot}4$; (c) $\omega = 2{\cdot}28$, $k = 2{\cdot}03$.

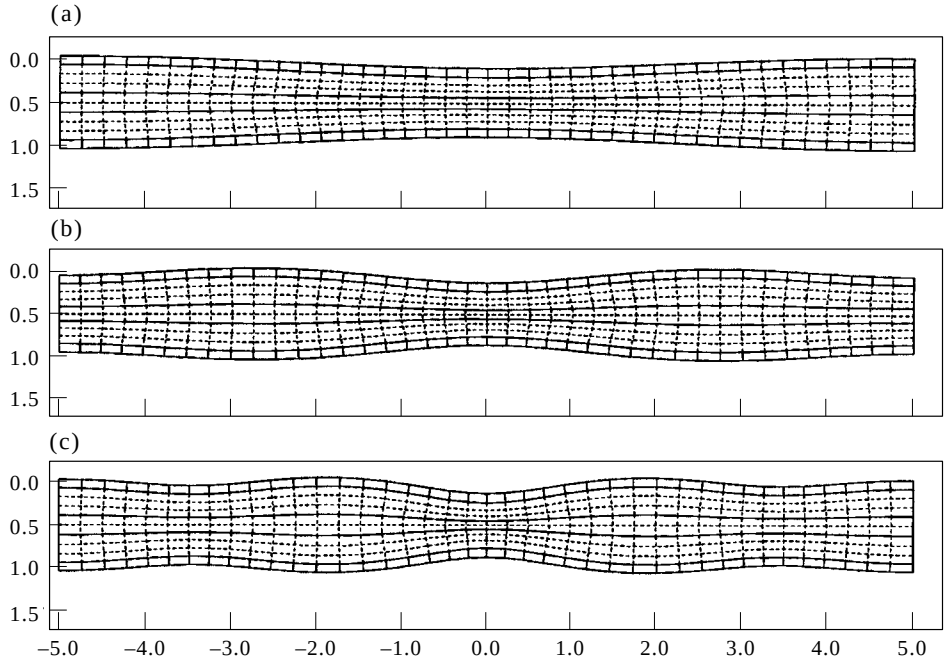

Figure 27. The first three (radially varying) symmetric thickness–stretch modes for case 1: (a) $\omega = 3{\cdot}06$, $k = 0{\cdot}766$; (b) $\omega = 3{\cdot}08$, $k = 1{\cdot}4$; (c) $\omega = 3{\cdot}32$, $k = 2{\cdot}03$.

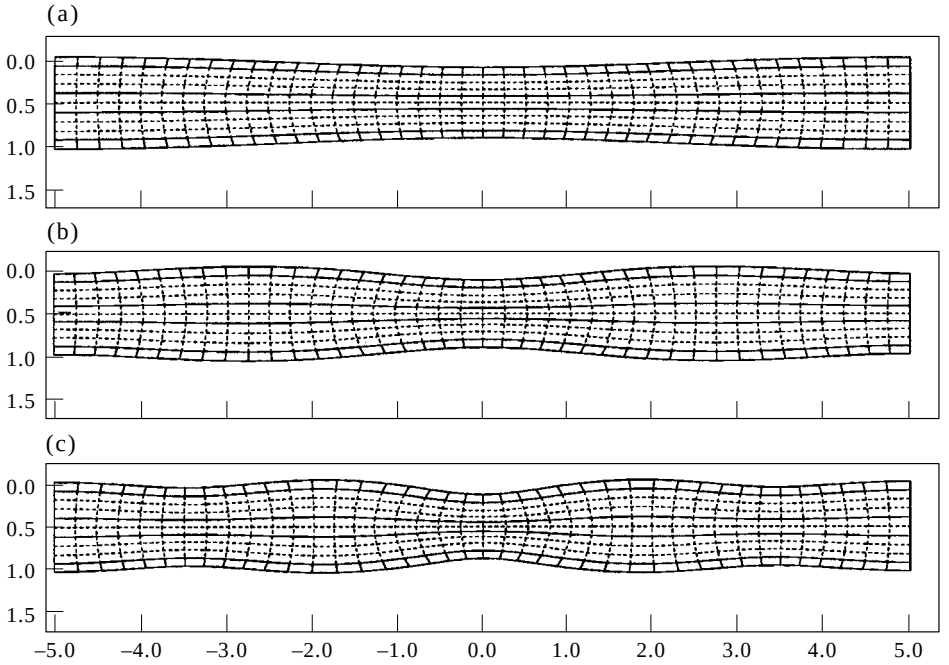

Figure 28. The first three (radially varying) symmetric thickness–stretch modes for case 2: (a) $\omega = 2{\cdot}88$, $k = 0{\cdot}766$; (b) $\omega = 2{\cdot}76$, $k = 1{\cdot}4$; (c) $\omega = 2{\cdot}7$, $k = 2{\cdot}03$.

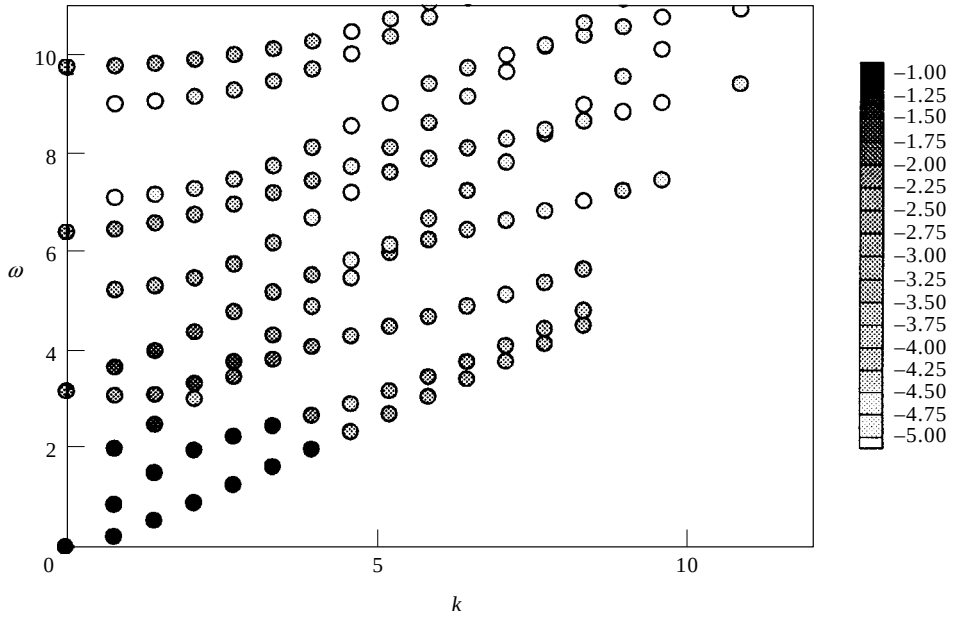

Figure 29. Modal participation spectrum of sandwich plate impacted by "long duration load": case 1 (stiff face sheets). Degree of shading indicates relative contribution of mode according to $\log_{10}$ scale of amplitude shown at right.

where ω_0 shall be referred to as the "impact frequency", and k_0 shall be referred to as the "impact wavenumber". The impact loading is thus imposed as a body force applied to a cylindrical volume of radius r_0 that is infinitesimally thin and infinitesimally close to the

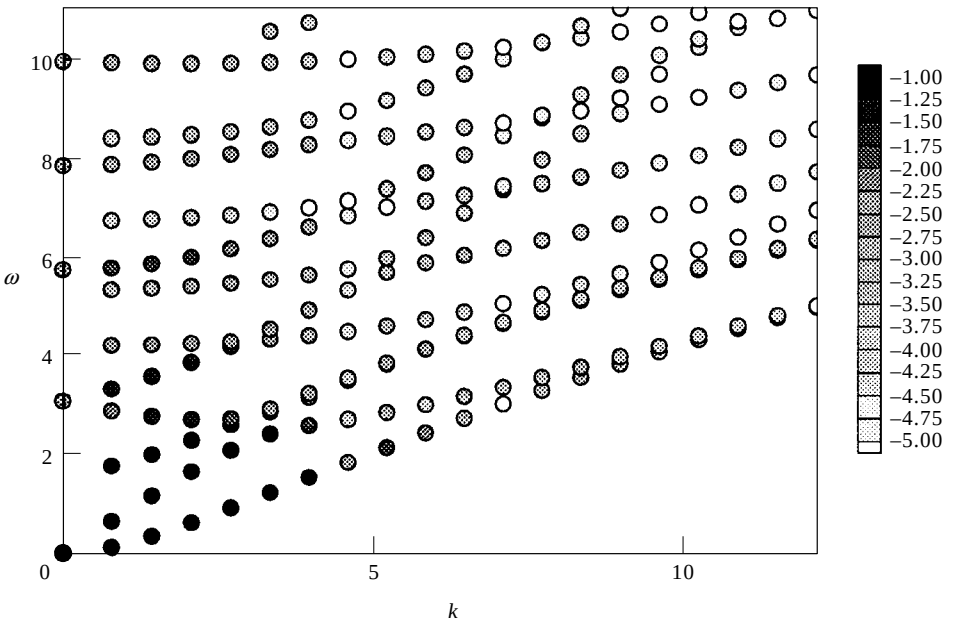

Figure 30. Modal participation spectrum of sandwich plate impacted by "long duration load": case 2 (compliant face sheets). Degree of shading indicates relative contribution of mode according to $\log_{10}$ scale of amplitude shown at right.

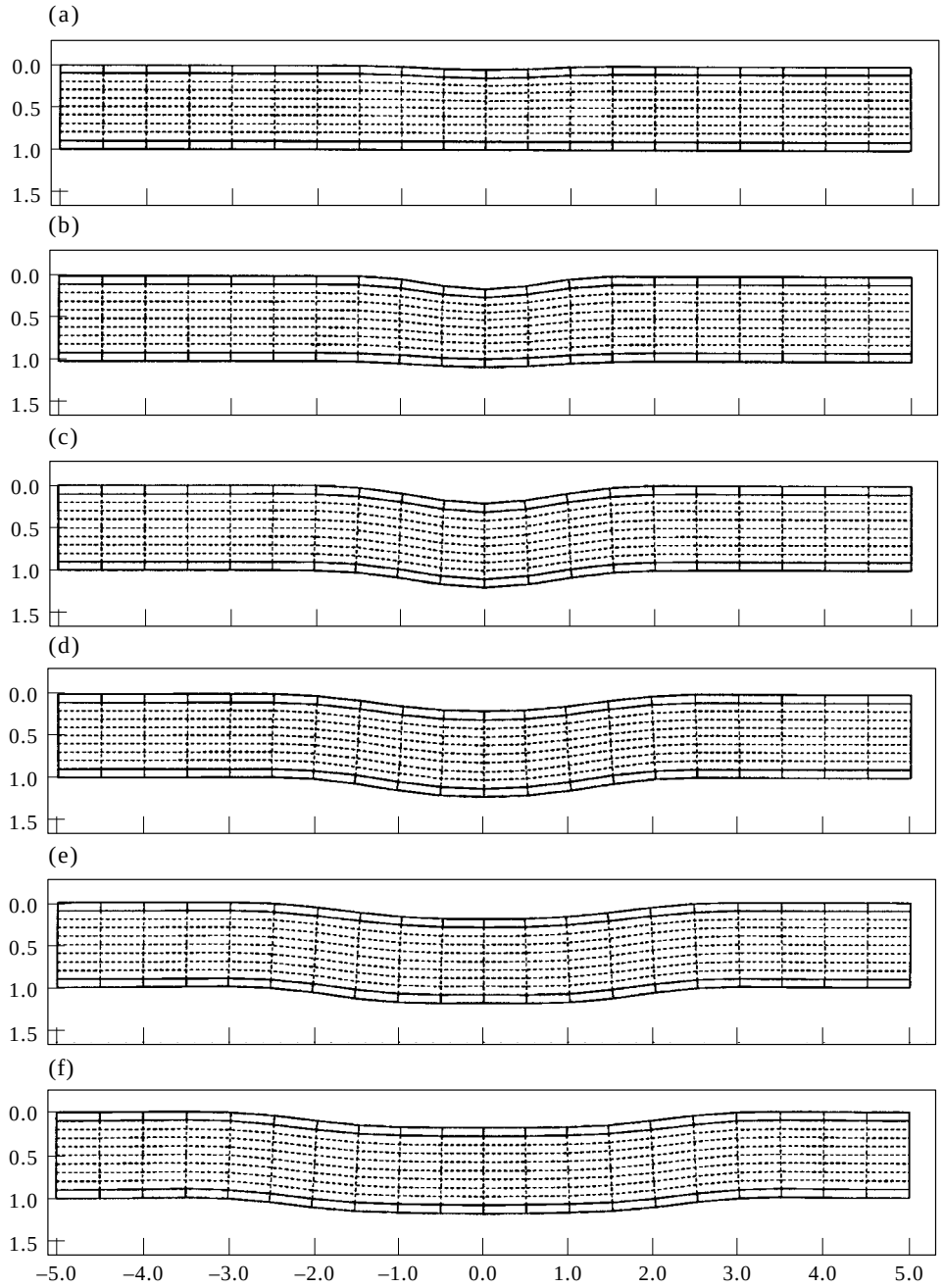

Figure 31. Transient response of case 1 subjected to "long duration load". "Freeze frames" of deforming plate at sequential instants in (normalized) time: (a) $t = 1$, (b) 2, (c) 3, (d) 4, (e) 5, (f) 6.

surface $z = z_0$. The radial variation of this body force per unit intensity is shown in Figure 2(a) and the corresponding time variation is shown in Figure 2(b).

The response of multilayered structures loaded by the forcing function (25a, b) will be considered for various values of impact radius and impact duration. The forcing function is standardized by choosing the value of D such that the forcing function imparts a unit impulse to the structure for each case.

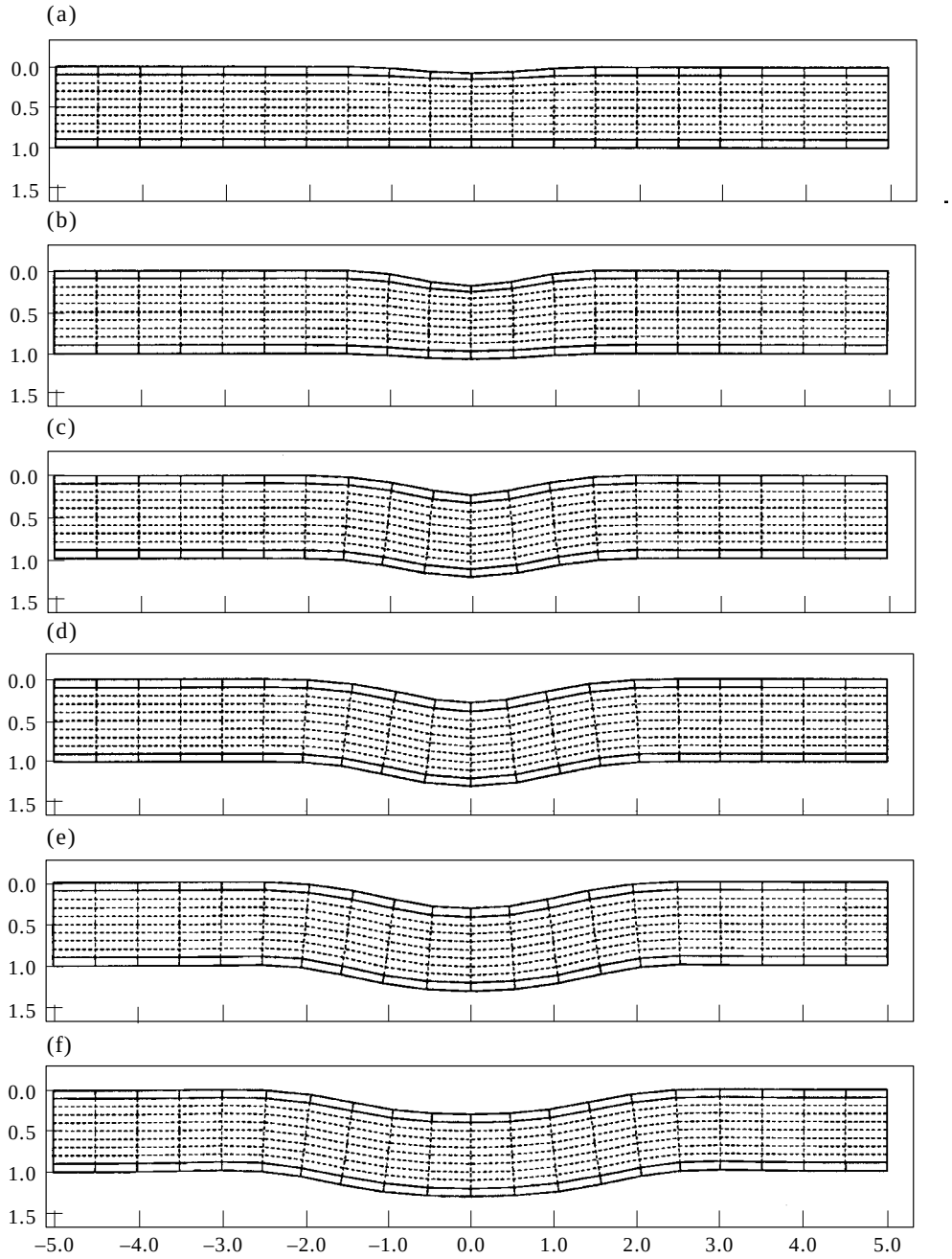

Figure 32. Transient response of case 2 subjected to "long duration load". "Freeze frames" of deforming plate at sequential instants in (normalized) time: (a) $t = 1$, (b) 2, (c) 3, (d) 4, (e) 5, (f) 6.

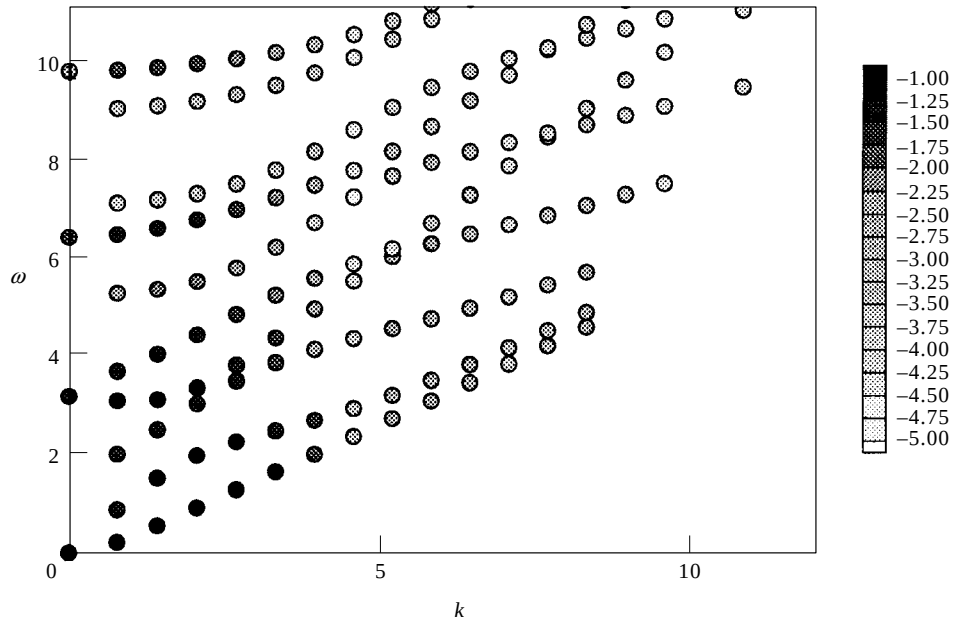

Figure 33. Modal participation spectrum of sandwich plate impacted by "short duration load": case 1 (stiff face sheets). Degree of shading indicates relative contribution of mode according to $\log_{10}$ scale of amplitude shown at right.

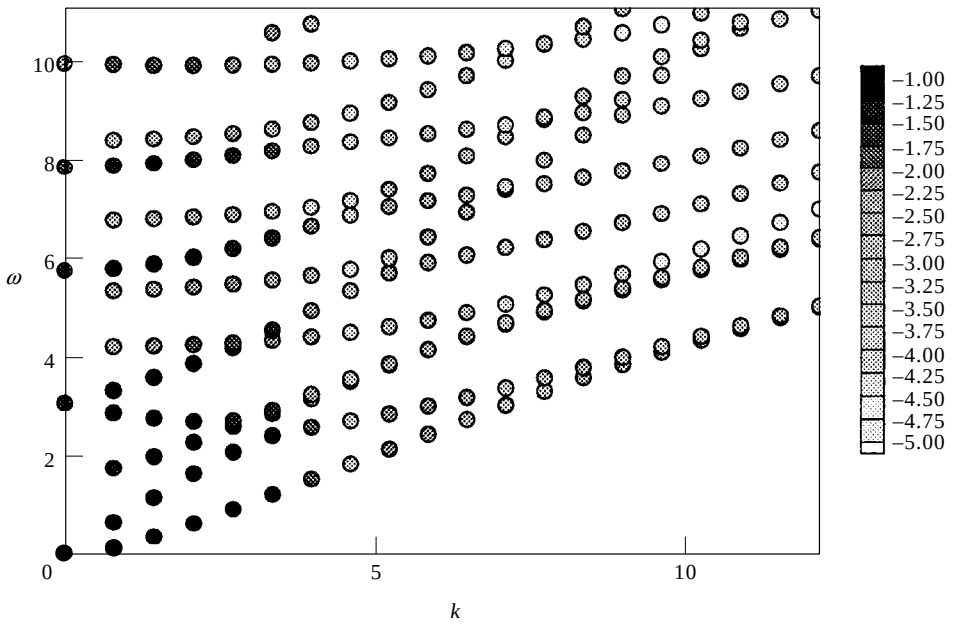

Figure 34. Modal participation spectrum of sandwich plate impacted by "short duration load": case 2 (compliant face sheets). Degree of shading indicates relative contribution of mode according to $\log_{10}$ scale of amplitude shown at right.

4. IMPLEMENTATION

In this work, the response of several structures is considered. These include single layer plates, sandwich structures, and bilaminates with a finite adhesive layer. Results will be in the form of frequency spectra, elastodynamic modes, and time dependent response of the entire structure under transient load. These results are achieved as discussed below.

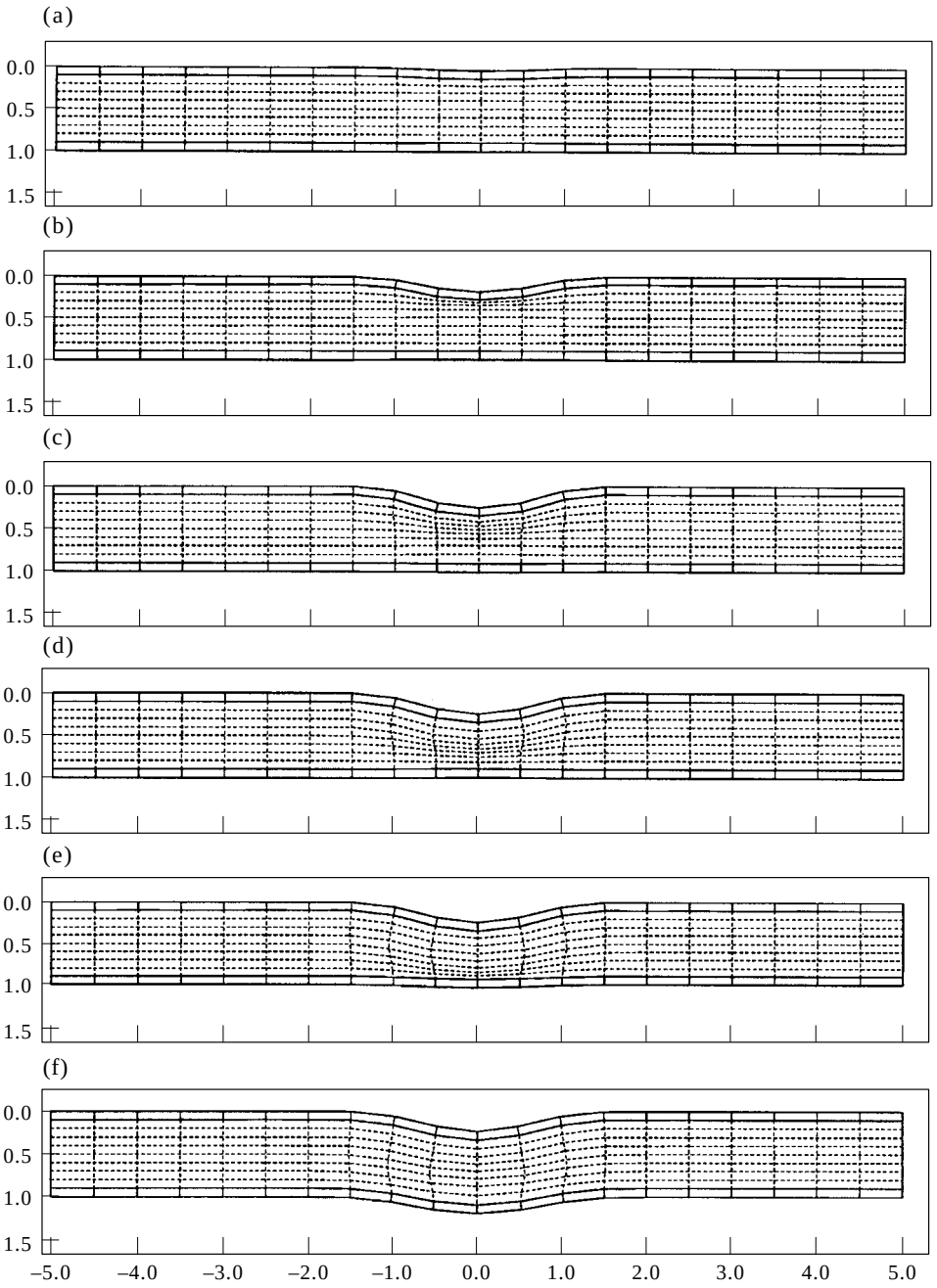

Fig. 35a-f

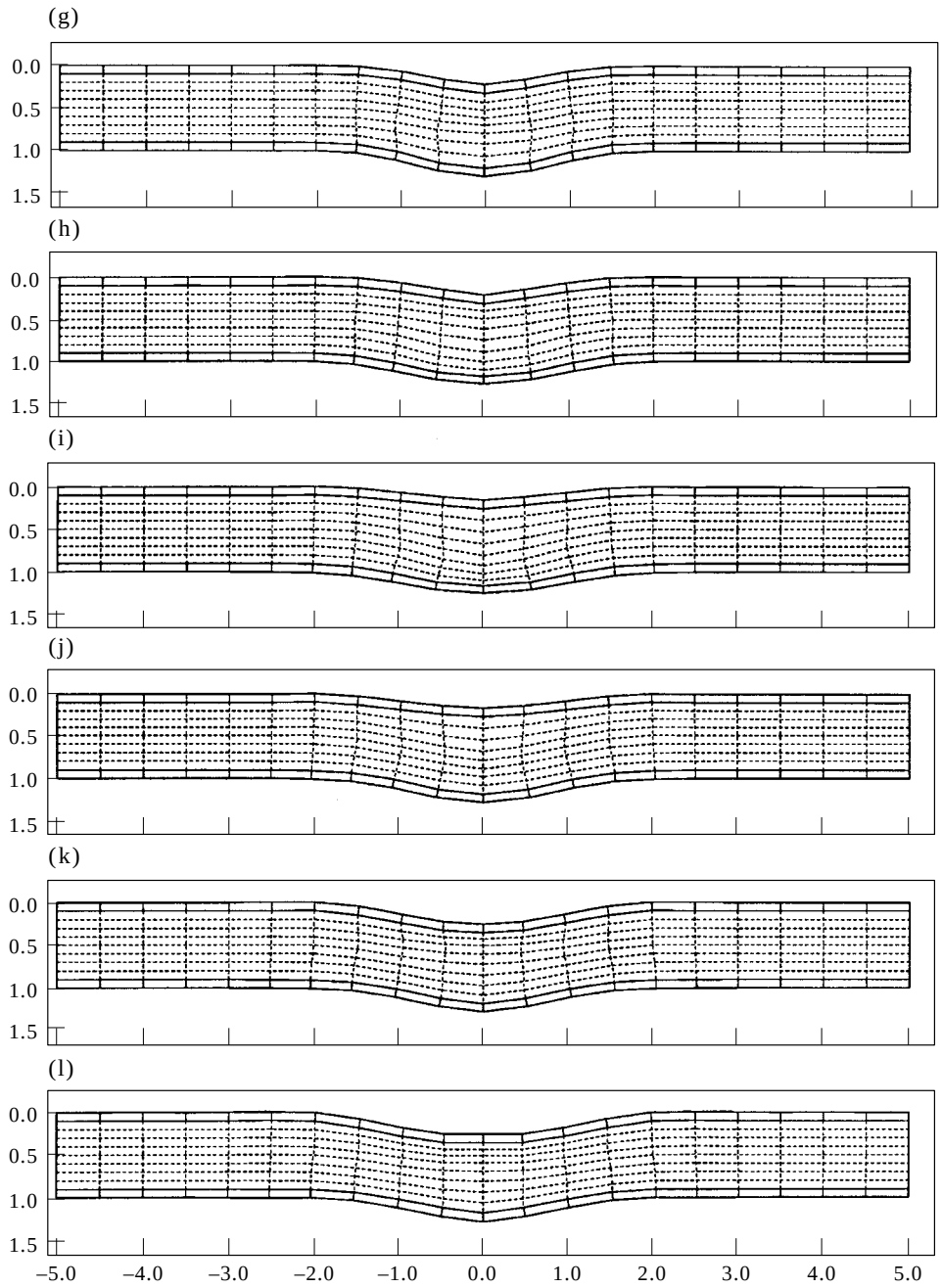

Fig. 35g-l.

Figure 35. Transient response of case 1 subjected to "short duration load". "Freeze frames" of deforming plate at sequential instants in (normalized) time: (a) $t = 0{\cdot}2$, (b) 0·4, (c) 0·6, (d) 0·8, (e) 1·0, (f) 1·2, (g) 1·4, (h) 1·6, (i) 1·8, (j) 2·0, (k) 2·2, (l) 2·4.

4.1. NORMALIZATION OF PARAMETERS

In the simulations presented in the sections that follow, the parameters of the system are normalized as follows; all length scales are normalized with respect to the total dimensional thickness $\bar{H}$ of the multilayer plate, mass density is normalized with respect

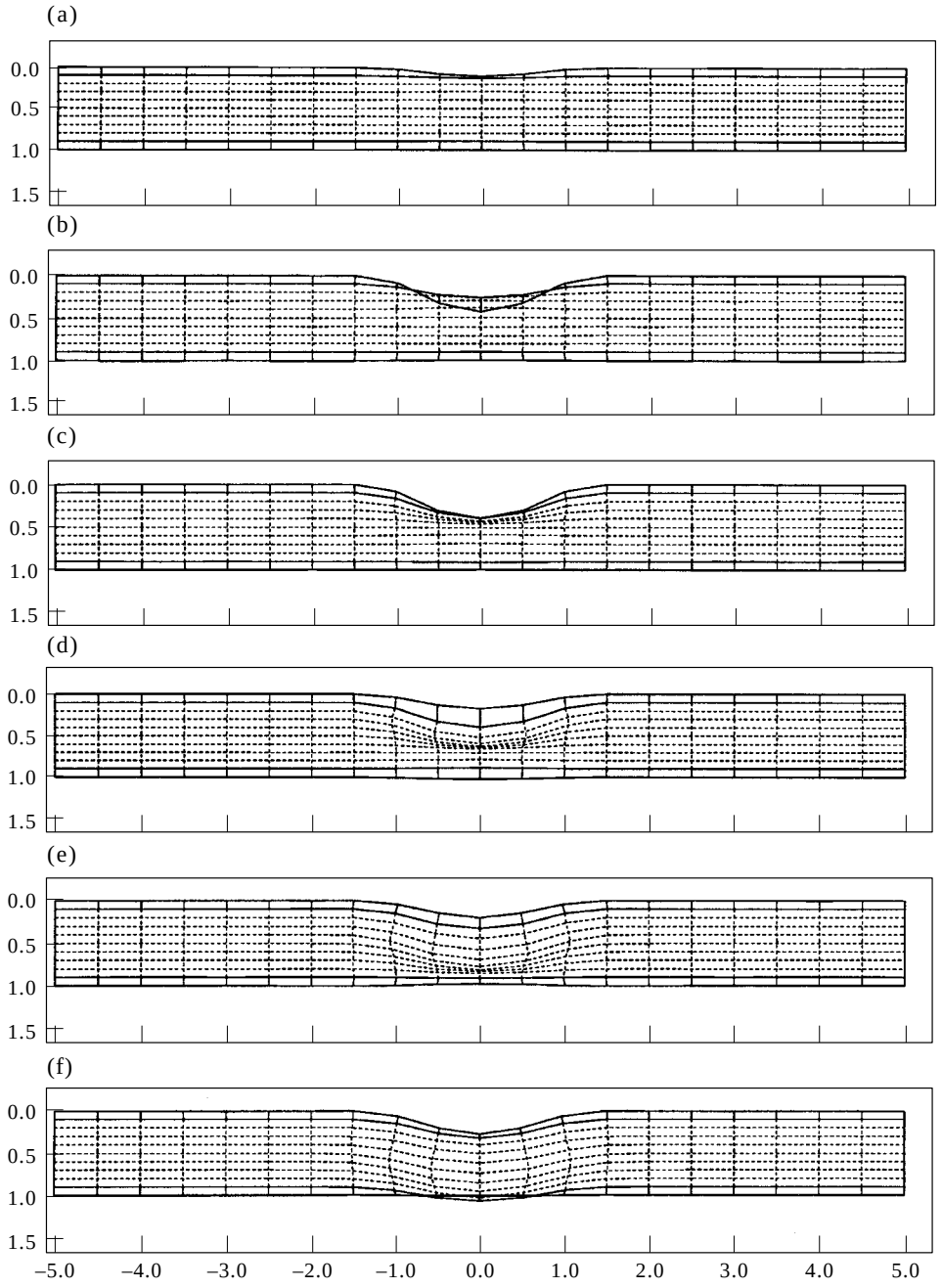

Fig. 36a-f.

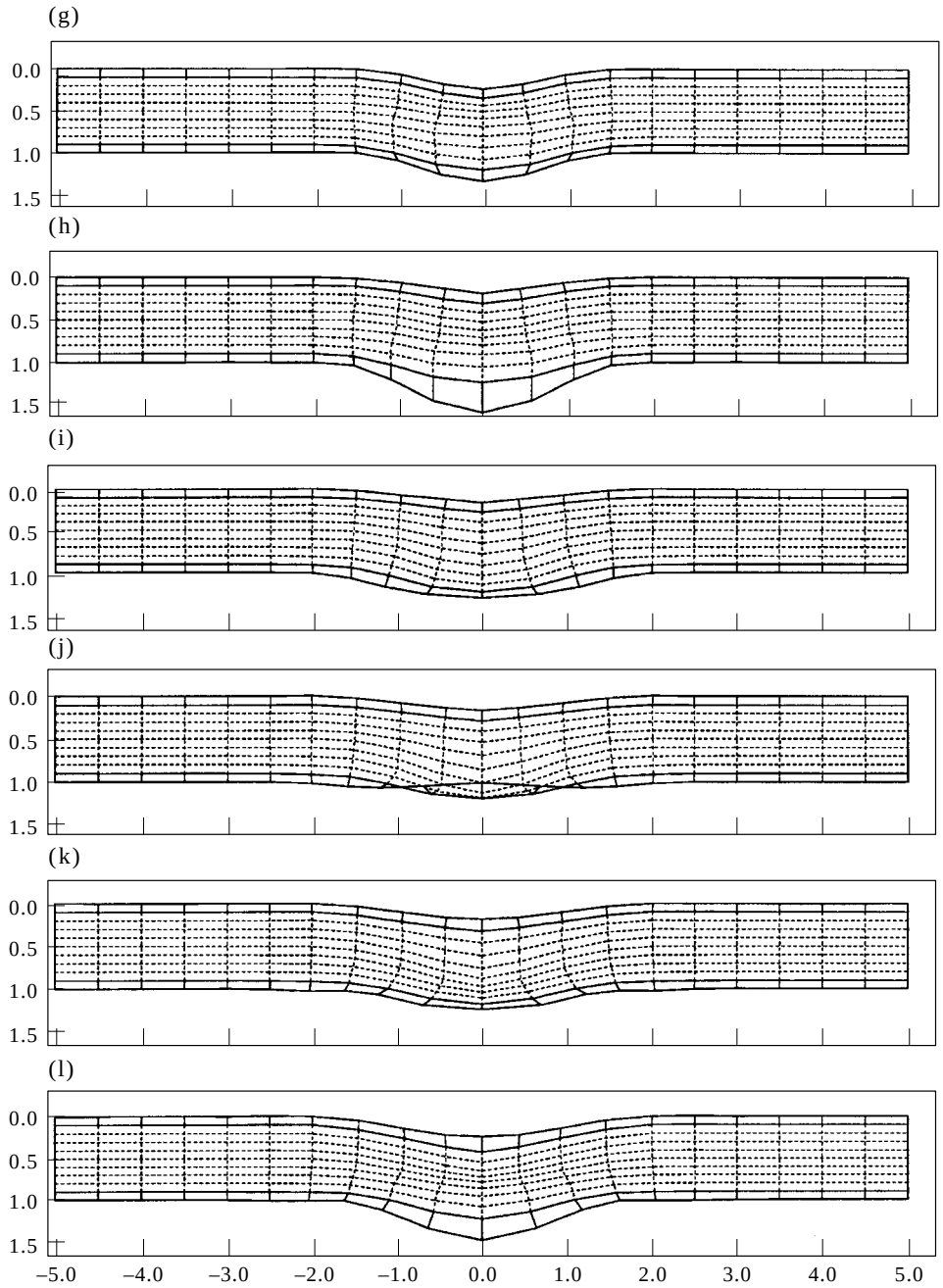

Fig. 36g-l.

Figure 36. Transient response of case 2 subjected to "short duration load". "Freeze frames" of deforming plate at sequential instants in (normalized) time: (a) $t = 0{\cdot}2$, (b) 0·4, (c) 0·6, (d) 0·8, (e) 1·0, (f) 1·2, (g) 1·4, (h) 1·6, (i) 1·8, (j) 2·0, (k) 2·2, (l) 2·4.

to the dimensional mass density $\bar{\rho}_*$ of an identified reference layer, and time rates with respect to the primary wave speed $\bar{c}_*$ of the reference layer. Thus, letting superposed bars denote dimensional quantities in general, and superposed bars with asterisk subscripts denote dimensional quantities of the reference layer in particular, then the normalized (unbarred) parameters are related to their dimensional counterparts as delineated below. (Superscripts identifying the layer numbers are implied, where appropriate, but have been omitted below for clarity.)

Lengths: plate dimensions $H = 1$, $R = \bar{R}/\bar{H}$; co-ordinates, $r = \bar{r}/\bar{H}$, $z = \bar{z}/\bar{H}$; displacements $u = \bar{u}/\bar{H}$, $w = \bar{w}/\bar{H}$; wavenumbers, $k = \bar{k}\bar{H}$, $\alpha = \bar{\alpha}\bar{H}$, $\beta = \bar{\beta}\bar{H}$. Rates: time, $t = \bar{t}\bar{c}_* / \bar{H}$; frequency, $\omega = \bar{\omega}\bar{H}/\bar{c}_*$; wave speeds, $c_p = \bar{c}_p / \bar{c}_*$, $c_s = \bar{c}_s / \bar{c}_*$.

It is seen that $t = 1$ corresponds to the time it takes for a transversely propagating primary wave to travel the total thickness of an equivalent plate comprised of the material of the reference layer. Material properties: it follows that the dimensionless mass density and Lamé constants are related to their dimensional counterparts as mass density, $\rho = \bar{\rho}/\bar{\rho}_*$; Lamé constants, $\lambda = \bar{\lambda}/\bar{\rho}_* \bar{c}_*^2$, $\mu = \bar{\mu}/\bar{\rho}_* \bar{c}_*^2$.

Specific results corresponding to impact of a single layer plate are presented in section 5. These results will form the basis for interpretation and comparison of results pertaining to specific multilayered plates presented in sections 6 and 7. A description of the specific structures to be considered and an outline of the analysis to be performed is discussed below.

4.2. ANALYSIS

The analytical model and techniques presented earlier will be used to investigate the elastodynamic behavior of a single layer plate as a benchmark, and two specific types of multilayer structures. The latter two types correspond to sandwich plates consisting of a core material sandwiched between two face sheets, and to bilaminates possessing a central "adhesive" layer. The overall dimensions and geometries of the three types of structures to be considered correspond directly, as shown in Figure 3. In each multilayer case, the material properties of the face sheets or adhesive layer are varied above and below those of the base material so as to provide a basis for comparison, with the base material corresponding to that of the single layer plate. In both multilayer cases the base material comprises 80% of the structure. For each of the three-layer plates under consideration the layers are numbered sequentially from 1 to 3, as per the notation and normalization introduced earlier, with the impacted surface being layer number one and thus the central or core layer labeled layer number 2. For the sandwich plate, the core layer is comprised of the reference material, while for the bilaminate with central adhesive layer, the two outer layers are comprised of the reference material. Frequency spectra and physical depictions of the elastodynamic modes, as well as the response to impact loads, are presented for each case so as to provide a consistent basis for comparison. All computations are implemented in parallel, as the problems of interest are particularly suited for parallel programming because of the independent nature of the modes as presented in section 2. For responses associated with time-dependent loads, the calculations are executed in parallel by distributing the total number of precalculated modes among the available processors. Each processor then calculates the response due to its subset of modes. The responses of the subsets are subsequently added to give the total response of the forced system. First, the response of the single layer plate is considered.

5. RESPONSE OF A SINGLE LAYER PLATE

A special case of the class of multilayered structures considered for this work is that of a single layer plate. An understanding of the dynamics of a single layer plate will be

necessary in order to discuss the response of the multilayered structures presented in sections 6 and 7 of this study. Thus, the present section will be concerned with a single layer cylindrical plate. In particular, we shall consider a structure with a radius that is five times its thickness ($R = 5$) comprised of linearly elastic material possessing a Poisson's ratio of $v = 0{\cdot}3$ (hence $\rho = c_p = 1$ and $c_s = 0{\cdot}5345$, where the superscripts have been dropped since there is only one layer). This plate will be referred to as the isotropic plate. (It will be seen that the radius to thickness ratio of 5 is large enough to qualify as a "thick plate", i.e., to show local behavior without boundary interaction, and yet small enough to limit the number of modes necessary for computation to a workable number.) First, the frequency spectrum for the structure in question is presented.

5.1. FREQUENCY SPECTRA AND ELASTODYNAMIC MODES

The frequency spectrum for the isotropic plate is shown in Figure 4. In that figure, the circles represent natural frequency–radial wavenumber pairs of the isotropic plate found as roots of equations (15) and (19), each of which corresponds to a natural elastodynamic mode of the plate. As may be expected, the frequency–wavenumber pairs fall on the branches of the classical Rayleigh–Lamb frequency spectrum for circular crested waves in a plate† (see for example reference [29] or [30]). Each branch in the Rayleigh–Lamb spectrum corresponds to a mode of radial wave propagation in an infinite plate. These branches have been well studied [21, 31, 32]. The lowest branch corresponds to radially propagating flexural waves which are often approximated using thin plate theory. The second lowest branch corresponds to radially propagating dilatational waves which are analogous to longitudinal waves in a thin rod. The higher branches correspond to radially propagating "thickness shear" and "thickness stretch" waves. Each mode for the finite plate is thus seen to correspond to a standing wave comprised of propagating wave trains traveling in opposite directions. We will therefore categorize the natural modes into groups corresponding to the branches of the Rayleigh–Lamb spectrum.

The modes corresponding to the frequency–wavenumber pairs along the $k = 0$ axis in Figure 4 are "thickness-stretch" modes with no radial variation, and are comprised purely of transversely propagating dilatational waves. These modes, for which the shapes of the first three are plotted in Figure 5, correspond directly to the longitudinal modes of a thin rod and will be referred to as "transverse–longitudinal" ("rod-like") modes. The uppermost shape in Figure 5 is that of the rigid body mode which has a vanishing frequency as well as a vanishing wavenumber. It is noted that there are no "thickness-shear" modes that are radially invariant, as such a mode would violate the boundary conditions at $r = R$. Figure 6 shows the shapes of the first three "flexural" modes which correspond to the lowest branch of the Rayleigh–Lamb spectrum. An important observation of the "flexural" branch of the Rayleigh–Lamb spectrum is that the slope of that branch, which gives the radial group propagation velocity, is asymptotic to the Rayleigh surface wave speed. This suggests that for motion with high radial wavenumber, or small radial wavelength, the transverse dimension of the plate is comparatively large compared to the associated wavelength such that each surface of the plate acts as if it bounds an effective half-space and thus supports surface wave motion. The shapes of the first three "radial–longitudinal" modes corresponding to the second branch of the

† The Rayleigh–Lamb frequency spectrum for circular crested waves in a plate has exactly the same form as that for straight crested waves [29].

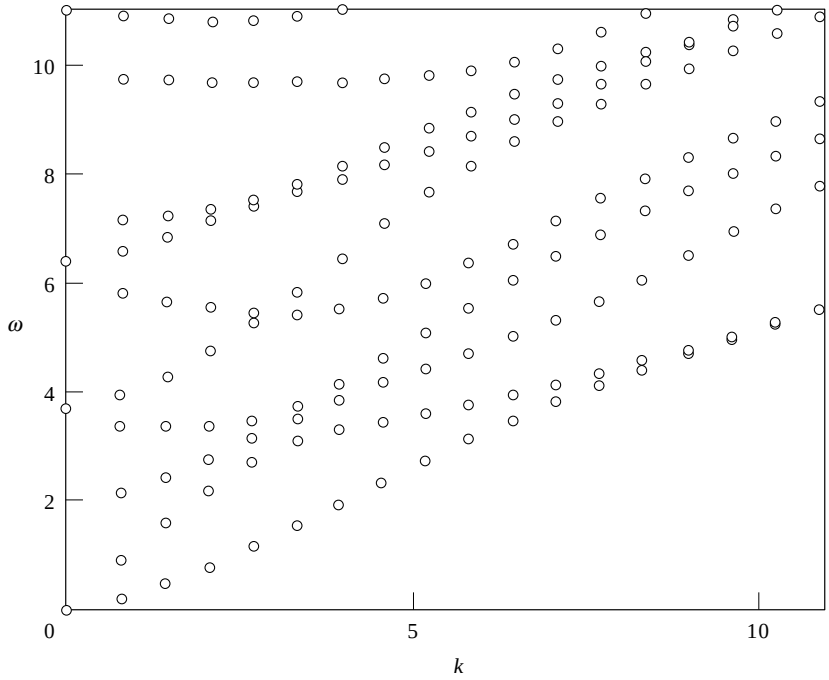

Figure 37. Frequency spectrum for bilaminate with central "adhesive" layer: case 3 (stiff central layer).

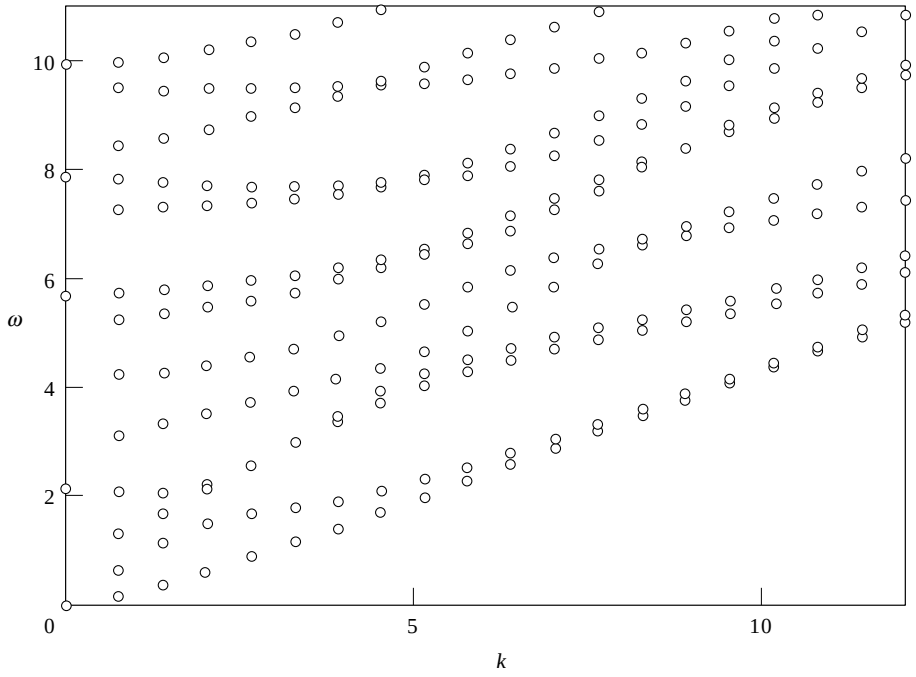

Figure 38. Frequency spectrum for bilaminate with central "adhesive" layer: case 4 (compliant central layer).

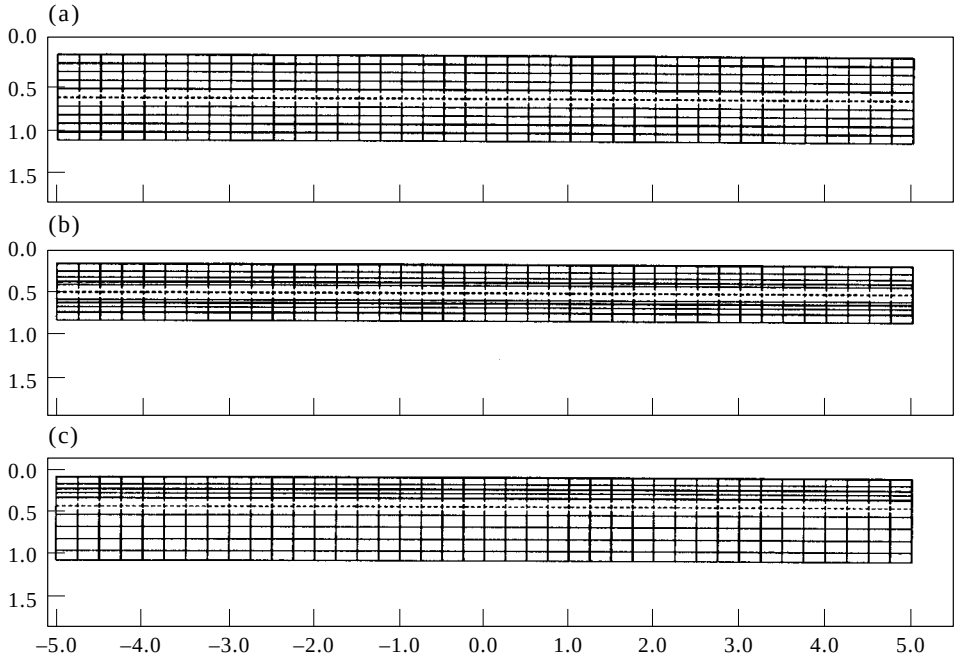

Figure 39. The first three "transverse–longitudinal" ("rod-like") modes for case 3: (a) $\omega = 0$, $k = 0$; (b) $\omega = 3{\cdot}69$, $k = 0$; (c) $\omega = 6{\cdot}39$, $k = 0$.

Rayleigh–Lamb spectrum are plotted in Figure 7. These modes are analogous in the radial direction to the longitudinal modes of a thin rod. The second branch of the Rayleigh–Lamb spectrum is also asymptotic to the Rayleigh surface wave speed. Consideration of Figure 8 shows the shapes of the first three modes corresponding to the third branch of the Rayleigh–Lamb spectrum. The modes of this branch are characterized by a twisting or shearing through the thickness of the plate and are thus referred to as "thickness–shear" modes. Thickness–shear modes may be antisymmetric (Figure 8) or symmetric (Figure 9). Modes corresponding to the fourth branch are depicted in Figure 10. These modes are characterized by regions of stretch and compression through the thickness and are thus referred to as (symmetric) "thickness–stretch" modes. Like modes may also be antisymmetric (Figure 11). All of the remaining branches correspond to higher order thickness–stretch and thickness–shear modes.

5.2. TRANSIENT RESPONSE

Next, the response of the isotropic plate due to two separate impact loads is considered. The first load, which will be denoted as the "long duration" load, has an impact duration $t_0 = 3{\cdot}14$ that is comparatively longer than the time it would take for a plane dilatational wave to travel through the thickness of the plate. The second load, which will be denoted as the "short duration" load, has an impact duration $t_0 = 0{\cdot}449$ which is comparatively shorter than the time it would take for a plane dilatational wave to travel through the thickness of the plate. Both loads considered have an impact radius $r_0 = 1{\cdot}2$, that is on the order of the thickness of the plate.

The contribution of each mode to the response of the plate due to the long duration impact load is shown in Figure 12. In that figure, circles representing the modes of the previously presented frequency spectrum are shaded according to the base 10 logarithm

of their corresponding modal amplitudes. Thus dark circles correspond to modes that contribute highly to their response and light circles correspond to modes which contribute less. It can be seen in Figure 12 that the flexural and radial longitudinal modes dominate this response. Several of the antisymmetric thickness–shear modes also participate.

The response of the plate due to the long duration impact load is shown in Figure 13. In this figure, the deformed geometry of the plate due to the loading is exaggerated and plotted at sequential time points. It can be seen from Figure 13 that this load creates a flexural disturbance in the vicinity of the impact, the neighborhood of $r = 0$, which propagates radially outward from the center of the plate. It is noted that the flexural wave front reaches the point $r = 3$ in approximately 6 time units.

The modal amplitudes due to the short duration impact load are shown in Figure 14. In this figure, it can be seen that many of the higher frequency modes are more active in the response to this load than they were in the previous response, as would be expected since the "frequency" of the forcing is higher. Especially active are the transverse–longitudinal modes and the thickness–stretch modes.

The response due to the short duration impact load is shown in Figures 15 and 16. This response is similar to the long duration load response in that the load causes a disturbance which propagates radially away from the area of impact and reaches the point $r = 3$ in approximately 6 time units. In this response, however, a compressive pulse appears which originates at the point of impact and propagates transversely through the thickness of the plate in approximately one time unit. The compressive pulse is then reflected from the free bottom surface as a tensile pulse. This pulse is seen more readily in Figure 16, which displays a sequence of smaller time steps during the first time unit. The reflection of this compressive pulse at the free surface is pertinent to the spalling phenomenon characteristic to impact loading of brittle materials.

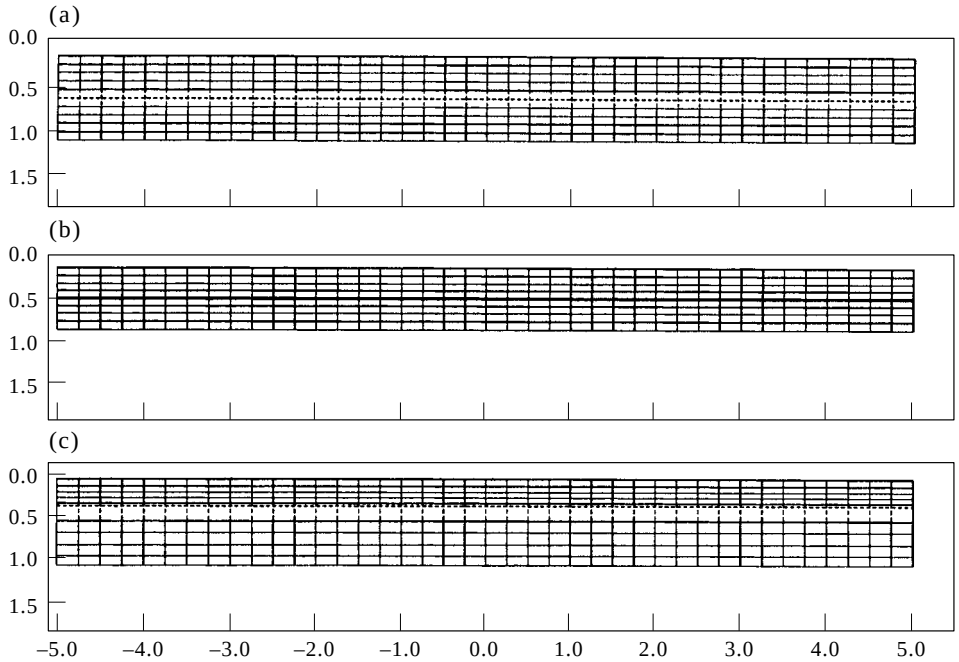

Figure 40. The first three "transverse–longitudinal" ("rod-like") modes for case 4: (a) $\omega = 0$, $k = 0$; (b) $\omega = 2{\cdot}1$, $k = 0$; (c) $\omega = 5{\cdot}75$, $k = 0$.

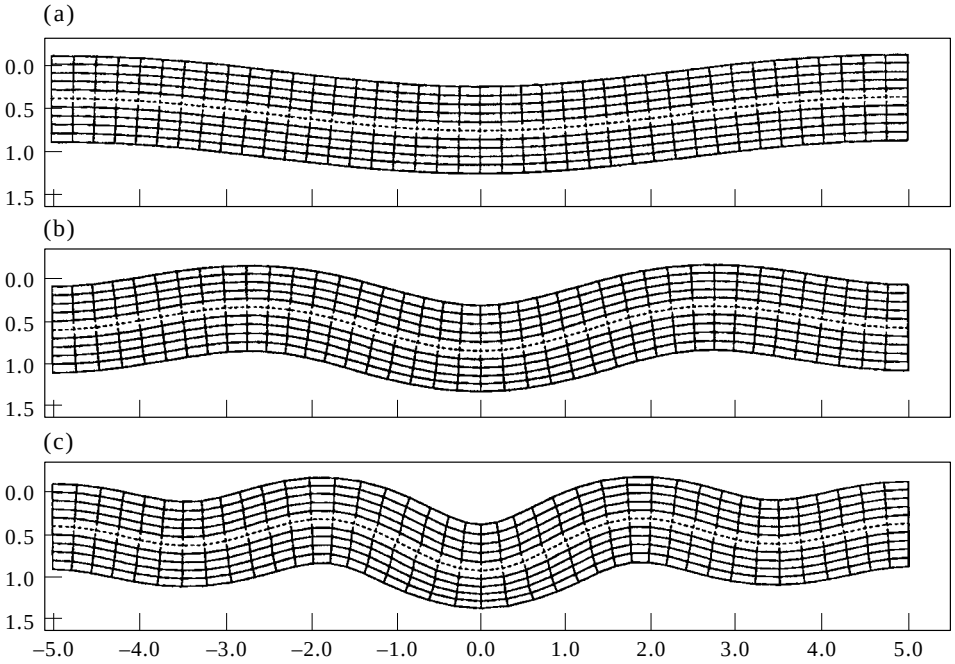

Figure 41. The first three "flexural" modes for case 3: (a) $\omega = 0{\cdot}144$, $k = 0{\cdot}766$; (b) $\omega = 0{\cdot}425$, $k = 1{\cdot}4$; (c) $\omega = 0{\cdot}775$, $k = 2{\cdot}03$.

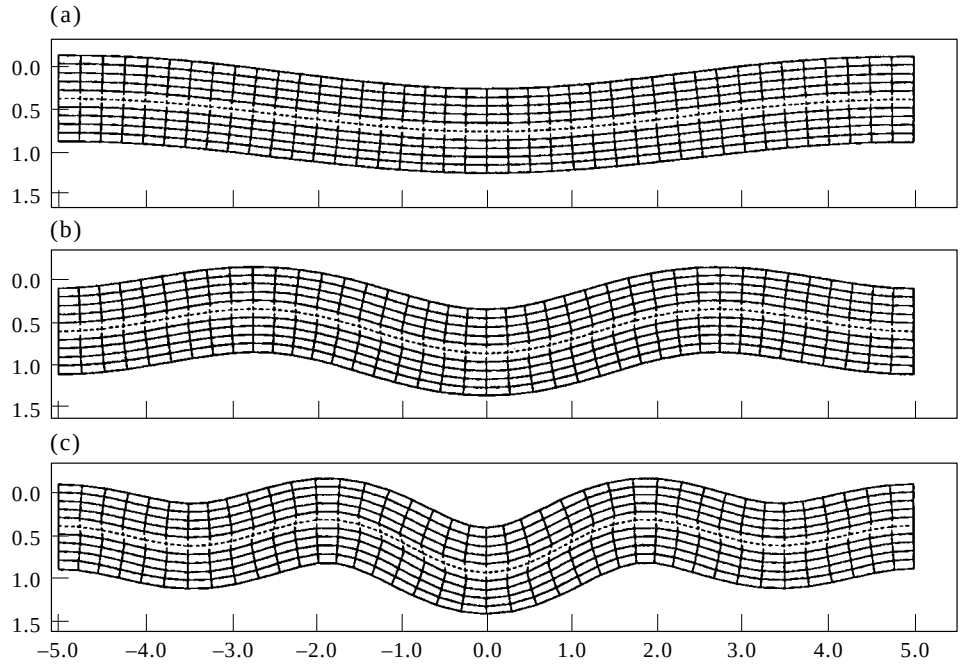

Figure 42. The first three "flexural" modes for case 4: (a) $\omega = 0{\cdot}131$, $k = 0{\cdot}766$; (b) $\omega = 0{\cdot}349$, $k = 1{\cdot}4$; (c) $\omega = 0{\cdot}597$, $k = 2{\cdot}03$.

6. RESPONSE OF SANDWICH PLATES

Sandwich structures generally consist of a thick "core layer" bonded, over each of its two major bounding surfaces, to thinner "face sheets". In this section, the response of two such sandwich structures which we will denote as case 1 and case 2 are considered. For both cases the core material will be taken as the reference material and hence its properties will be identical to those of the single layer (isotropic) plate considered in the previous section, providing a basis for comparison. The differences between these cases and the case of the isotropic plate are in the properties of the face sheets, each of which is one-tenth of the thickness of the overall structure. The configuration of the sandwich plates under consideration may be seen in Figure 3(b). The plate corresponding to case 1 is comprised of identical face sheets which are stiffer than the core layer (having four times higher elastic modulus), while the structure corresponding to case 2 possesses identical face sheets which are more compliant than the core layer (having four times lower modulus). We thus consider structures such that $c_p^{(2)} = 1$, $c_s^{(2)} = 0{\cdot}5345$ and $\rho^{(1)} = \rho^{(2)} = \rho^{(3)} = 1$ for both case 1 and case 2, while for case 1: $c_p^{(1)} = c_p^{(3)} = 2{\cdot}0$, $c_s^{(1)} = c_s^{(3)} = 1{\cdot}069$; and for case 2: $c_p^{(1)} = c_p^{(3)} = 0{\cdot}5$, $c_s^{(1)} = c_s^{(3)} = 0{\cdot}26725$.

6.1. FREQUENCY SPECTRA AND ELASTODYNAMIC MODES

The frequency spectrum corresponding to case 1 is shown in Figure 17 and that corresponding to case 2 is shown in Figure 18. Comparison of these figures with the frequency spectrum for the isotropic plate (Figure 4) shows that all of the branches for case 1 are higher in frequency than the corresponding branches of the isotropic (single layer) plate, and that the branches for case 2 are lower in frequency than those of the isotropic plate. This may be expected since 20% of the material for case 1 has a higher elastic modulus than the isotropic plate and 20% of the material for case 2 has a lower

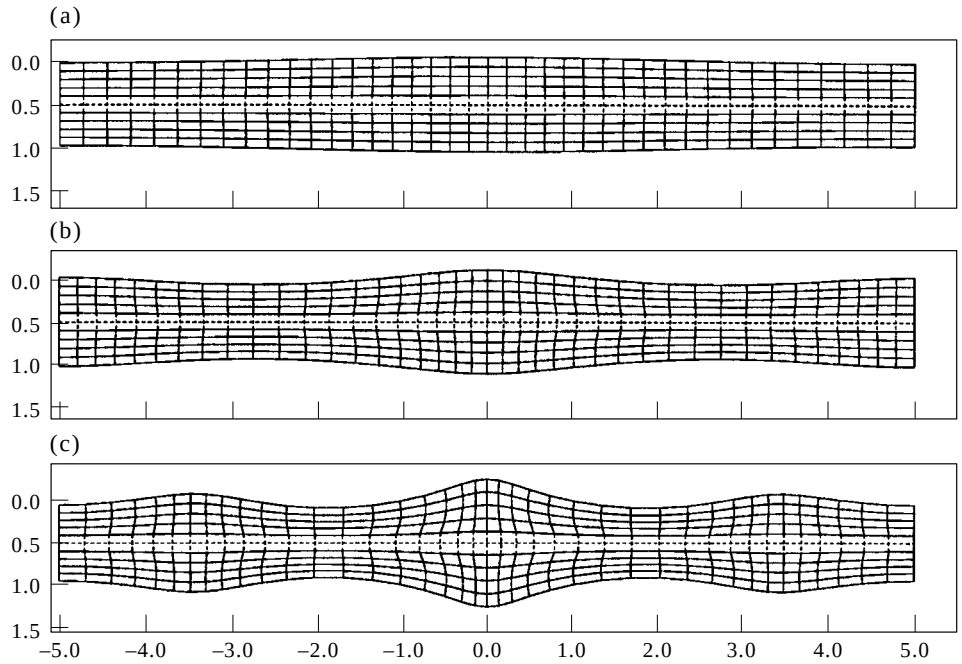

Figure 43. The first three radial–longitudinal modes for case 3: (a) $\omega = 0{\cdot}868$, $k = 0{\cdot}766$; (b) $\omega = 1{\cdot}56$, $k = 1{\cdot}4$; (c) $\omega = 2{\cdot}18$, $k = 2{\cdot}03$.

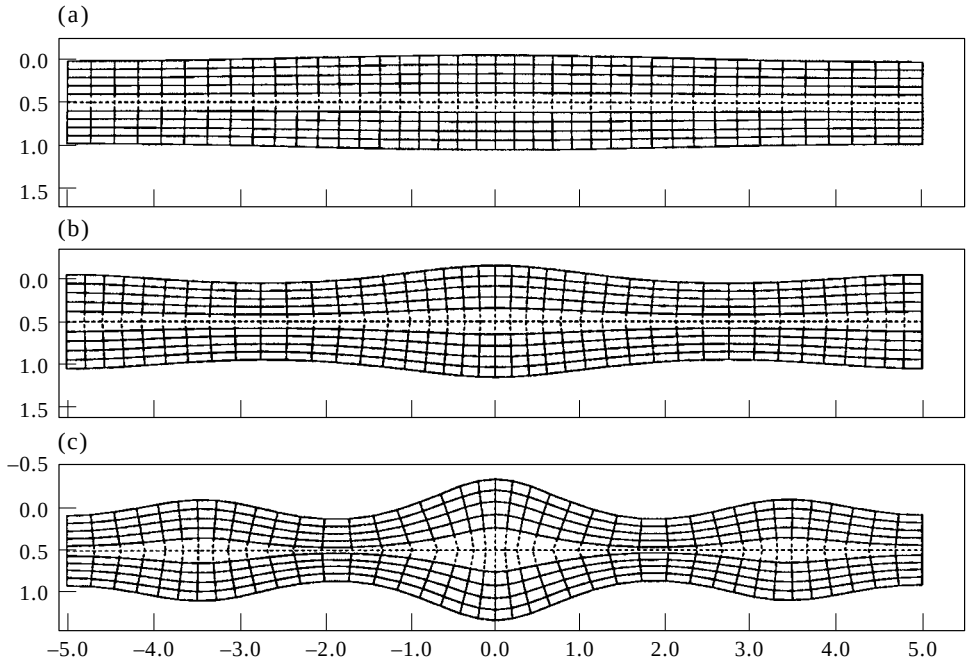

Figure 44. The first three radial–longitudinal modes for case 4: (a) $\omega = 0{\cdot}633$, $k = 0{\cdot}766$; (b) $\omega = 1{\cdot}12$, $k = 1{\cdot}4$; (c) $\omega = 1{\cdot}49$, $k = 2{\cdot}03$.

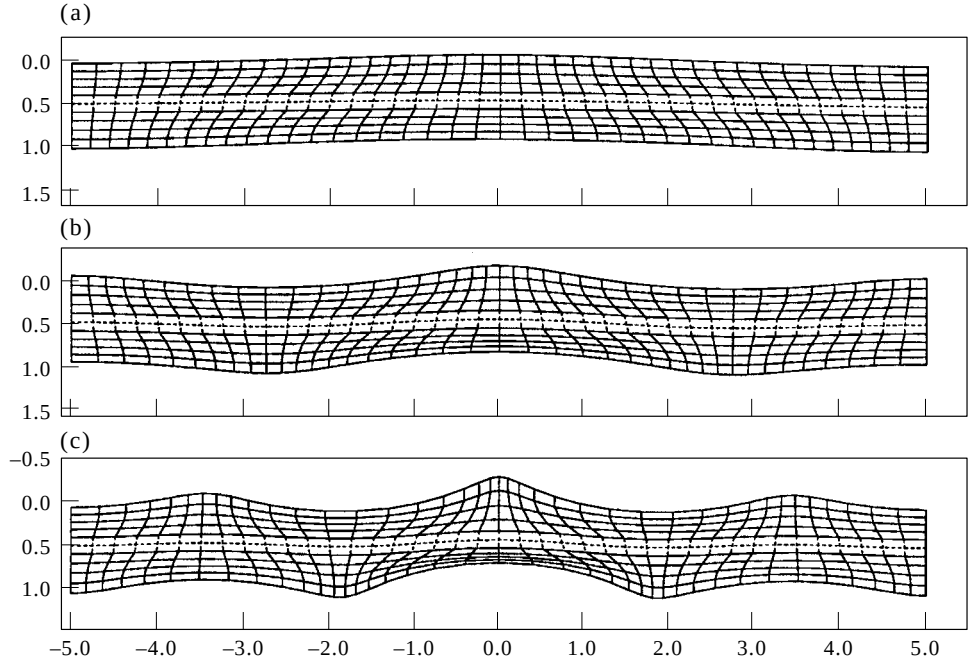

Figure 45. The first three antisymmetric thickness–shear modes for case 3: (a) $\omega = 2{\cdot}12$, $k = 0{\cdot}766$; (b) $\omega = 2{\cdot}41$, $k = 1{\cdot}4$; (c) $\omega = 2{\cdot}76$, $k = 2{\cdot}03$.

elastic modulus than the isotropic plate. It can be seen for both cases 1 and 2 that the lowest two branches of the frequency spectrum which, as discussed earlier, correspond to flexural and radial longitudinal modes, deviate from those for the isotropic case monotonically as the radial wavenumber increases. This may be explained by considering that both of these branches are asymptotic to the Rayleigh surface wave speed as the radial wavenumber increases. Thus the surface motion of these modes increases with radial wavenumber and the face sheets have a greater effect on the frequency of the elastodynamic mode. (The opposite trend may be expected for the case of bilaminate plates with a central adhesive layer considered in section 7.)

Several of the elastodynamic modes corresponding to both cases 1 and 2 are displayed in Figures 19–28. Upon consideration of these figures, small differences between cases 1 and 2 may be observed within the face sheets or near the interfaces, for the transverse–longitudinal modes (Figures 19 and 20), while no pronounced differences between cases 1 and 2 are observed for the flexural modes (Figures 21 and 22). Upon comparing the radial–longitudinal modes of case 1 which are shown in Figure 23 with those of case 2 which are shown in Figure 24, the biggest difference that can be seen is that deformed transverse surfaces (surfaces whose normals were originally in the radial direction) in Figure 23 are curved away from the vertical, while those in Figure 24 are not. The corresponding modes for the isotropic plate possess transverse surfaces which are curved less after deformation than those for case 1 but more than those for case 2, as can be verified by consideration of Figure 7. An explanation for this is rooted in the characteristic that these modes consist primarily of radial motion. For case 1, the radial motion of the core material is resisted by the stiff face sheets and thus the motion is greater in the center than near the bounding surface, thus the transverse surfaces are curved more than those for the isotropic plate. For case 2, the compliant face sheets allow increased

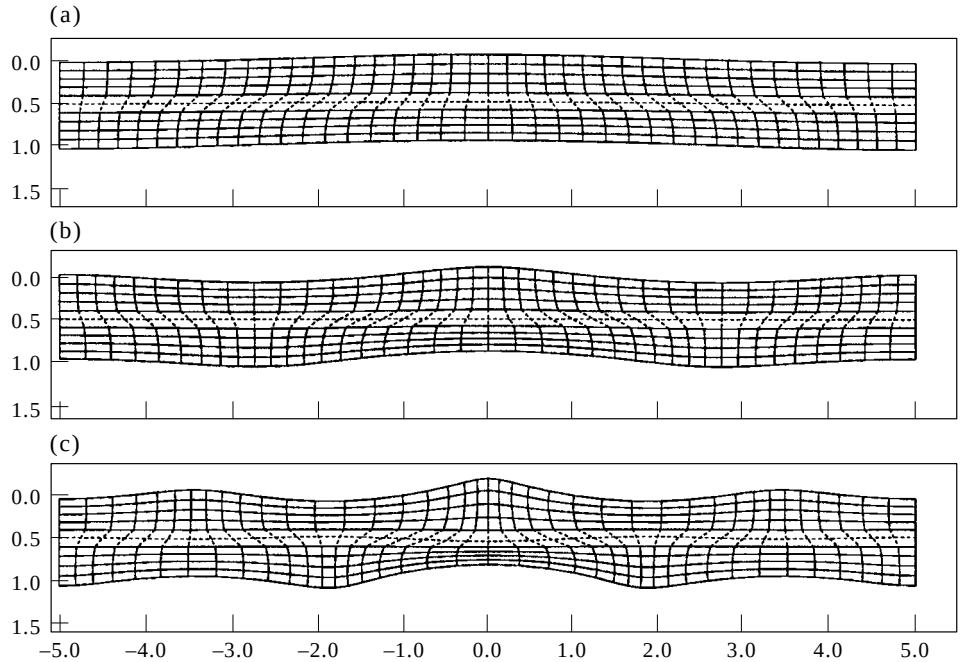

Figure 46. The first three antisymmetric thickness–shear modes for case 4: (a) $\omega = 1{\cdot}32$, $k = 0{\cdot}766$; (b) $\omega = 1{\cdot}68$, $k = 1{\cdot}4$; (c) $\omega = 2{\cdot}1$, $k = 2{\cdot}03$.

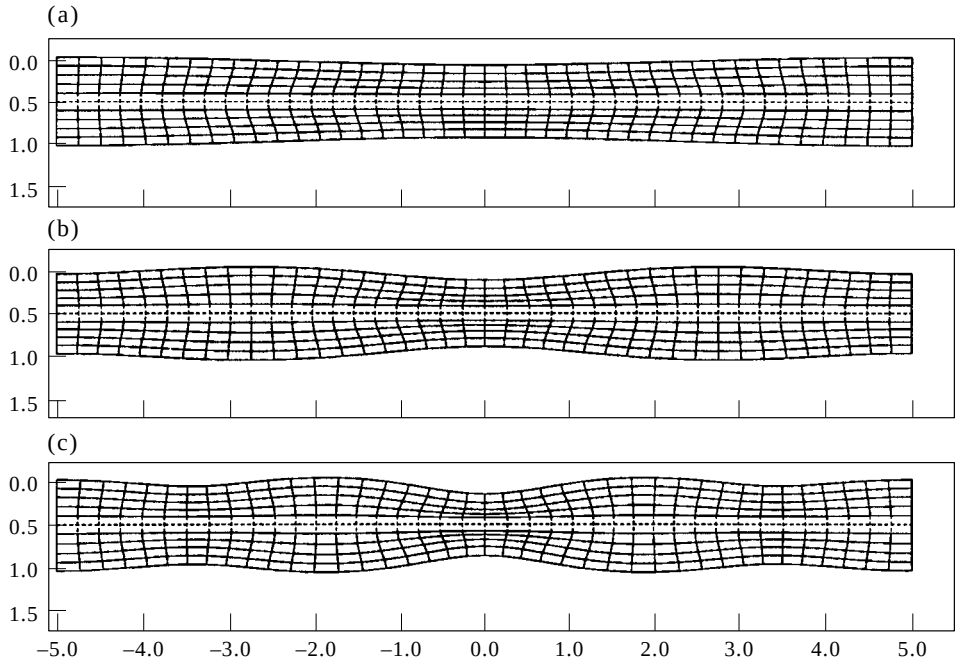

Figure 47. The first three (radially varying) symmetric thickness–stretch modes for case 3: (a) $\omega = 3{\cdot}37$, $k = 0{\cdot}766$; (b) $\omega = 3{\cdot}35$, $k = 1{\cdot}4$; (c) $\omega = 3{\cdot}37$, $k = 2{\cdot}03$.

radial motion of the bounding surface so that it moves with the core and hence the curvature of the transverse surfaces is reduced. Next, compare the thickness stretch modes shown for case 1 in Figure 27 and for case 2 in Figure 28. In these figures, the opposite trend is seen because the motion is primarily transverse. The stiff face sheets of case 1 resist bending due to the transverse motion and thus reduce the curvature of transverse surfaces, while the compliant face sheets of case 2 bend with the transverse motion and thus increase the curvature of transverse surfaces. These effects help to clarify the differences between the radial–longitudinal modes and the thickness–stretch modes which have similar looking shapes. That is, radial–longitudinal modes consist primarily of radial motion while thickness–stretch modes consist primarily of transverse motion.

If the thickness–shear modes for case 1 shown in Figure 25 are compared with those of case 2 shown in Figure 26, it can be seen that the compliant face sheets of case 2 are deformed more than the stiff face sheets of case 1. Conversely, the core is deformed more for case 1 than for case 2 near the interfaces between the face sheets and the core. [This suggests that excitation of these modes for the sandwich with stiff face sheets (case 1) could lead to debonding of the layer interfaces.] In a manner similar to those of the previous discussion, the shear motion of the core is resisted by the stiff face sheets for case 1, causing curvature of transverse surfaces, while the compliant face sheets of case 2 move with the shear motion of the core thus reducing the curvature of transverse surfaces.

6.2. TRANSIENT RESPONSE

Next, the responses of the sandwich structures of cases 1 and 2 to the same impact loads considered for the isotropic plate are examined. Recall that for each load, the forcing function is scaled so that the total imparted impulse is the same. The impact load is characterized by its (non-dimensional) "impact duration" time t_0 (or equivalently the

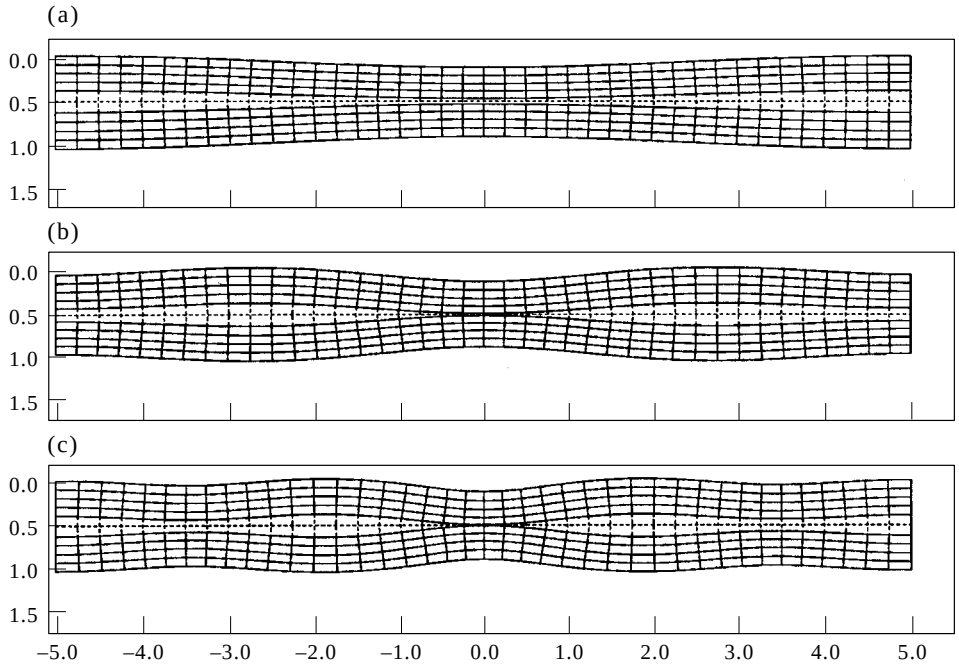

Figure 48. The first three (radially varying) symmetric thickness–stretch modes for case 4: (a) $\omega = 2{\cdot}07$, $k = 0{\cdot}766$; (b) $\omega = 2{\cdot}06$, $k = 1{\cdot}4$; (c) $\omega = 2{\cdot}17$, $k = 2{\cdot}03$.

"impact frequency" $\omega_0 = \pi/t_0$) and the "impact radius" r_0 (or equivalently the "impact wavenumber" $k_0 = 2{\cdot}405/r_0$). Two impact durations are considered, the "long duration" ($t_0 = 3{\cdot}14$) and the "short duration" ($t_0 = 0{\cdot}449$), both for an impact radius of $r_0 = 1{\cdot}2$.

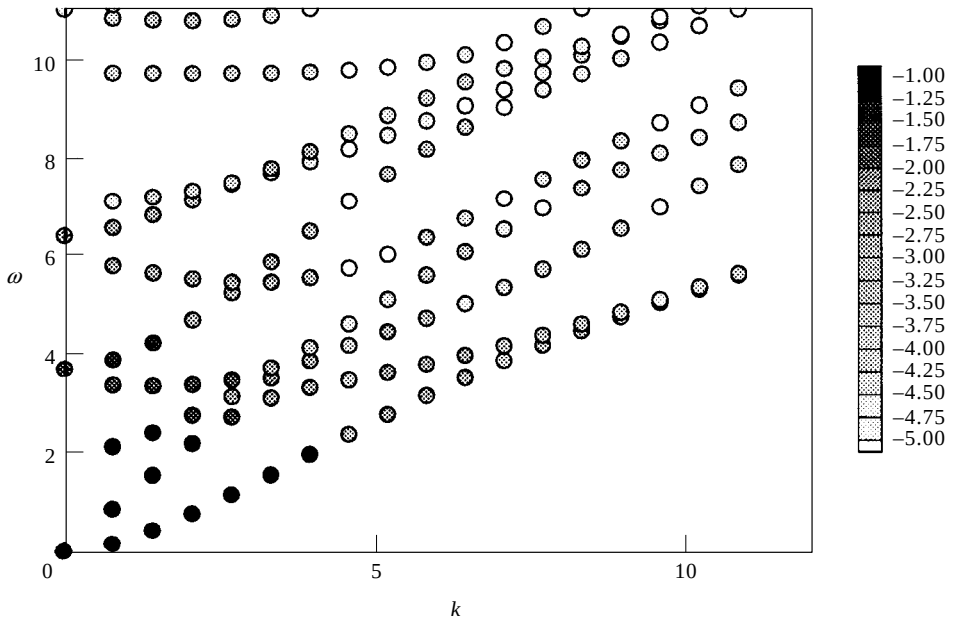

Figure 49. Modal participation spectrum of bilaminate with central "adhesive" layer impacted by "long duration load": case 3 (stiff central layer). Degree of shading indicates relative contribution of mode according to $\log_{10}$ scale of amplitude shown at right.

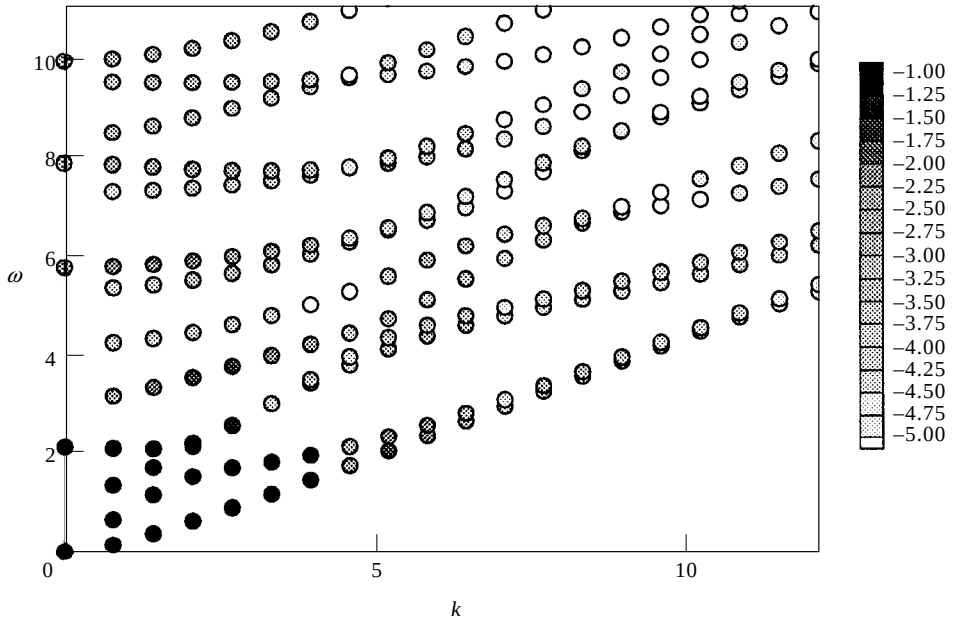

Figure 50. Modal participation spectrum of bilaminate with central "adhesive" layer impacted by "long duration load": case 4 (compliant central layer). Degree of shading indicates relative contribution of mode according to $\log_{10}$ scale of amplitude shown at right.

Before proceeding, it is pointed out to the reader that in the corresponding figures the response is shown by *exaggerated* plots of the deformed geometry. For these plots, a consistent scale of deformation was chosen so that the responses can be compared and also so that the range of behavior can be easily observed. A consequence of this scale is that large displacement gradients may cause the lines of the plots to overlap. It is emphasized that this does not correspond to any kind of material failure or discontinuity but is simply a result of the exaggerated scale of the deformed geometry.

The modal amplitudes of the response of the structure corresponding to case 1 to the long duration impact load are shown in Figure 29 and those for case 2 are shown in Figure 30. In these figures, it can be seen that the majority of the modal amplitudes are greater for case 2. This is expected since case 2 is more compliant than case 1 and thus will respond to the same load with larger displacements. Figures 31 and 32 show the responses, of cases 1 and 2, respectively, to this load. Upon consideration of these figures, the only significant difference seen between these responses is that the resulting displacement, when compared with the corresponding results for the isotropic plate, is larger for case 2 and smaller for case 1 as might be expected.

The modal amplitudes for the "short duration load" are shown in Figures 33 and 34. Although most of the modal amplitudes are greater for case 2, as seen previously, it is noted that the transverse–longitudinal modes, particularly those corresponding to the thickness–stretch modes, participate more for case 2 than for case 1. The response of case 1 to this load is shown in Figure 35. Similarly, the response of case 2 is shown in Figure 36. The first observation that may be made upon consideration of these figures is that the displacements of the face sheets are significantly larger for case 2 than for case 1. This is expected since the face sheets of case 1 are stiffer than those of case 2. It can also be observed, however, that the transversely propagating stress pulse which is initiated in the top face sheet induces significantly larger stresses (deformation) for case 2 even after it has

propagated into the core layer, which is the same for both cases. This result may have been anticipated due to the higher degree of participation, for case 2, of the thickness–stretch modes which correspond to transverse dilatational motion. This difference between the responses of case 1 and case 2 suggests that the stiff face sheets tend to protect the softer core from impact as may be expected. What is perhaps more interesting, however, is that

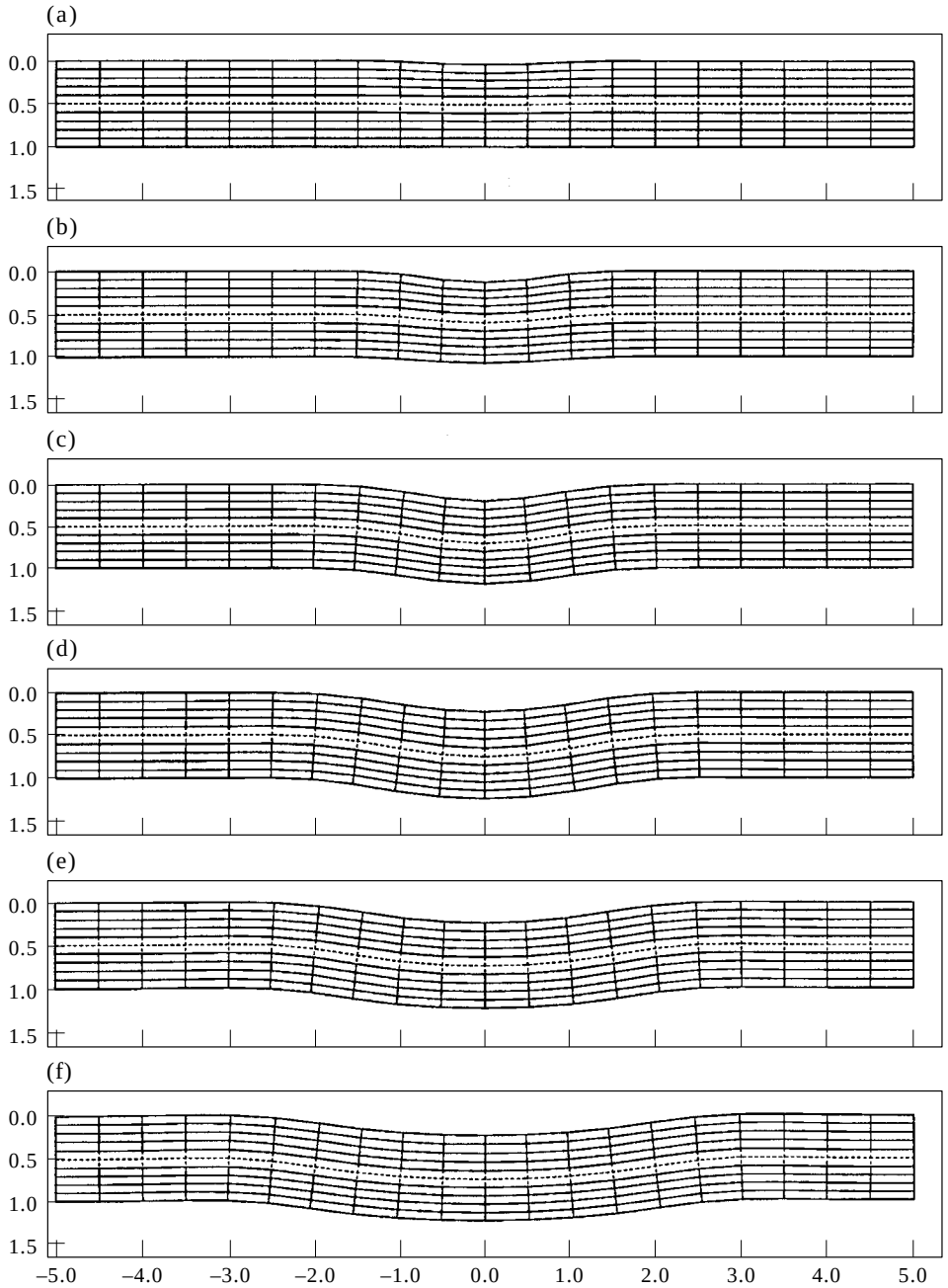

Figure 51. Transient response of case 3 subjected to "long duration load". "Freeze frames" of deforming plate at sequential instants in (normalized) time: (a) $t = 1$, (b) 2, (c) 3, (d) 4, (e) 5, (f) 6.

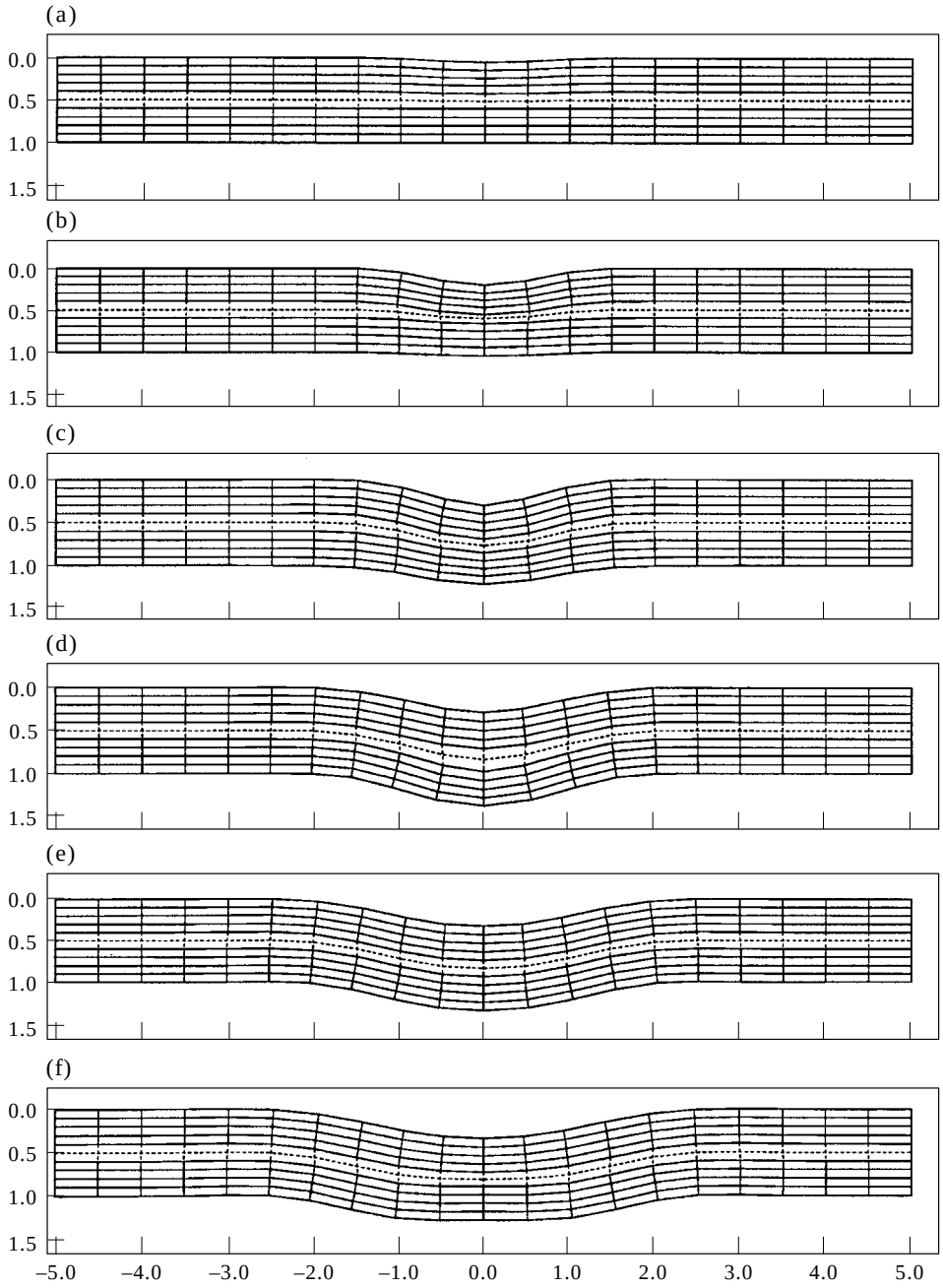

Figure 52. Transient response of case 4 subjected to "long duration load". "Freeze frames" of deforming plate at sequential instants in (normalized) time: (a) $t = 1$, (b) 2, (c) 3, (d) 4, (e) 5, (f) 6.

the compliant face sheet exposes the core to higher stresses due to transverserly propagating pulses than would be experienced by an isotropic plate without any face sheet at all. This result can be verified by comparing Figure 36 with Figure 16.

From the results presented in this section, it can be seen that the sandwich structures considered behave very much like the isotropic plate in response to the "long duration

loads''. The main effect of the face sheets was to increase or decrease the total stiffness of the plate and thus reduce or increase the overall displacements accordingly. The character of the response was not seen to be significantly affected by the face sheets. For the ''short duration loads'', however, the face sheets were observed to have a much greater effect on the form of the response. Compliant face sheets were seen to expose the structure to higher compressive stresses at the interface between the top face sheet and the core. These stresses may be transmitted through the core and reflected as tensile pulses at the opposite interface. Such tensile reflection could promote interfacial damage such as layer debonding at the interface of the core and the face sheet opposite the impact surface. The stiff face sheets, on the other hand, tended to protect the core from the transversely propagating pulses due to the impact.

7. RESPONSE OF BILAMINATES WITH A CENTRAL ''ADHESIVE'' LAYER

In this section, the response of bilaminate structures with a central layer simulating, for example, the situation of an adhesive layer, is considered. Two such structures, denoted as case 3 and case 4, are examined, each of which has two identical outer layers and a thinner layer in between them as represented in Figure 3(c). The material of the outer layers will be considered as the base or reference material and hence will be identical to the material of the isotropic plate examined in section 5 or the core material of the sandwich plates considered in section 6. The thickness of the ''adhesive'' layer is chosen to be two-tenths of the total thickness of the plate, hence these cases are of the same general ''make up'' as cases 1 and 2 but configured differently. Specifically, structures are considered where the layers are characterized by the non-dimensional properties given by $c_p^{(1)} = c_p^{(3)} = 1$, $c_s^{(1)} = c_s^{(3)} = 0{\cdot}5345$ and $\rho^{(1)} = \rho^{(2)} = \rho^{(3)} = 1$ for both cases 3 and 4, with the

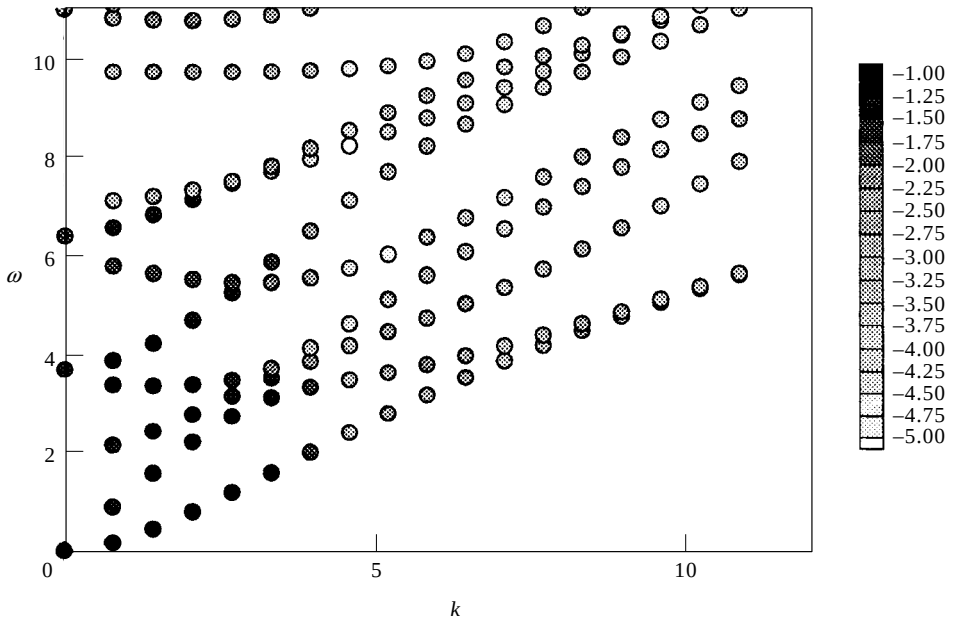

Figure 53. Modal participation spectrum of bilaminate with central ''adhesive'' layer impacted by ''short duration load'': case 3 (stiff central layer). Degree of shading indicates relative contribution of mode according to $\log_{10}$ scale of amplitude shown at right.

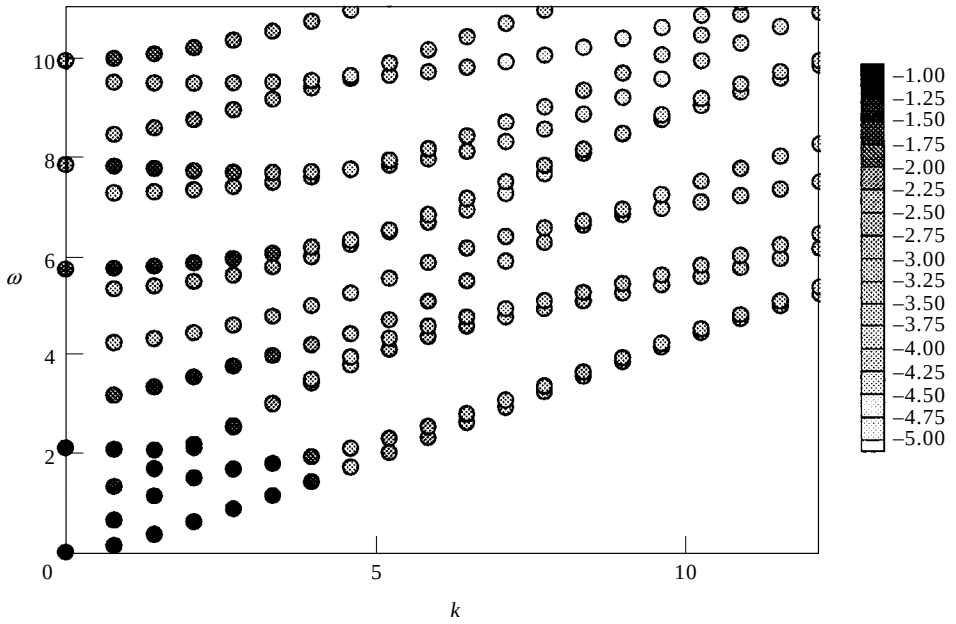

Figure 54. Modal participation spectrum of bilaminate with central "adhesive" layer impacted by "short duration load": case 4 (compliant central layer). Degree of shading indicates relative contribution of mode according to $\log_{10}$ scale of amplitude shown at right.

normalized wave speeds in the central layer distinguished for each case as: case 3: $c_p^{(2)} = 2{\cdot}0$, $c_s^{(2)} = 1{\cdot}069$; case 4: $c_p^{(2)} = 0{\cdot}5$, $c_s^{(2)} = 0{\cdot}26725$.

7.1. FREQUENCY SPECTRA AND ELASTODYNAMIC MODES

The frequency spectrum corresponding to case 3 is shown in Figure 37 while that corresponding to case 4 is shown in Figure 38. As may be anticipated from the behavior observed for the sandwich plates discussed in the previous section, the frequencies for case 3, where the adhesive layer is relatively stiff compared to the "adherends", are generally higher than the corresponding frequencies for the isotropic plate which are generally higher than those for the structure corresponding to case 4. For case 4, it is noted that the fourth branch, which corresponds to symmetric thickness–stretch modes, has much lower associated frequencies than it has had in any of the previous cases. It is curious that the other higher order thickness–stretch branches have not been lowered in frequency as much as the fourth branch. As anticipated at the end of the previous section, the frequencies associated with the lowest two branches of case 3 are asymptotic to those of the isotropic plate for large radial wavenumbers, a reason being that these modes consist largely of surface motion as discussed earlier. The lowest branches of case 4, however, are not asymptotic to the isotropic case within the range of radial wavenumbers considered. This may generally be attributed to the effective decoupling of the motion of the two adherends for this case as may be seen upon examination of the corresponding figures. The structures are thus effectively thinner in this sense and hence the surface motion becomes apparent for shorter wavelengths and hence higher wavenumbers than for the other cases considered. Next, several of the corresponding elastodynamic mode shapes are examined more closely.

The elastodynamic modes corresponding to cases 3 and 4 are plotted in Figures 39–48. Figure 43 shows the radial longitudinal modes for case 3. These modes are very similar

to those for the isotropic case and, as stated previously, the corresponding frequencies are asymptotic to the Rayleigh surface wave speed in the outer layer because most of the motion of these modes is at the surface for large wavenumbers. The radial longitudinal modes for case 4 are shown in Figure 44. These modes are somewhat different than the corresponding modes for the isotropic case. Because the inner layer is compliant, a large portion of the deformation corresponding to these modes occurs in the inner layer and

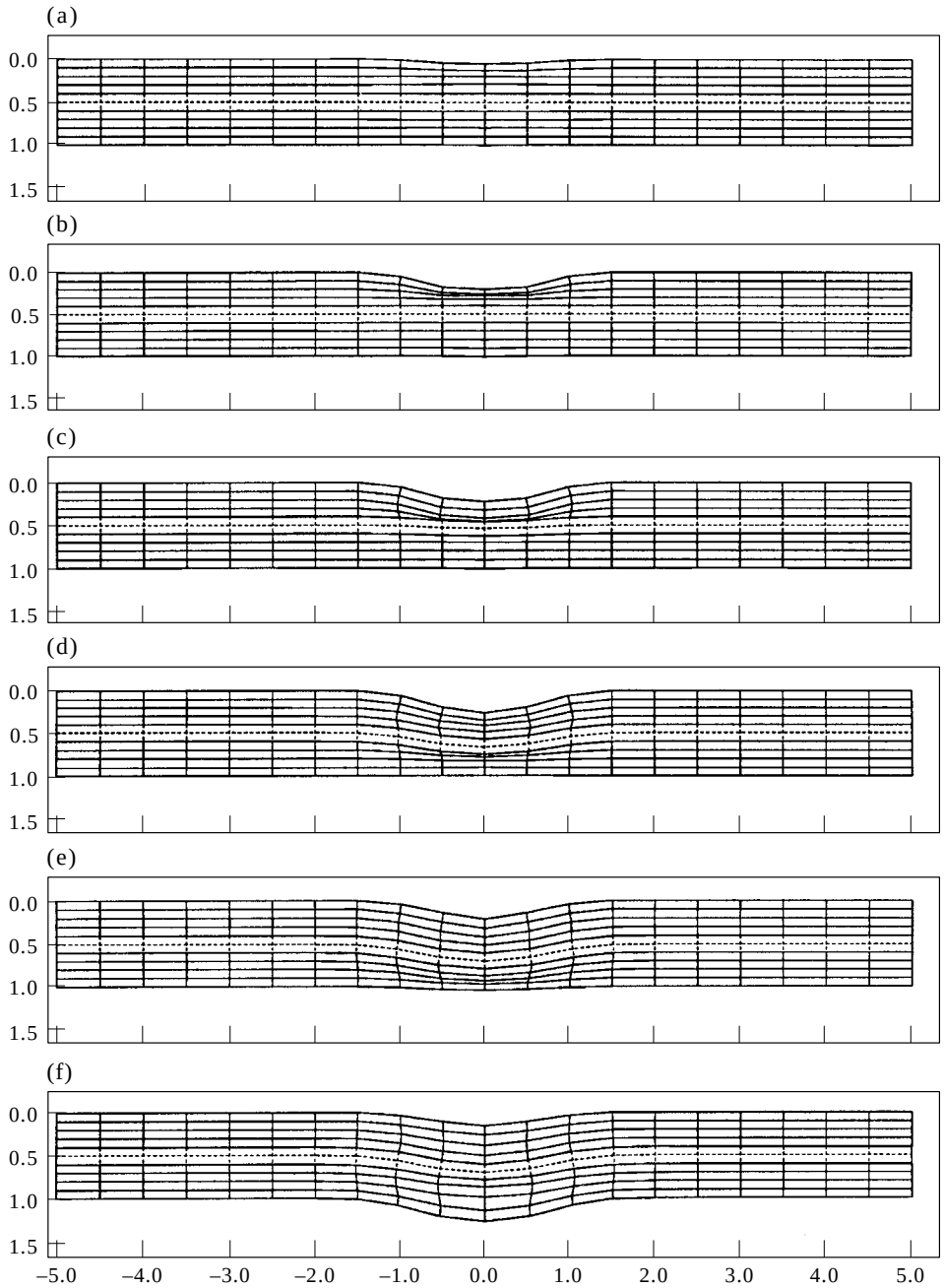

Fig. 55a-f.

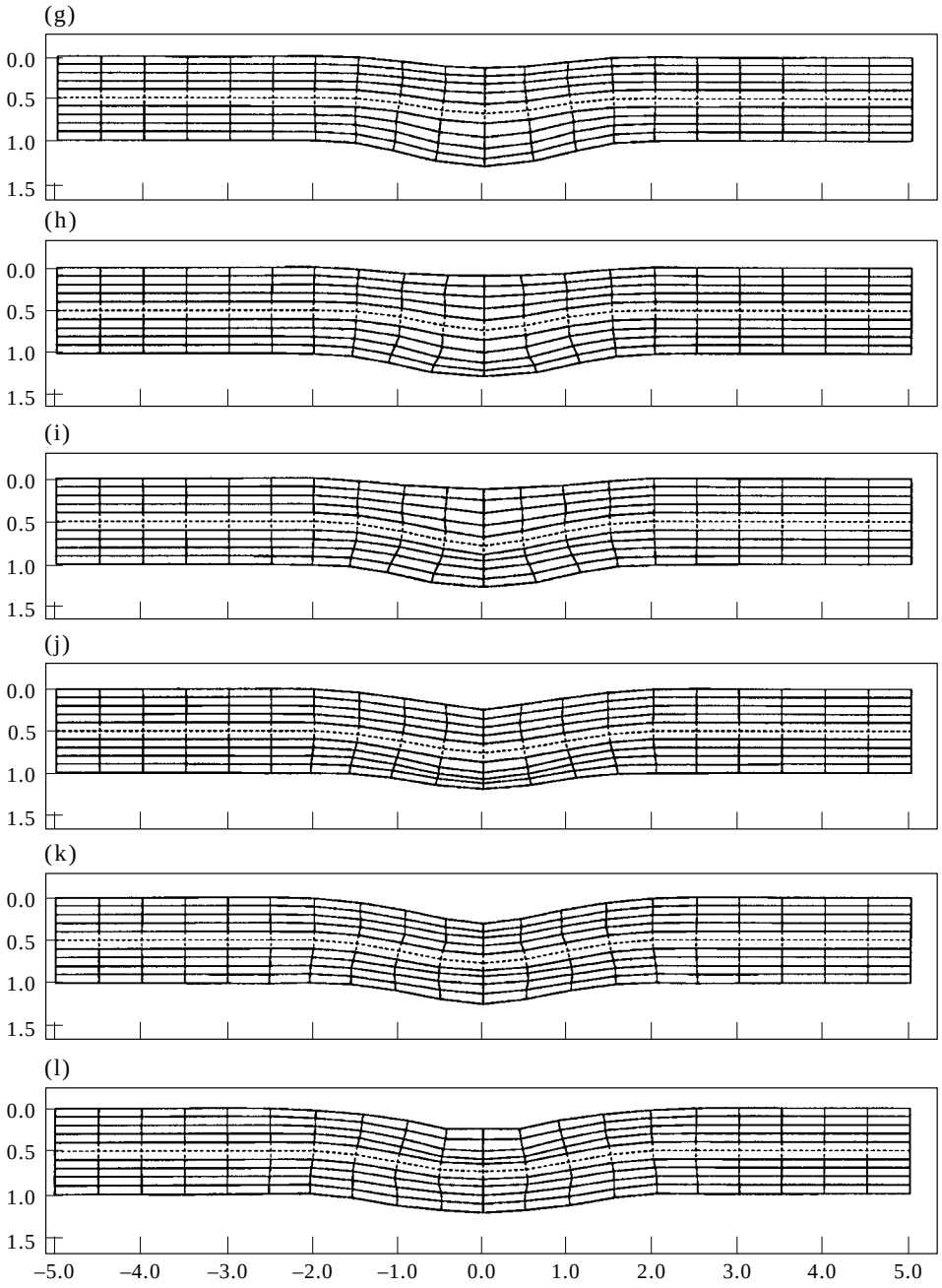

Fig. 55g-l.

Figure 55. Transient response of case 3 subjected to "short duration load". "Freeze frames" of deforming plate at sequential instants in (normalized) time: (a) $t = 0{\cdot}2$, (b) 0·4, (c) 0·6, (d) 0·8, (e) 1·0, (f) 1·2, (g) 1·4, (h) 1·6, (i) 1·8, (j) 2·0, (k) 2·2, (l) 2·4.

thus the material properties of the inner layer contribute more to the frequencies of these modes. Thus, the corresponding frequencies are not asymptotic to the Rayleigh surface wave speed in the outer layer, at least for the range of wavenumbers considered. The

thickness–shear modes are shown in Figures 45 and 46 for cases 3 and 4, respectively. Like the radial–longitudinal modes, the thickness–shear modes for case 3 appear similar to those of the isotropic plate while those for case 4 have greater deformation in the compliant inner layer.

Figures 47 and 48 depict the first three thickness stretch modes for cases 3 and 4, respectively. Again, the modes for case 3 appear to be similar to those for the isotropic

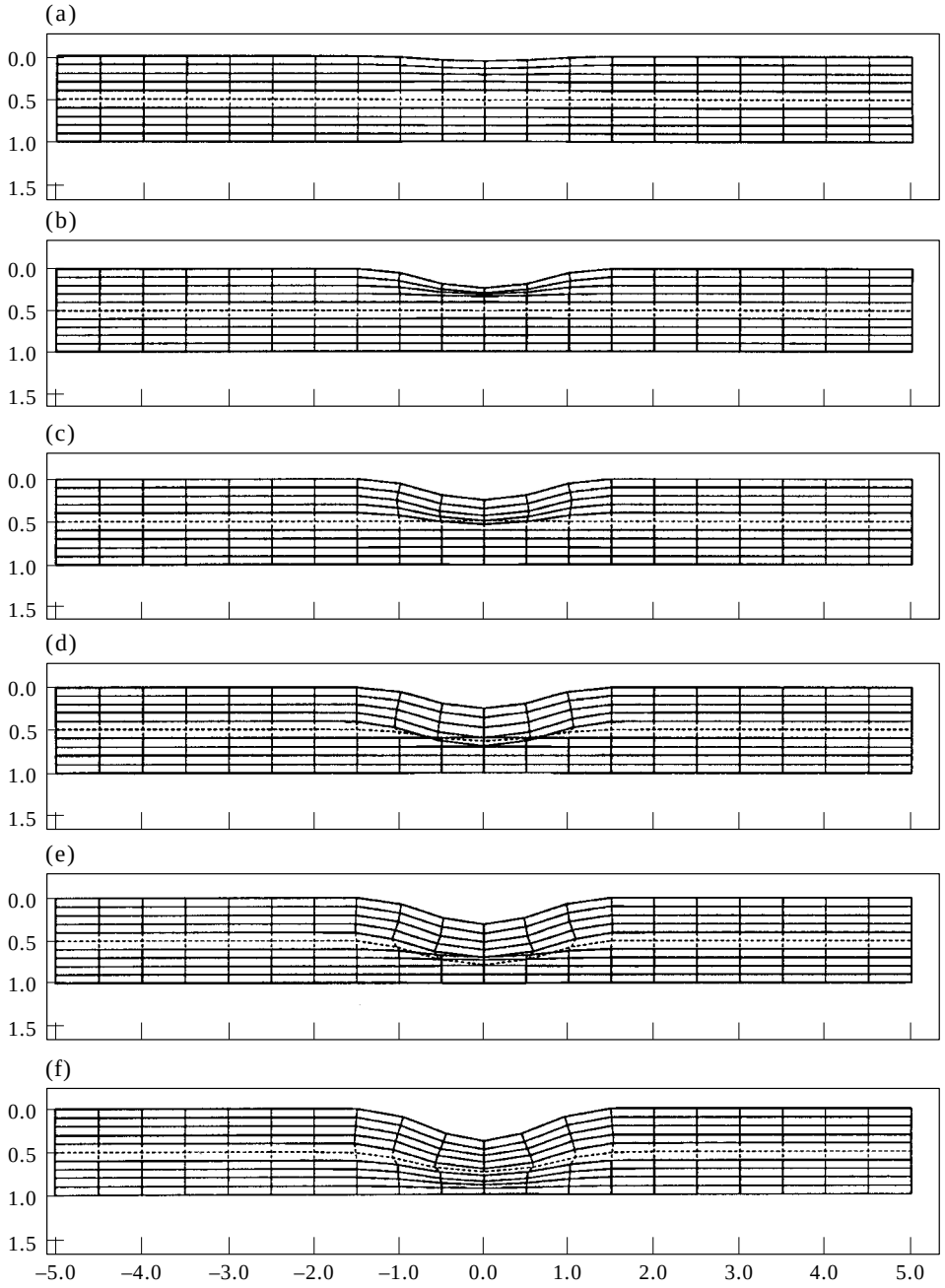

Fig. 56a-f.

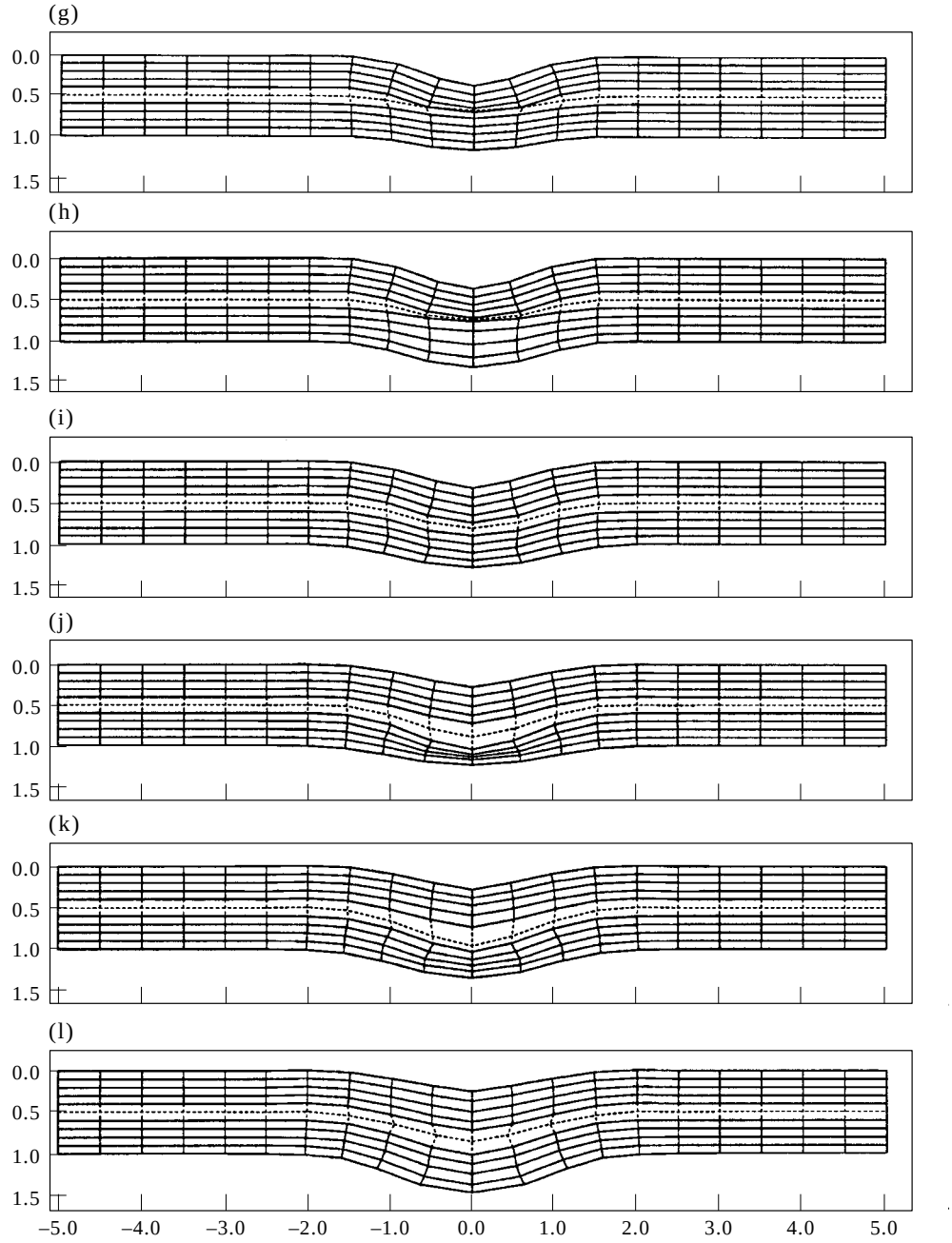

Fig. 56g-l.

Figure 56. Transient response of case 4 subjected to "short duration load". "Freeze frames" of deforming plate at sequential instants in (normalized) time: (a) $t = 0{\cdot}2$, (b) 0·4, (c) 0·6, (d) 0·8, (e) 1·0, (f) 1·2, (g) 1·4, (h) 1·6, (i) 1·8, (j) 2·0, (k) 2·2, (l) 2·4.

plate while those for case 4 appear to differ. The symmetric thickness stretch modes for case 4 are interesting in that the outer layers each individually take on the shape of the flexural modes for the isotropic plate, while the inner layer keeps the form of the thickness

stretch modes. The outer layers of these modes appear to stretch very little if at all in the transverse direction. This combination of modes makes sense if the isotropic plate modes are considered for each layer separately. The reduced stiffness of the inner layer will lower the frequencies of the thickness stretch modes for that layer so that they tend to match the lower frequencies of the flexural modes in the outer layers. Referring back to Figure 27, it can be seen that a similar mode shape occurs for the sandwich plate with stiff face sheets. In that figure, the face sheets take on the form of the flexural modes and bend around the thickness stretch modes of the less stiff inner layer. This suggests an explanation for the significant reduction in frequency of the symmetric thickness stretch modes (fourth branch). For these modes, a large percentage of the corresponding deformation is seen to occur in the middle layer which has reduced stiffness. The material properties of this layer dominate the resulting motion and therefore the frequencies associated with these modes are reduced more than those of the other modes. In light of the low frequencies of the symmetric thickness stretch modes for case 4, we will expect strong participation of these modes in the responses of case 4 to impact loading. Next, the responses are examined of bilaminates with central adhesive layers (cases 3 and 4) to the same impact loads as considered for the sandwich plates in the previous section, and for the isotropic plates in section 5.

7.2. TRANSIENT RESPONSE

The modal amplitudes associated with the response of case 3 to the "long duration" impact load are shown in Figure 49 while those for case 4 are shown in Figure 50. As for the sandwich structures, the modal amplitudes are lower for the case with added stiffness (case 3). The symmetric thickness stretch modes (fourth branch) appear to contribute significantly more for case 4 than for case 3 or for the isotropic plate (Figure 12). Figures 51 and 52 display the responses of the structures corresponding to cases 3 and 4, respectively, to this load. The response for case 3 appears to be similar to that for the isotropic plate with a somewhat smaller displacement due to the added stiffness of the thin middle layer. In the response for case 4, however, the outer layers can be seen to separate slightly due to transverse stretch of the compliant middle layer. This may be attributed to the excitation of the symmetric thickness stretch modes mentioned previously.

The modal amplitudes for the short duration impact load are shown in Figures 53 and 54 for cases 3 and 4, respectively. For both cases, participation of the thickness stretch modes is seen but the modes corresponding to the fourth branch participate significantly more than the others for case 4. The impact response of case 3 is shown in Figure 55 and the response of case 4 is shown in Figure 56. For case 3, an increase in the stress (deformation) of the transversely propagating compressive pulse can be seen when comparing Figure 55 with Figure 16 which corresponds to the same load for the isotropic plate (compare $t = 0{\cdot}6$). This increase is due to the overlap of the compressive pulse with its compressive reflection from the stiff central layer. This effect may be thought of as a pinching of the outer layer between the impact load and the stiff central layer. In the response of case 4, the familiar transversely propagating stress pulse travels through the thickness of the plate and is reflected from the opposite surface. In this case, however, the reflected tensile pulse does not appear to be transmitted through the compliant inner layer, but is instead reflected back again into the lower layer in compression. The vibrational energy appears to remain trapped in the bottom layer causing it to stretch and contract repeatedly until the energy disperses radially via the flexural wave.

It was seen in this section that the bilaminate with a stiff "adhesive" layer (case 3) behaves very much like the isotropic plate when subjected to the "long duration" impact load. This may be attributed to the observation that the responses to this load are

dominated by the flexural modes, which consist mainly of surface motion, and thus are not significantly altered by the presence of a stiff thin central layer. In the response of case 3 to the short duration impact load, a ''pinching'' of the impacted outer layer was observed. It would appear that this phenomenon would tend to promote internal damage at the layer interface. The responses of the bilaminate with a compliant ''adhesive'' layer (case 4) were seen to be strongly influenced by the symmetric thickness stretch modes (fourth branch) which allow the outer layers to separate from each other and flex almost independently. This independent flexing may lead to internal damage such as layer debonding as well as core crushing.

8. CONCLUDING REMARKS

The foundations for the analysis of the transient axisymmetric response of thick layered plates have been outlined, and a mathematical representation of an impact load has been presented. The analysis, based on an exact elasticity solution, was seen to lend itself well to parallel computation, and subsequent computations were implemented accordingly. A benchmark study with regard to a single layer plate was presented, followed by parallel studies for two types of layered plates, sandwich plates and bilaminates with a central ''adhesive'' layer. In each case, frequency spectra and elastodynamic modes were discussed and compared. Further, the response to both ''short duration'' and ''long duration'' impact loads was examined, with the results presented in the form of ''freeze frames'' of the deforming structure at various time increments revealing important local behavior.

The response of the isotropic plate to impact loading was seen to be sensitive to the impact duration. It was observed that after impact occurred, the energy imparted to the plate was dispersed radially by flexural waves. When the ''frequency'' of the impact was small compared with the frequency of the flexural modes (long duration of impact), the energy was seen to be dispersed as it was imparted and hence the local stresses in the vicinity of impact were of the order of the stresses at the radially propagating flexural wave front. When the ''frequency'' of impact was large compared with the frequency of the flexural modes (short duration of impact), then the imparted energy was not dispersed by the flexural waves, but instead was seen to build up in the region local to the impact. This energy was seen to be channeled to the higher frequency thickness–stretch and thickness–shear modes resulting in transversely propagating pulses and hence high stress levels in the region local to the impact. Since these local stresses are much higher than those associated with the flexural wave front, the present results suggest that thin plate theories which do not include transverse (thickness) effects are not adequate for the prediction of damage due to short duration impact loading.

The responses of the several laminate structures examined support the notion that transverse wave propagation is a dominant mechanism for initiating internal damage in layered structures as a result of impact. It was seen that transversely propagating compressive pulses were initiated in the first layer by the impact, and that these pulses travel transversely while dispersing radially. If the compressive pulse reaches an interface between layers before dispersing, then it will reflect and refract. A stiff embedded layer was seen to cause the compressive pulse to reflect in compression and overlap with itself near the layer interface. Such behavior would encourage damage at the layer interface due to large compressive stress. The refracted pulse was observed to continue on in compression. When an embedded compliant layer was reached, the compression pulse was seen to reflect in tension. The reflected tensile pulse tended to pull the layers apart and hence would encourage debonding. When a thin compliant layer was situated in between two stiffer layers, a compressive pulse was seen to be transmitted into the soft layer and to become

trapped there, repeatedly reflecting in compression between the two stiff layers until the vibrational energy was dispersed radially by flexural waves or refracted into the stiff layers. This situation would cause the compliant inner layer to stretch and contract while the stiff outer layers flex against each other. This kind of resonance would also tend to pull the layers apart, and hence encourage debonding. Thus, it was seen that the internal damage that has been observed in laminates impacted by masses (see for example reference [28]) may be attributed to transverse wave propagation. It is apparent that this phenomenon cannot be properly understood by studying plate theories or models of laminate response that do not include transverse wave propagation. (Parallel studies were also conducted for an impactor with a smaller radius of $r_0 = 0{\cdot}345$ for each of the structures considered herein and revealed the same general behavior [25]. The specific results corresponding to this smaller impact radius have therefore been excluded for brevity.)

REFERENCES

1. J. M. Whitney and N. J. Pagano 1970 *ASME Journal of Applied Mechanics* **37**, 1031–1036. Shear deformation in heterogeneous anisotropic plates.
2. P. C. Yang, C. H. Norris and Y. Stavsky 1966 *International Journal of Solids and Structures* **2**, 665–684. Elastic wave propagation in heterogeneous plates.
3. R. D. Mindlin 1951 *ASME Journal of Applied Mechanics* **18**, 31–38. Influence of rotatory inertia and shear on flexural motions of isotropic, elastic plates.
4. S. Abrate 1991 *Applied Mechanics Reviews* **44**, 155–190. Impact of laminated composite materials.
5. S. Abrate 1994 *Applied Mechanics Reviews* **47**, 517–544. Impact of laminated composite: recent advances.
6. S. Abrate 1997 *Applied Mechanics Reviews* **50**, 69–82. Localized impact of sandwich structures with laminated facings.
7. C. T. Sun and R. Y. S. Li 1974 *AIAA Journal* **10**, 1415–1417. Exact and approximate analyses of transient wave propagation in an anisotropic plate.
8. C. T. Sun and S. Chattopadhyay 1975 *ASME Journal of Applied Mechanics* **41**, 693–698. Dynamic response of anisotropic laminated plates under initial stress to impact of a mass.
9. M. G. Koller 1986 *Journal of Applied Mathematics and Physics* (*ZAMP*) **37**, 256–269. Elastic impact of spheres on sandwich plates.
10. A. P. Christoforou and S. R. Swanson 1991 *International Journal of Solids and Structures* **27**, 161–170. Analysis of impact response in composite plates.
11. L. J. Lee, K. Y. Huang and Y. J. Fann 1993 *Journal of Composite Materials* **27**, 1238–1256. Dynamic response of composite sandwich plate impacted by a rigid ball.
12. C. B. Prasad, D. R. Ambur and J. H. Starnes 1994 *AIAA Journal* **32**, 1270–1277. Response of laminated composite plates to low-speed impact by impactors.
13. C. C. Chao, T. P. Tung, C. C. Sheu and J. H. Tseng 1994 *ASME Journal of Vibration and Acoustics* **116**, 371–378. A consistent higher order theory of laminated plates with nonlinear impact modal analysis.
14. R. Heuer, H. Irschik, P. Fotiu and F. Ziegler 1992 *International Journal of Solids and Structures* **29**, 1813–1818. Nonlinear flexural vibrations of layered plates.
15. A. Nosier, R. K. Kapania and J. N. Reddy 1994 *Computational Mechanics* **13**, 360–379. Low velocity impact of laminated composites using a layerwise theory.
16. C. T. Sun, J. D. Achenbach and G. Herrmann 1968 *ASME Journal of Applied Mechanics* **35**, 408–411. Time-harmonic waves in a stratified medium propagating in the direction of layering.
17. D. Li and H. Benaroya 1994 Wave Motion **20,** 315–358. Waves, normal modes and frequencies in periodic and near periodic rods.
18. R. L. Weaver and Y.-H. Pao 1980 *ASME Journal of Applied Mechanics* **47**, 833–840. Multiple scattering of waves in irregularly laminated composites.
19. A. N. Norris and Z. Wang 1994 *Journal of Sound and Vibration* **169**, 485–502. Low frequency bending waves in periodic plates.

20. W. J. Bottega 1988 *Mechanics Research Communications* **15**, 11–20. An axisymmetric solution for the transient problem of a multilayered elastic solid of finite extent.
21. R. L. Weaver and Y.-H. Pao 1982 *ASME Journal of Applied Mechanics* **49**, 821–836. Axisymmetric elastic waves excited by a point source in a plate.
22. W. J. Bottega 1988 *Mechanics Research Communications* **15**, 237–241. On the orthogonality of the normal modes for multilayered elastic solids.
23. S.-S. Lih and A. K. Mal 1995 *Wave Motion* **21**, 17–34. On the accuracy of approximate plate theories for wave field calculations in composite laminates.
24. M. El-Raheb and P. Wagner 1996 *Journal of the Acoustical Society of America* **99**, 3513–3527. Transient elastic waves in a finite layered media.
25. K. A. Lange 1996 *M.S. Thesis*, *Rutgers University*. On the elastodynamic response of thick multilayered plates subjected to impact loads.
26. W. J. Bottega and A. Maewal 1983 *International Journal of Nonlinear Mechanics* **18**, 449–463. Dynamics of delamination buckling.
27. W. J. Bottega 1994 *International Journal of Solids and Structures* **31**, 1891–1909. On circumferential splitting of a laminated cylindrical shell.
28. M. D. Rhodes, G. J. Williams and J. H. Starnes, Jr. 1977 *NASA Technical Note D*-8411. Effect of low-velocity impact damage on the compressive strength of graphite–epoxy hat-stiffened panels.
29. K. F. Graff 1991 *Wave Motion in Elastic Solids*. New York: Dover Publications; 1975 re-issue.
30. H. Kolsky 1963 *Stress Waves in Solids*. New York: Dover Publications.
31. J. W. S. Rayleigh 1889 *Proceedings of the London Mathematical Society* **10**, 225–234. On the free vibrations of an infinite plate of homogeneous elastic matter.
32. H. Lamb 1917 *Proceedings of the Royal Society of London*, *series A* **93**, 114–128. On waves in an elastic plate.